MRV5

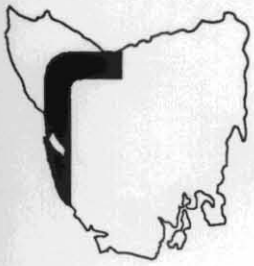

MT READ VOLCANICS PROJECT
GEOLOGICAL REPORT 5

The origin of gold-tin-copper mineralisation at the Lakeside Deposit, Western Tasmania

TASMANIA DEPARTMENT OF RESOURCES & ENERGY
DIVISION OF MINES AND MINERAL RESOURCES

MRV5

TASMANIA DEPARTMENT OF
RESOURCES AND ENERGY

Division of Mines and Mineral Resources

1990

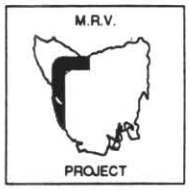

MT READ VOLCANICS PROJECT
GEOLOGICAL REPORT 5

The origin of gold-tin-copper mineralisation at the Lakeside Deposit, western Tasmania

by J. TAHERI, B.Sc., M.Sc., Ph.D. and G. R. GREEN, B.Sc. (Hons), Ph.D.

DIVISION OF MINES & MINERAL RESOURCES, PO BOX 56, ROSNY PARK, TASMANIA 7018 ISBN 0 7246 2115 6

TAHERI, J.; GREEN, G. R. 1990. The origin of gold-tin-copper mineralisation at the Lakeside Deposit, western Tasmania. *Geol. Rep. Mt Read Volc. Proj. Tasm.* 5.

ISBN 0 7246 2115 6

CONTENTS

Introduction 5
Geology 5
Regional geology 5
Local geology 5
Mineralisation in and/or alongside the Henty Fault Zone 5
Lakeside Prospect 7
Location 7
Alteration/Mineralisaxtion 7
Alteration and mineralisation in Mt Black Volcanics 7
Mineralisation within Farrell Slates 9
Stage 1 9
Stage 2 9
Stage 3 11
Stage 4 11
Mineralogical Zonation 11
Fluid Inclusions 12
Introduction 12
Fluid inclusions in the Lakeside Prospect 12
Description and classification of inclusions 12
Fluid Inclusion Homogenisation Data 14
Fluid Inclusion Composition — Freezing Experiments 15
Discussion 15
Oxygen isotope data 17
Sulphur isotope data 17
Geochemistry of mineralised zones 19
Origin and physicochemical conditions of hydrothermal fluids 30
Thermal history 30
Transport, deposition and origin of gold 30
Tin transport and deposition 31
Lead isotope data 33
Granite Tor and its bearing on mineralisation 33
Implications for exploration 33
Conclusions 37
Acknowledgements 37
References 37

APPENDIX 1: Chemical composition of pyrite, Lakeside Prospect 51
APPENDIX 2: Chemical composition of arsenopyrite, Lakeside Prospect 52
APPENDIX 3: Chlorite (composition and geothermometry), Lakeside Prospect 54
APPENDIX 4: Chemical composition of gold, Lakeside Prospect 55
APPENDIX 5: Fluid inclusion data 56
APPENDIX 6: Thermochemical data used in construction of diagrams 58
APPENDIX 7: $^{206}Pb/^{204}Pb$ data 59

LIST OF FIGURES

1. Simplified geology of western Tasmania, showing Mt Read Volcanics between Hellyer mine and South Darwin Peak. 6
2. Simplified stratigraphic columns for the Cambrian of central western Tasmania. 7
3. Geology of the Lakeside Prospect area, showing the locations of main deposits along the Henty Fault. 8
4. Longitudinal projection showing the drill holes intersecting gold-tin mineralisation at the Lakeside Prospect. 10
5. Th histograms for fluid inclusion types. 14
6. Th vs freezing points for types B-1 and B-2 fluid inclusions. 16
7. P-X plot of isotherms for the system CO_2–H_2O showing the range of pressure and compositions for the fluid inclusions with critical points. 17
8. Frequency distribution of sulphur isotope compositions of sulphides from the Lakeside Prospect, Sterling Valley Tin area, Murchison Mine, New North Mt Farrell Mine, and Sterling Valley Mine. 18
9. Variation diagrams for As, Sn, Au, Pb, Zn, Ag, Cu from mineralised sections of drill core from the Lakeside Prospect. 22
10. Log fO_2—log fS_2 diagrams at 300° and 350°C for Fe-O-S and Sn-O-S systems. 31
11. $^{206}Pb/^{204}Pb$ vs lead concentration for the Lakeside Prospect, Sterling Valley and Murchison Mines together with representative data from Cambrian massive sulphide deposits and vein-type post-Cambrian mineralisation, western Tasmania. 32

12. Relationship between locations of Devonian veins and replacement deposits to subsurface granite ridge connecting the Heemskirk and Granite Tor Granites. 34
13. Spatial relationship between $\delta^{34}S$ values and mineral assemblages, and the intrusion of the Granite Tor Granite along the Henty Fault. 35
14. Metal zoning and suggested pre-faulting construction for the Lakeside Prospect and Sterling Valley Tin Prospect. 36

LIST OF PLATES

1. Early-formed As-poor pyrite partially replaced and overgrown by As-rich pyrite. 41
2. Late-forming As-rich pyrite along the fracture and on the surface of the As-poor pyrite. 41
3. Finely brecciated pyrite and arsenopyrite healed by quartz and carbonate infillings. 42
4. Partial replacement of pyrrhotite by pyrite and carbonates. 42
5. Quartz, fluorite, tourmaline, arsenopyrite and cassiterite assemblage. 43
6. Partial replacement of pyrite by arsenopyrite. 43
7. Occurrence of twinned cassiterite crystals in close association with chlorite. 44
8. Cassiterite, quartz, chlorite and arsenopyrite assemblage. 44
9. Occurrence of chalcopyrite along the fractures in arsenopyrite and as patches. 45
10. Occurrence of chalcopyrite and gold as fissure-filling within brecciated arsenopyrite. 45
11. Occurrence of gold and chalcopyrite along the micro-fractures in brecciated arsenopyrite. 46
12. Occurrence of gold in micro-fractures in pyrite or at the arsenopyrite–pyrite boundary. 46
13. Replacement of sphalerite by stannite. 47
14. Occurrence of late pyrite on margins of carbonate veinlets. 47
15. Occurrence of gold as inclusion in pyrite. 48
16. Galena enclosing and partially replacing stannite, arsenopyrite, pyrite and chalcopyrite. 48
17. Fluid inclusion types from the Lakeside Prospect. 49

LIST OF TABLES

1. Paragenesis of ore and gangue minerals. 9
2. Classification of fluid inclusion types and their distributions 13
3. Oxygen isotope analyses from quartz samples and their equilibrating fluids at indicated temperatures. 19
4. Sulphur isotope data. 20
5. Average and standard deviation of Au and Sn contents of mineralised rocks from drill core 21
6. Correlation coefficient between Cu, As, Ag, Au, Pb,Zn, Sn from mineralised core samples. 30

INTRODUCTION

Despite considerable debate about the origin of mineralisation for the Mt Farrell Mine (i.e. Devonian versus Cambrian), no detailed studies have been undertaken on the mineralisation along the Henty Fault Zone. Recent intense exploration along the Henty Fault Zone resulted in the discovery of the Henty Gold Prospect. This stimulated further exploration activities in which a metallogenetically rare Sn-Au association was discovered at the Lakeside Prospect.

The objects of this investigation are to determine:

(a) Relative importance of Devonian and Cambrian mineralising processes; and

(b) possible controls on Au distribution for the mineralisation along the Henty Fault.

GEOLOGY

Regional Geology

The geology of western Tasmania has been reviewed by Williams (1978), Solomon (1981), Corbett (1981), and Corbett and Lees (1987), from which a brief outline is presented here. Two Precambrian blocks, termed Tyennan Nucleus and Rocky Cape Region, form the eastern and western margins of a relatively narrow basin, the Dundas Trough (fig. 1), which is mainly filled with Cambrian sedimentary sequences. A belt of felsic to intermediate volcanic rocks, called the Mt Read Volcanics, occupies the eastern margin of the Dundas Trough (fig. 1). The Mt Read Volcanics have been divided into three lithological groups (figs 1 and 2).

(1) Central Volcanic Complex, mainly consisting of rhyolitic and andesitic lavas, pyroclastic rocks, shale, and siltstone, with minor granitic intrusions. The rocks in the northern portion of the Mt Read Volcanics (Que–Hellyer Volcanics) are more mafic and may represent younger volcanics (Corbett and Komyshan, 1989). The Central Volcanic Complex and the Que–Hellyer Volcanics host the main Pb-Zn-Cu-Ag and Au mineralisation in western Tasmania (e.g. Rosebery, Que River, Hellyer, Mt Lyell; fig. 1).

(2) The Tyndall Group, comprising felsic to intermediate tuffs and lavas with interbedded sandstone, shale and volcaniclastic conglomerates.

(3) A western volcano-sedimentary succession of tuffs, shale, quartz-feldspar porphyries and minor sandstone and volcaniclastic turbidites.

A major north–northeast-trending fault system (Henty Fault) divides the Mt Read Volcanics into two parts. The fault extends from north of Tullah to south of Mt Read (fig. 1). The Farrell Slates, consisting mainly of slate and tuffaceous sandstone, occur along the eastern side of the Henty Fault Zone, and host Pb, Zn, Ag, Au, Sn mineralisation in the Tullah area. The Cambrian and younger (to early Middle Devonian) rocks in western Tasmania have been affected by a widespread Devonian deformation correlated with the Tabberabberan Orogeny of south-east Australia. This was followed by the emplacement of high level granitoid plutons (e.g. Granite Tor Granite, Heemskirk Granite, Pine Hill Granite; fig. 1). Tin mineralisation and remobilisation of some Cambrian sulphides are related to this orogeny in western Tasmania.

Local Geology

The Henty Fault in the vicinity of the Lakeside Prospect (fig. 3) separates the Mt Black Volcanics (Central Volcanics) to the west from the Farrell Slates and Murchison Volcanics (Tyndall Group) to the east (McNeill, 1987; Corbett and McNeill, 1986). The fault strikes NNE and dips steeply west (65°). There are some small faults parallel to the main fault in the Farrell Slates to the east.

A complex movement history for the Henty Fault has been reported by Berry (1989). The fault appears to have been active from the early Palaeozoic to the Tertiary. The earliest movement is east-directed thrusting, predating the Devonian folding, and may correlate with the early Ordovician movement on the Great Lyell Fault. Brittle-ductile deformation is indicated for this phase of movement. Devonian movements include high-angle reverse faulting, post-dating Devonian folding, but synchronous with the Granite Tor intrusion and the mineralisation. Later Devonian sinistral wrench faults involved displacements of less than five kilometres. These are generally exposed as brittle deformation overprinting the earlier brittle-ductile fabric. There are also late phases of reactivation of the Henty Fault, including a sinistral wrench movement possibly in the Jurassic, and a normal fault of Tertiary age (Berry, 1989).

The rocks to the west of the Henty Fault are predominantly feldspar-phyric andesite and dacite. Chlorite alteration is common, and the rocks are intensely silicified close to the Henty Fault.

The Farrell Slates are either underlain conformably by the Murchison Volcanics (Polya *et al.*, 1986) or are in faulted contact with them (Berry, 1989). They are approximately 700 m thick and strike NNE (i.e. parallel to the Henty Fault) for some 26 km and dip steeply to the west, with a foliation approximately parallel to the bedding. The sequence mainly consists of grey to black slate, shale, greywacke and volcaniclastic arenite. The main constituents of the rocks are muscovite, quartz, chlorite, siderite, calcite, albite and volcanic rock fragments.

MINERALISATION IN AND/OR ALONGSIDE THE HENTY FAULT ZONE

Several small vein-type Pb-Ag to polymetallic Sn-Au bearing deposits occur within the Henty Fault zone, or are hosted by the Farrell Slates and the Mt Black Volcanics adjacent to the Henty Fault (fig. 3). The Farrell Slates are the main host for the mineralisation alongside the Henty Fault. The mineralisation within the Farrell Slates was first discovered in 1897 (Hall *et al.*, 1953) and has been described by Brooks (1962), Richardson (1951), Hall and Solomon (1962), Jensen (1959), and Hall *et al.* (1987, 1988).

The total recorded production from the Mt Farrell deposits, including the North Mt Farrell, New North Mt Farrell, Mt Farrell, Murchison and Mackintosh Mines, was 735 064 t of ore containing 96 092 t of lead and 319 695 kg of silver (Collins *et al.*, 1981). More than 99% of this total was mined from the North Mt Farrell and New North Mt Farrell mines.

Drilling by the Electrolytic Zinc Company (e.g. McDonald, 1985) in the Sterling Valley Tin area (fig. 3) showed that vein-type polymetallic mineralisation (As, Cu, Sn, Au, Ag, Pb, Zn) also occurs within the Mt Black Volcanics west of the Henty Fault.

The mineralisation associated with the Henty Fault occurs mainly as veins or fissure lodes in shears.

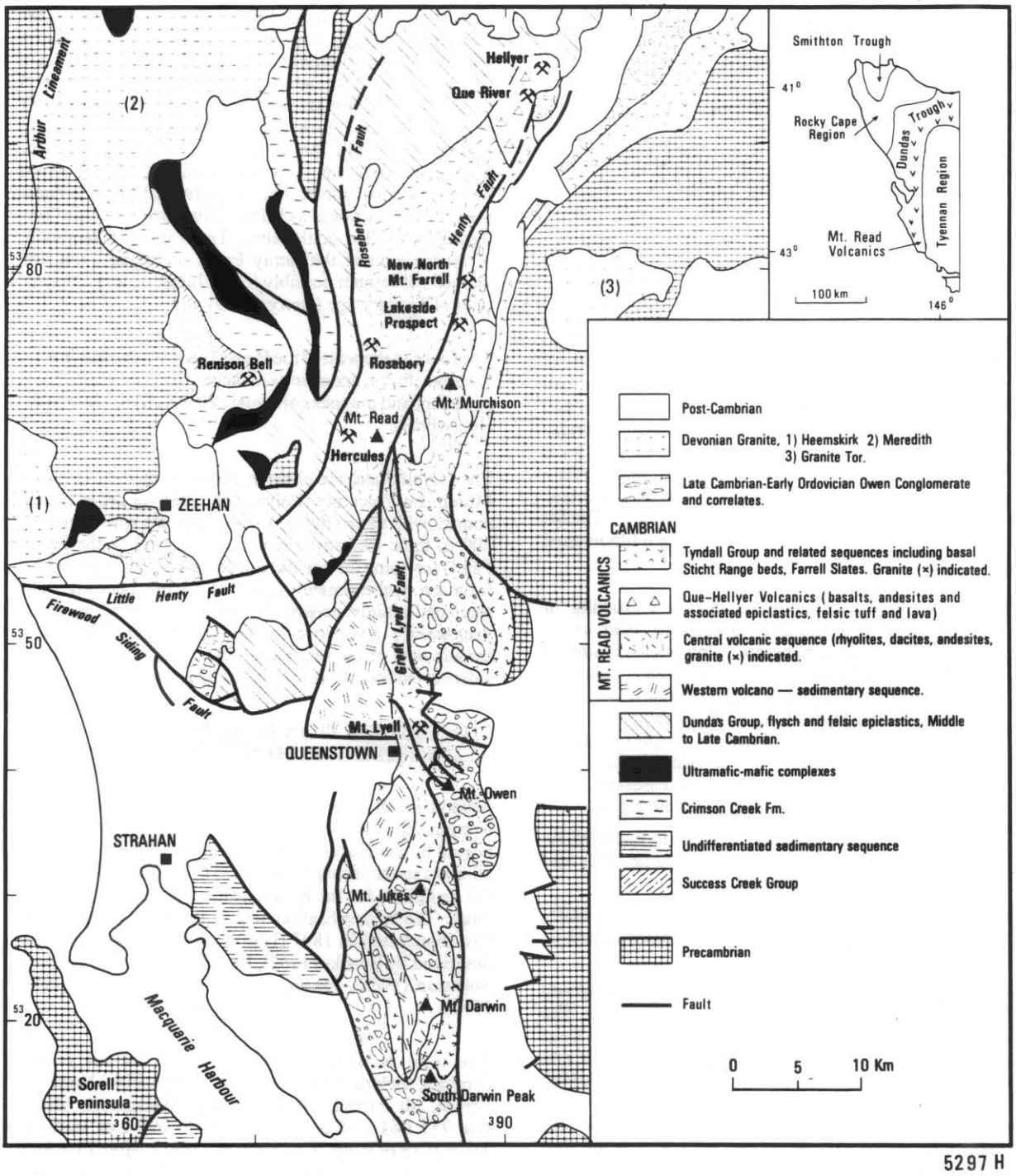

Figure 1. *Simplified geology of western Tasmania showing the Mt Read Volcanics between Hellyer and South Darwin Peak. Inset shows the major palaeogeographic elements in western Tasmania (after Corbett and McNeill, 1987; Corbett and Komyshan, 1989).)*

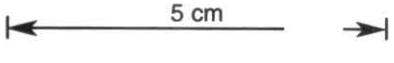

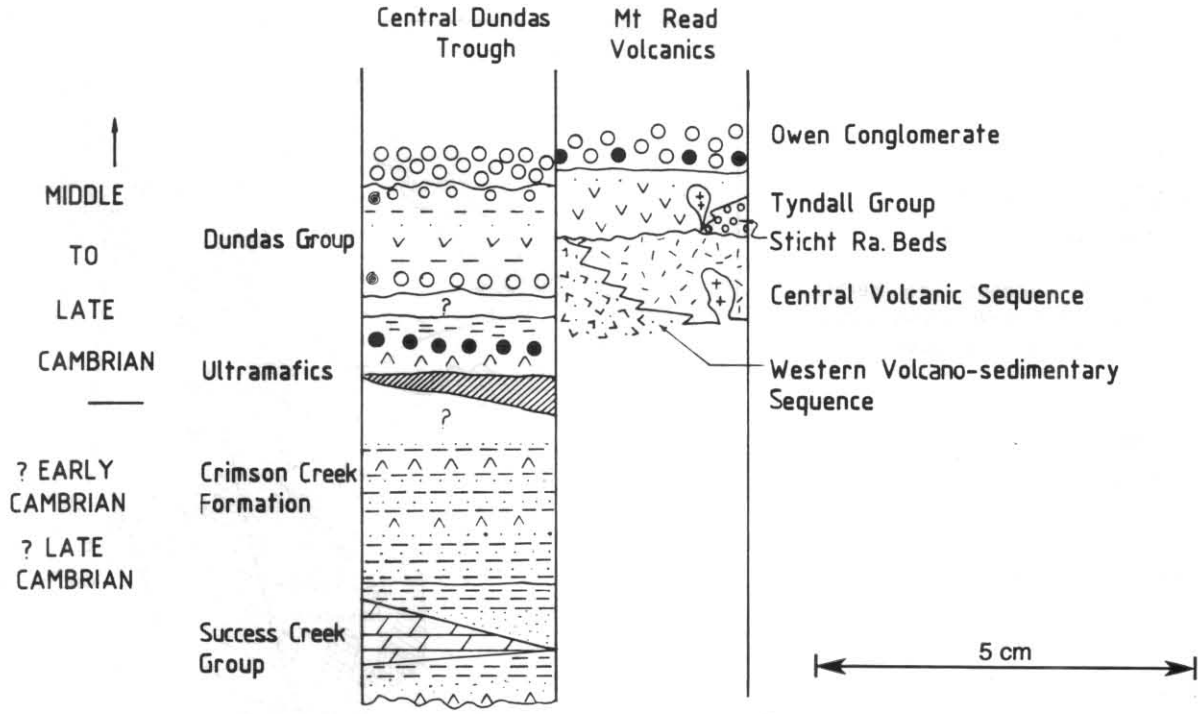

Figure 2. *Simplified stratigraphic columns for the Cambrian of central western Tasmania.*

Based on mineral contents, proportions of different minerals and/or ore genesis, the mineralisation may be divided into three broad categories:

(1) Pb-Ag dominated deposits within the Farrell Slates in the Tullah area (e.g. New North Mt Farrell Mine; fig. 3). The deposits mainly consist of several sub-parallel lenticular fissure lodes/veins in shears striking from NNW to NNE. General mineral assemblages include galena ± sphalerite ± chalcopyrite ± tetraheddrite ± siderite. A similar type of mineralisation occurs in the Sterling Valley Mine, however arsenopyrite is a common mineral and minor gold also occurs in this deposit.

(2) Polymetallic Sn-Au bearing mineralisation hosted by the Farrell Slates and/or Mt Black Volcanics (e.g. Lakeside Prospect). Mineralisation is mainly of vein and/or fissure-filling type, and the common minerals include pyrite, arsenopyrite, stannite, chalcopyrite, pyrrhotite, cassiterite, tourmaline, carbonates and fluorite. Massive arsenopyrite is the dominant phase in some places in the Sterling Valley Tin area (fig. 3).

(3) Massive to disseminated pyrite, sphalerite, galena and gold-bearing veinlets of pyrite and chalcopyrite in felsic to intermediate lavas and tuffs (e.g. Henty Gold Prospect).

No detailed geological information is available for this deposit. As part of the Mt Read Volcanics Project, detailed geological, petrochemical, stable isotopes and fluid inclusion studies are being undertaken to investigate the possible origin(s) of the mineralisation and its relationship to other mineral deposits occurring alongside the Henty Fault Zone.

LAKESIDE PROSPECT

Location

The Lakeside Prospect is located 3 km south Tullah, over a length of 1 km from 375 000 mN to 376 000 mN along the Henty Fault (fig. 3).

Alteration/Mineralisation

The area is covered by glacial gravel, and geological information is based on drill core. A total of 13 holes have been drilled within the area by Billiton Australia and the EZ Company (Hall *et al.*, 1987, 1988; Mill *et al.*, 1980; Sainty, 1982; fig. 8). All of these holes were collared on the western side of the Henty Fault in the Mt Black Volcanics, and intersected the Henty Fault zone and the Farrell Slates.

The main mineralisation occurs within the Farrell Slates east of the Henty Fault. However the rocks to the west of the fault (Mt Black Volcanics) are pervasively altered and weakly mineralised in places.

(a) Alteration and mineralisation in the Mt Black Volcanics. The main rock types are feldspar-phyric andesitic tuffs and lavas. The rocks are intensely altered and finely brecciated. Basaltic dykes and flows are also common, and are intensely chloritised. Chlorite, sericite, albite and quartz have totally replaced the original rock-forming minerals, however the primary textures of the rocks have been preserved. Minor minerals include rutile, leucoxene and sphene, which appear to be the alteration products of pre-existing titaniferous oxides. Vesicles are rare and are commonly filled by quartz and/or chlorite.

The Mt Black Volcanics, close to the Henty Fault zone, have been strongly silicified, and in places the silicification extends over 100 m (e.g. DDH RED88-4, fig. 4) from the fault.

Andesitic rocks are cut by veins of albite, chlorite± quartz, sericite ± quartz, quartz ± cassiterite ± sulphides (pyrite ± arsenopyrite ± galena ± sphalerite) and late carbonates.

Brecciation is followed by fissure filling, and the rocks appear to have been mildly deformed after veining. However some late carbonate veins represent a post-deformation stage.

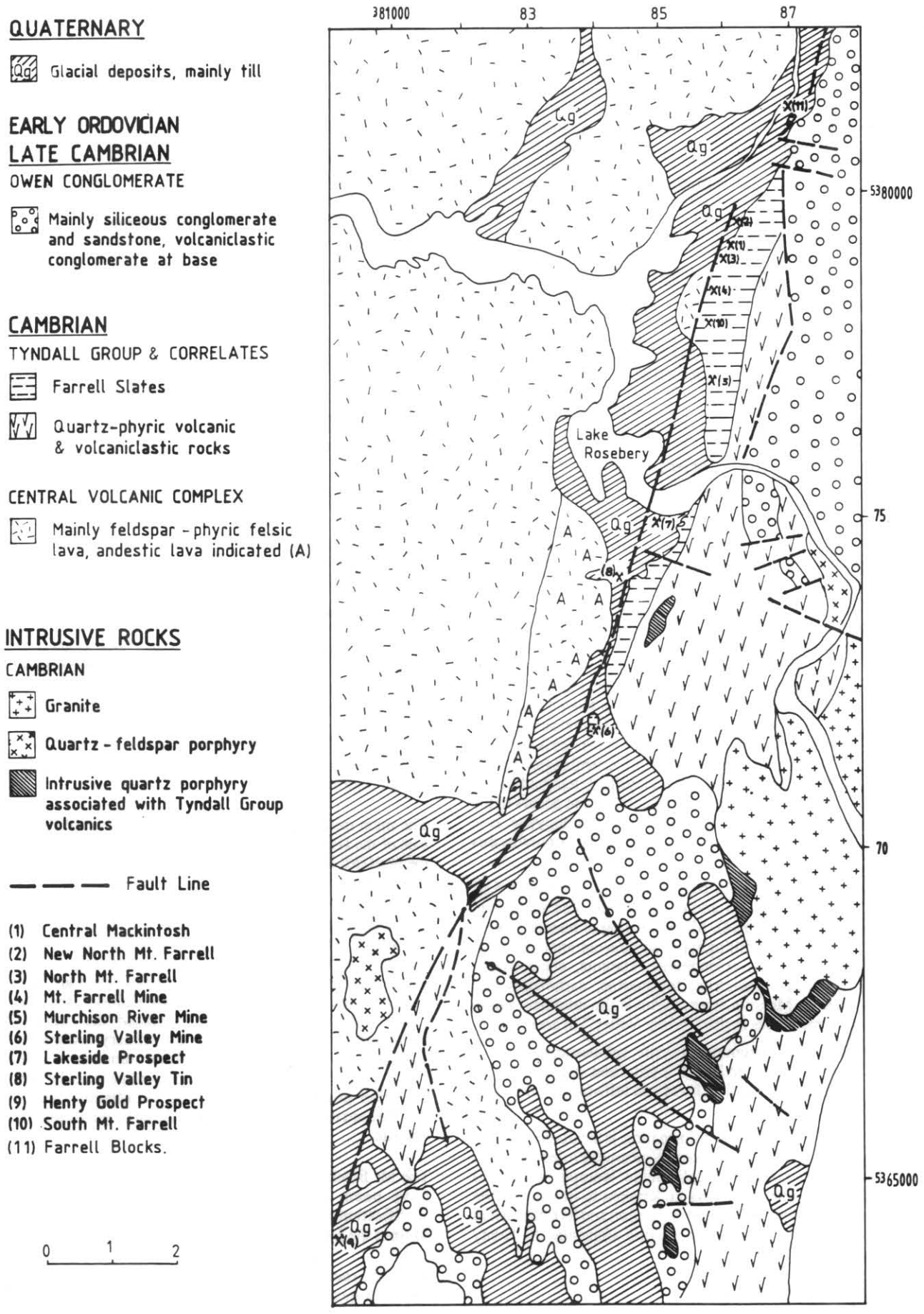

Figure 3. *Geology of the Lakeside Prospect area, showing the locations of main deposits along the Henty Fault (compiled from Corbett and McNeill, 1986; McNeill, 1987; Green and Bamford, 1986).*

5 cm

(b) Mineralisation within the Farrell Slates. Mineralisation occurs as disseminations, fissure veins and stringers within and/or immediately below the Henty Fault in the Farrell Slates. The mineralised zones intersected by the drill holes vary from few metres to more than 70 m thick.

The host rocks mainly consist of sandstone, slate, shale and quartzose arenite. They are commonly foliated, deformed and are brecciated. Several barren veins of different mineralogy, including chlorite ± quartz, carbonate, quartz ± tourmaline cut the Farrell Slates. It is not possible to establish timing for different vein types, as a vein of particular mineralogy may appear at different stages of mineralisation. However based on cross-cutting relationships, some chlorite and carbonate veins appear to have been formed in the late stage of mineralisation.

Mineralisation at the Lakeside Prospect may be divided into four different stages (Table 1). These stages are recognised by cross-cutting relationships and replacement textures. It is difficult to recognise replacement textures and/or sequences of events, as the mineralisation has been affected by brecciation at different stages, deformation, repetition in veining, and overprinting of early-formed minerals by later phases.

Table 1. *Paragenesis of ore and gangue minerals, Lakeside Prospect.*

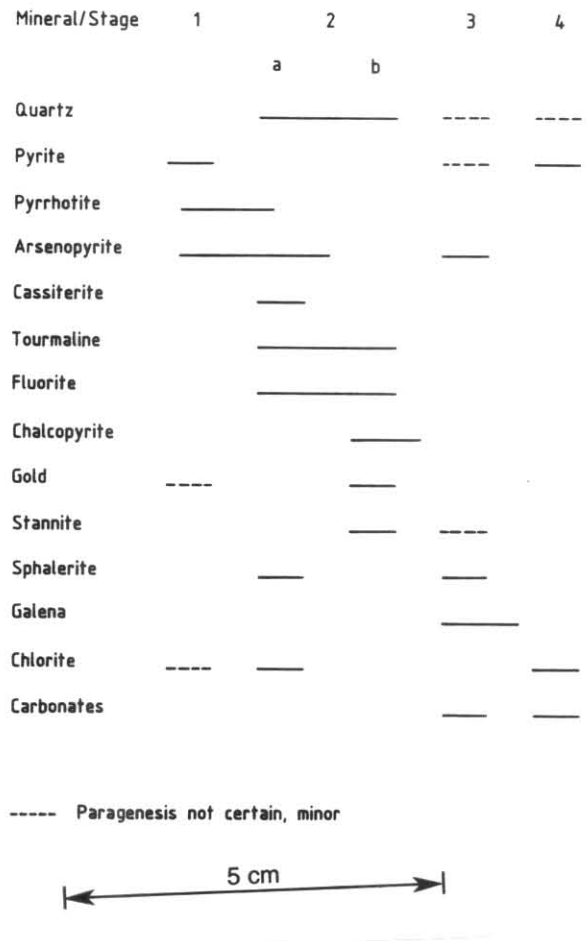

STAGE 1: PYRITE ± PYRRHOTITE ± ARSENOPYRITE

Massive to coarse-grained pyrite is the dominant mineral at this stage. It is mildly anisotropic, pale yellow to white in colour, and intensely brecciated (Plate 3). The staining method of Fleet *et al.* (1988) was used to examine whether the anisotropic character of pyrite is related to zones of high arsenic content and/or the occurrence of small crystals of arsenopyrite within pyrite. It revealed areas of two distinctly different colours (Plates 1 and 2), and micro-probe analyses showed that the different colours are directly related to differences in the As content of pyrite.

As-rich pyrite is mainly formed on margins and/or in fractures within As-poor pyrite (Plate 2). However the pyrite with low As content may itself form on the surface of As-rich pyrite (Plate 2). This may indicate fluctuations in As contents of the ore-forming solution at this stage of mineralisation. The high contents of As in pyrite (up to 5.7 wt%, Appendix 1) are probably related to the occurrence of submicroscopic crystals of arsenopyrite rather than substitution of As for S in the pyrite structure, as the solubility of As in pyrite appears to be less than 0.6 wt% and is temperature independent (Clark, 1960). Pyrite also occurs at late stages of mineralisation, post-dating pyrrhotite and stannite formation (Plates 4 and 14). The association of gold and As is well documented in the literature (e.g. Boyle, 1979). However gold in the Lakeside Prospect appears to have been deposited at later stages of mineralisation, possibly under different physicochemical conditions.

Pyrrhotite occurs in semi-massive and mildly brecciated forms. It has been partially replaced by pyrite and/or veined by carbonates and chlorite (Plate 4). Pyrrhotite is not a common sulphide mineral in the Lakeside Prospect, and only occurs in deeper drill hole intersections including RED87-2, RED88-4, and RED88-1, at depths of 208 m, 272 m and 279 m respectively (fig. 4). The mineralisation at these depths is generally dominated by pyrite, pyrrhotite, arsenopyrite and cassiterite, with minor to rare occurrences of galena, sphalerite, chalcopyrite, gold and stannite. This is different from the mineralisation occurring at shallow depths (e.g. RED87-3, RED87-5), in which pyrrhotite is absent and galena, sphalerite, chalcopyrite, stannite and gold are more common (fig. 4).

STAGE 2: TIN AND GOLD MINERALISATION ASSOCIATED WITH QUARTZ ± TOURMALINE ± FLUORITE

Quartz, tourmaline and fluorite are the common gangue minerals for this stage of mineralisation (Plate 5). The mineralisation at this stage may be subdivided into two substages:

2a: Arsenopyrite ± cassiterite ± chlorite. Mild to intensely brecciated arsenopyrite occurs as aggregates of fine-grained euhedral crystals (≅ 20 μm) developing a semi-massive habit replacing pyrite (Plate 6). Arsenopyrite is the most common sulphide at the Lakeside Prospect and appears to have been formed over several stages; however it is most abundant at this substage. Chemically, arsenopyrite from the Lakeside Prospect has low but consistent As contents (X=29.5 ± 0.7 atom%, Appendix 2), and the concentrations of minor elements such as Zn, Ni, Sb and Co are generally less than 0.2 wt%. Low As concentration of arsenopyrite may be indicative of low temperature of formation (i.e.<350°C) However lack of sufficient experimental work at low temperature (<400°C) makes the application of arsenopyrite geothermometry (Kretschmar and Scott, 1976) for the Lakeside Prospect unreliable. Cassiterite is closely associated with arsenopyrite and occurs as fine-grained disseminated crystals (up to 10 μm) or as coarse, euhedral, mostly twinned crystals up to 0.7 mm in close association with pale green-blue chlorite (Plates 5, 7 and 8).

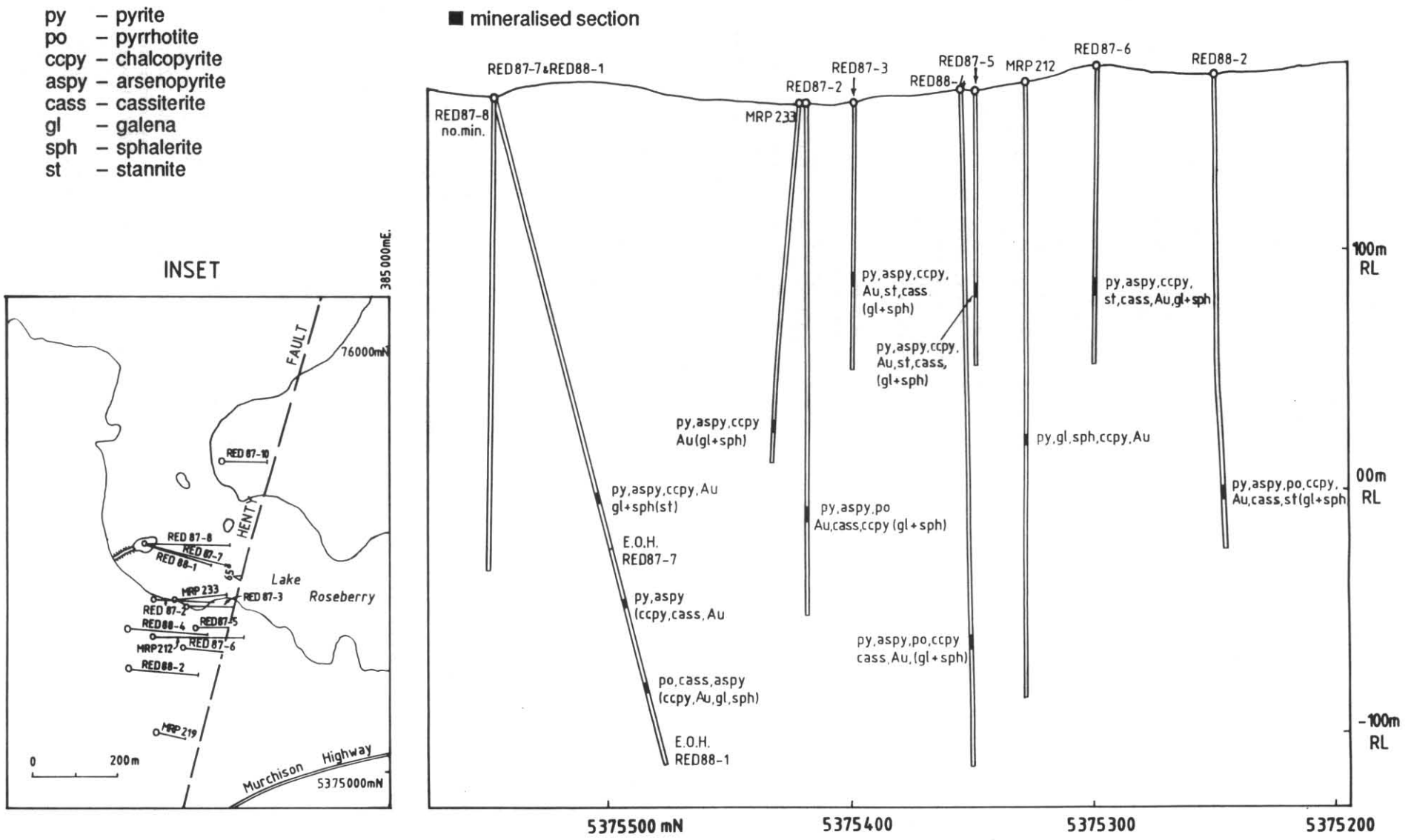

Figure 4. *Longitudinal projection showing the drill holes intersecting gold–tin mineralisation at the Lakeside Prospect. Note the occurrence of pyrrhotite (po) in deeper holes. For the contents and relationships between the base metal, tin and gold see Figure 9. Inset shows the location of the drill holes in the Lakeside Prospect area.*

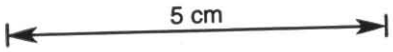

Chemically the chlorite associated with cassiterite is uncommonly enriched in iron (up to to 38 wt% FeO) and low in silica content (Appendix 3). The presence of quartz in this substage satisfies the conditions for the application of the six component chlorite geothermometer of Walshe (1986), although the method should be employed with caution in the case of iron-rich chlorites such as those at the Lakeside Prospect (Walshe, 1986; Walshe *et al.*, 1986). No solutions were obtained at pressures of the water–steam boundary, but seven chlorites provided temperature estimates of 305 to 326°C at a pressure of 1 kbar (Appendix 3), in good agreement with the empirical geothermometer of Cathelineau and Nieva (1985) and the fluid inclusion homogenisation temperatures.

Pyrrhotite also occurs in close association with cassiterite in deep drill holes, and texturally it appears to have been continuously formed after the deposition of early-formed pyrite.

2b: Chalcopyrite ± stannite ± gold. The assemblage post dates the deposition of the arsenopyrite ± cassiterite ± chlorite assemblage (substage 2a). Chalcopyrite appears as:

(a) semi-massive patches,
(b) fissure veins,
(c) inclusions and/or veinlets in stannite, and
(d) infilling brecciated pyrite and/or arsenopyrite (Plates 9 and 10).

This may suggest that chalcopyrite was formed over long periods in the late stages of mineralisation.

Texturally, there are two different styles of stannite: firstly irregular patches which may contain lamellar chalcopyrite bodies, inclusions and/or fracture fillings in arsenopyrite; and secondly disseminated fine-grained cassiterite pseudomorphs. The stannite at the Lakeside Prospect appears to be of low temperature type (i.e. β-stannite) because there is no microcline-like twinning characteristic of inversion from α to β-stannite (Ramdohr, 1969).

Electrum occurs as fine grains (≅ 5 μm) in close association with chalcopyrite, either as small inclusions within chalcopyrite or as micro-fracture fillings in pyrite and/or arsenopyrite (Plates 9, 10, 11, and 12). A few small gold inclusions (<3 μm) of unknown paragenesis were also observed in pyrite (Plate 15). Based on microprobe analyses, gold at the Lakeside Prospect is compositionally homogeneous with an atomic Au/Ag ratio of around 1.05 (i.e. ≅ 34 wt% Ag, ≅ 66 wt% Au; Appendix 4). Gold deposition appears to post-date most of the sulphides, and is closely related to a later stage of mineralisation. The possible origin and physicochemical conditions of tin and gold deposition are discussed in a later section.

STAGE 3: GALENA ± SPHALERITE.

Galena and sphalerite are the minor sulphides in the Lakeside Prospect. They generally occur as fissure fillings or as replacements of earlier-formed minerals (Plates 9, 10 and 16). The relationship between galena and sphalerite is not clear, as they do not co-exist in all samples. However galena is relatively more common and its formation appears to continue after deposition of sphalerite. This is based on textural evidence, as only galena commonly replaces all earlier-formed minerals (Plate 16). Sphalerite also occurs as coarse euhedral crystals partially replaced and/or veined by stannite (plate 13). This relationship indicates that either sphalerite or stannite has been formed in two different stages. Sphalerite may contain minor blebs of pyrite, chalcopyrite and/or stannite.

STAGE 4: CHLORITE ± CARBONATES ± PYRITE.

This stage represents the last stage of hydrothermal alteration replacing and/or cross-cutting earlier formed minerals. It is characterised by fine-grained light green chlorite, abundant carbonates (calcite, dolomite, siderite), and veinlets of pyrite. However chlorite and carbonates appear to be of several generations, and they are not restricted to this stage of hydrothermal alteration.

Mineralogical Zonation

In general, the mineral contents and/or proportions of different ore minerals change with increasing depth. Pyrite, galena, sphalerite, stannite and chalcopyrite contents decrease with increase in depth, whereas cassiterite content seems to increase with the depth of the mineralisation.

Occurrences of pyrrhotite and Fe-rich chlorite are restricted to drill holes intersecting the mineralisation at greater depth where the mineralised sections are closer to the Granite Tor ridge surface. The occurrence and/or abundance of arsenopyrite, quartz and tourmaline appear to be independent of the depth of the mineralisation. Stannite is rarely found in deeper mineralised sections.

Despite the low average gold content (<5 g/t) and erratic distribution of gold in the Lakeside Prospect, there seems to be a general decrease in gold content with increase in depth of mineralisation.

The mineralisation in the Lakeside Prospect is similar to the mineralisation in the Sterling Valley Tin area, in that pyrite appears as an early-formed mineral and is followed by deposition of arsenopyrite, pyrrhotite, chalcopyrite, tourmaline, cassiterite, and late-formed galena and sphalerite. However in the Sterling Valley Tin area, sulphides are less brecciated, and pyrrhotite and stannite are more common. Arsenopyrite also contains more As than at the Lakeside Prospect (X=30.6 ± 0.60 atom%, Appendix 2). The abundance of pyrrhotite and stannite, and the higher As contents of arsenopyrite, may indicate a higher temperature of formation for the mineralisation in the Sterling Valley Tin area than that in the Lakeside Prospect. The significance of the occurrence of higher temperature mineral assemblages in the Sterling Valley Tin area compared to those of the Lakeside Prospect will be discussed in a later section.

FLUID INCLUSIONS

Introduction

During processes of crystal growth or fracture healing small portions of the fluid medium are commonly trapped as fluid inclusions. If the fluid contains solid phases they may also be trapped to form the solid inclusions. However these solid inclusions are different from "daughter minerals", as the latter crystallise out of fluid upon cooling after trapping. Fluid(s) and/or solid(s) may be trapped either during the growth of the crystal by any process which interferes with a perfect growth, yielding primary fluid inclusions, or at some later time by recrystallisation along fractures from different fluids to form secondary fluid inclusions. Pseudosecondary fluid inclusions are those formed along the fractures during the growth of a crystal.

Fluid inclusions which have been formed in a heterogeneous system of two or even more immiscible phases (e.g. droplets of oil in an aqueous liquid) may contain one to all of the fluids with different ratios. A similar phenomenon may result from phase separation, for example, from a boiling solution in which the fluid inclusions may contain only gas, or vapour bubbles of different sizes in different fluid inclusions.

Fluid inclusions are rarely larger than one millimetre. However museum specimens with fluid inclusions containing hundreds of millilitres of fluid are known (e.g. Hidden, 1882; Prikazchikov, 1959; Rankin and Greenaway, 1978).

The composition of fluid inclusions varies widely. In general the major solvents are H_2O and less commonly CO_2, and the major solute ions include Na, K, Mg, Ca, Cl, SO_4, and HCO_3, with lesser amounts of Li, B, Fe, Mn, F, P. Major constituents in inclusions with organic liquid or gas include H_2, CH_4 and C_2H_6, as well as a variety of high molecular weight compounds.

Fluid inclusions normally have a vapour or gas bubble which may move constantly under the effects of a thermal gradient or of gravity. The volume coefficients of thermal expansion for minerals are less than water by up to 3 times. Therefore upon cooling, a fluid inclusion which has been formed from an homogeneous fluid at elevated temperatures will shrink more than the host mineral, and when the total vapour pressure of the fluid is more than the pressure in the inclusion a bubble will nucleate and grow. The process can be reversed simply by heating the fluid inclusion to the temperature at which the bubble disappears (i.e. homogenisation temperature). This was first suggested by Sorby (1858).

The salinity of fluid inclusions (wt% NaCl equivalent) can be estimated by freezing the fluid inclusions and measuring the depression of the freezing points of the inclusions. This is just an estimate, as other solute ions such as Mg, Ca etc. may also be present in the fluid. There are many methods (non-destructive and destructive) to determine the compositions of the fluid inclusions, and these have been explained in detail by many workers (e.g. Roedder, 1984).

In general fluid inclusions can be utilised in the studies of ore deposits either in problems of mineral exploration or in studies of the physicochemical conditions of ore-forming fluids. They can also be used in igneous and metamorphic terrains, in oil exploration, in active geothermal systems, and in many other fields.

For further general information about fluid inclusions, the reader is referred to Roedder (1984) and Hollister and Crawford (1981).

Fluid inclusions in the Lakeside Prospect

Preliminary fluid inclusion studies were undertaken on quartz and carbonates from quartz-sulphide, quartz and quartz-carbonate veins, and quartz in vugs within the Mt Black Volcanics and the Farrell Slates. More than 40 doubly-polished fluid inclusion sections were prepared from different mineralised zones and veins; however only five were found to contain useful fluid inclusions. Several factors made this study extremely difficult. These included:

(a) intense brecciation of rocks and recrystallisation of quartz crystals.

(b) small fluid inclusions (<4 μm), and

(c) abundance of two-phase low vapour to liquid ratio, low temperature inclusions which have apparently overprinted the high temperature, presumably primary or pseudosecondary fluid inclusions.

The major problems with the fluid inclusions observed were the lack of sufficient high temperature (primary ?) fluid inclusions and their small sizes.

The absolute distinction between primary and secondary fluid inclusions was not always possible, except for some low temperature inclusions which occur along obvious microfractures. Only very few and small primary fluid inclusions have survived the effects of brecciation and physical changes (e.g. necking down, leakage or overprinting by later low-temperature fluid inclusions).

The experimental measurements are shown in Appendix 5. The following terms and observations are used through this section:

L – Liquid
V – Vapour
I – Ice
C – Critical Point (the limit for two fluid phase behaviour; pressure, composition dependent)
Th– Homogenisation temperature of fluid phases: Th_L=L+V ⇒L (i.e. fluid inclusion homogenises to liquid phase); Th_V=L+V⇒V (i.e. fluid inclusion homogenises to vapour
Te– Eutectic temperature
Immiscibility–Immiscibility is defined as a system containing several homogeneous phases in equilibrium with each other, synonymous with a stable mechanical mixture (Pichavant *et al.*, 1982).

Description and Classification of Inclusions

Fluid inclusions in quartz have a variety of shapes (rounded, oval, negative crystal or irregular) and they range in size from <4 to >20 μm. Fluid inclusions in carbonates are generally larger than 6 μm, and mostly show negative crystal shapes. The fluid inclusion may be classified as follows (Plate 17*a* to 17*e*):

Type A: Carbon dioxide-bearing fluid inclusions consisting of L_{CO_2}+V_{CO_2} (A-1), L_{H_2O}+L_{CO_2}+ V_{CO_2} (A-2), and L_{H_2O}+$V_{(H_2O+CO_2)}$ (A-3).

Type B: Two-phase ($L_{H_2O}+V_{H_2O}$) fluid inclusions which can be divided into two subtypes on their vapour–liquid ratios, viz:

Type B-1: Inclusions with high vapour–liquid ratios (50–70% by volume).

Type B-2: Inclusions with low vapour–liquid ratios (10–20%) by volume.

Type C: Two-phase fluid inclusions ($L_{H_2O}+V_{H_2O}$) containing one solid phase.

Different types of fluid inclusions and their distribution in different samples are shown in Table 2.

TYPE A:

Type A inclusions are common in quartz from quartz-sulphide veins. They are generally small in size (<5 μm). Type A-1 ($L_{CO_2}+V_{CO_2}$) may contain a single liquid phase at room temperature and vapour CO_2 nucleates upon cooling of the fluid inclusions (i.e. higher density and internal pressure); they are less common than type A-2 ($L_{H_2O}+L_{CO_2}+V_{CO_2}$)and type A-3 ($L_{H_2O}+V_{(H_2O+CO_2)}$). Type A-2 fluid inclusions consist of aqueous solution and a CO_2 vapour bubble ringed by liquid CO_2 (Plate 21*a*). The CO_2–H_2O ratios vary from 20 to 70%. The CO_2 vapour bubble in some inclusions appears only on cooling, and at room temperature may contain only liquid H_2O and liquid CO_2. Type A-3 inclusions consist of aqueous solution CO_2 and vapour (Plate 17*b*) with a very dark meniscus around the vapour bubble.The occurrence of CO_2 can only be positively identified by freezing experiments (i.e. melting of solid CO_2 phase). Type A-1, A-2 and A-3 inclusions may all be observed in the same field of view under the microscope.

TYPE B:

Two-phase ($L_{H2O}+V_{H2O}$) fluid inclusions with high vapour–liquid ratios (Type B-1) are not common, and were observed only in a barren quartz vein (Plate 17*c*). They are similar to type A-3 inclusions, and can be distinguished on cooling as they either become completely frozen above -56.6°C (i.e. melting temperature of solid CO_2) or no phase change is observed at this temperature or above 0°C (i.e. melting point of clathrate). Type B-2 are the most common inclusions and may be observed in all samples (Plate 17*d*). Secondary fluid inclusions occurring along the fractures and in recrystallised quartz are very small in size (<2 μm), and contain very low vapour–liquid ratios (<5%). However Type B-2 inclusions in quartz and calcite from late quartz-carbonate veins, and in quartz in vug, appear to be of primary origin, considering the criteria used by Roedder (1984) for primary fluid inclusions (Plate 17*d*).

TYPE C:

This type of fluid inclusion (L_{H2O} + V_{H2O} + solid phase) is not common and was observed only in a barren quartz

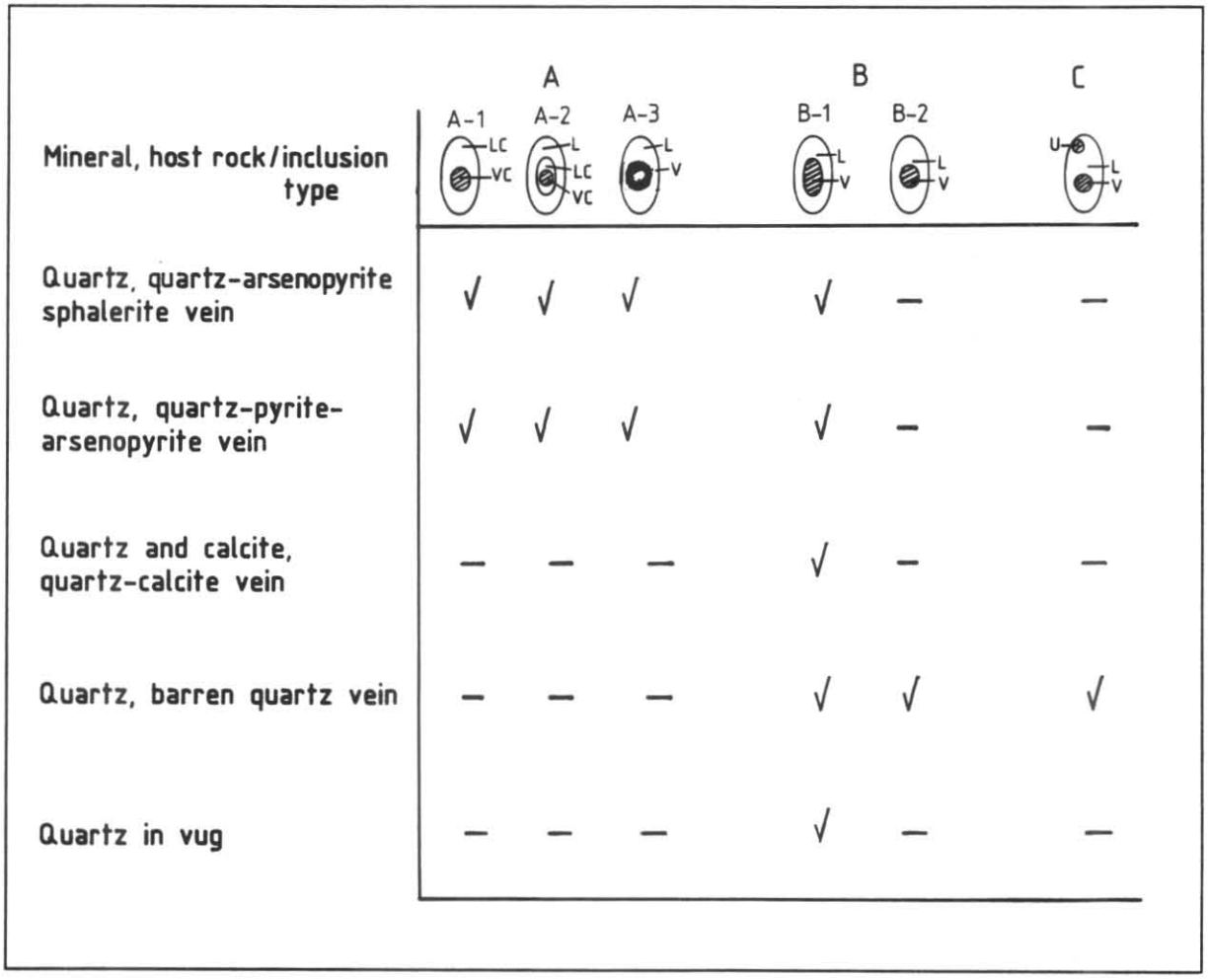

Table 2. *Classification of fluid inclusion types and their distributions, Lakeside Prospect.*

√	observed	–	not observed	L	liquid H_2O	V	vapour
LC	liquid CO2	VC	vapour CO_2	U	unknown solid inclusion		

vein (Plate 17*e*). The solid phase, as yet unidentified, is small in size, highly birefringent, and anisotropic with moderate relief. These inclusions show consistent solid–aqueous solution–vapour ratios.

Fluid Inclusion Homogenisation Data

Fluid inclusion homogenisation temperatures obtained for each type are shown as histograms in Figures 5*a* to 5*d*. Every attempt was made to obtain both freezing and heating data for each fluid inclusion. However because of the small size of fluid inclusions and decrepitation of some CO_2-bearing fluid inclusions before the homogenisation temperature, freezing and/or heating experiments were not always successful.

TYPE A:

The homogenisation temperatures of A-1 fluid inclusions ($L_{CO_2}+V_{CO_2}$) range from 13.7 to 28.9°C. These inclusions are not common but occur in close association with other types of CO_2-bearing fluid inclusions. Type A-1 fluid inclusions mainly homogenised to liquid, however a few homogenised to the vapour phase (Appendix 5).

Because of the low content of CO_2 in type A-3 fluid inclusions, the homogenisation temperatures for the CO_2 phase could not be measured.

The final homogenisation temperatures (to liquid or vapour) for A-2 and A-3 fluid inclusions range from 305 to 401°C. However more than 70% of the population fell in the range of 330–340°C (fig. 5*d*). Many Type A-2 fluid inclusions decrepitated before final homogenisation temperatures. This is a common phenomenon in CO_2-bearing fluid inclusions because of the high internal pressures generated by heating. The probability is very high for fluid inclusions homogenising to liquid if the fluid inclusion compositions fall on the two-phase region on the high pressure side of the critical point. Few inclusions did

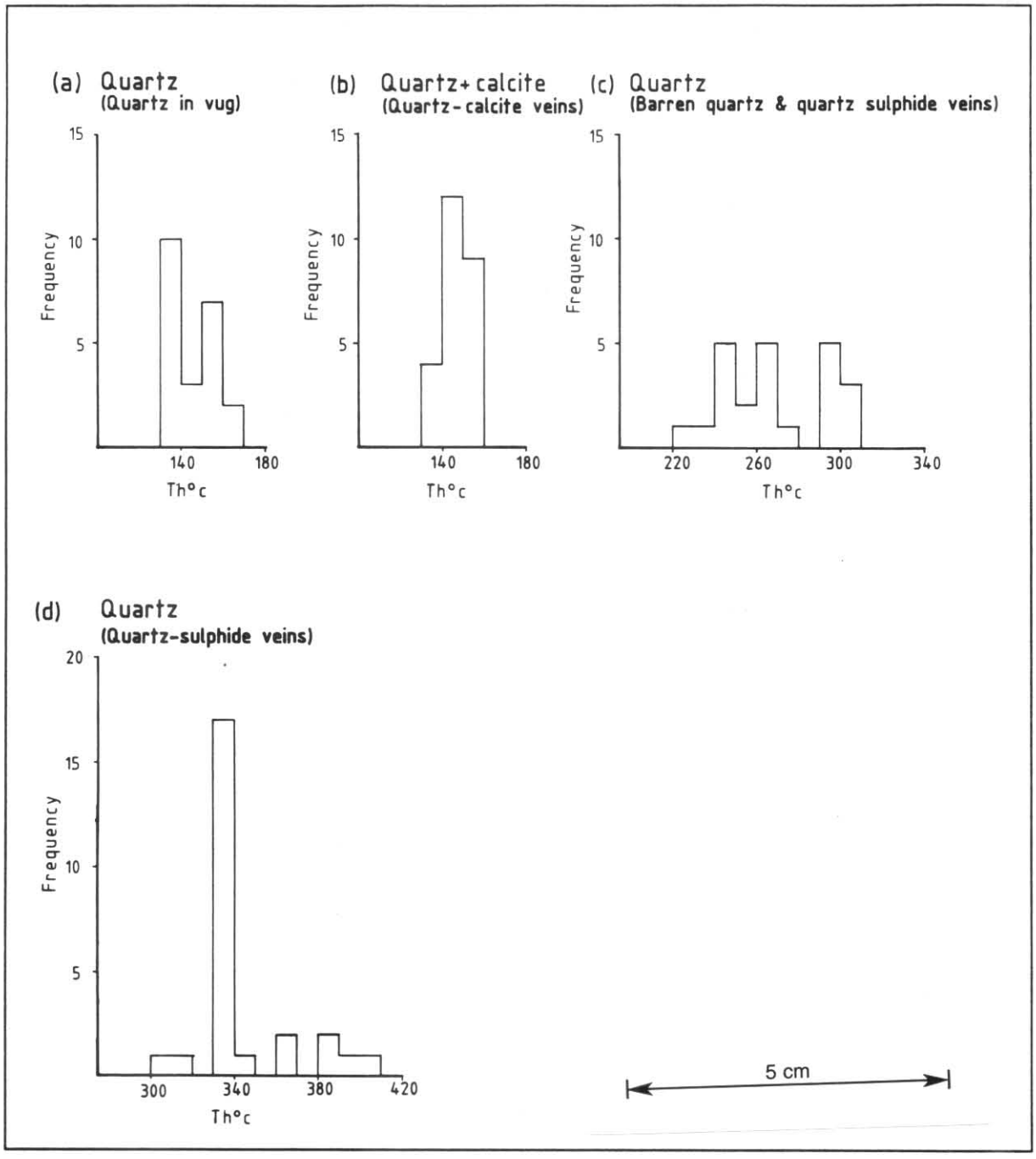

Figure 5. *Th histograms for types B-2 (a, b), B-1 (c), and A-2, A-3 (d) fluid inclusions, Lakeside Prospect.*

not exhibit any change upon heating. A few inclusions showed critical behaviour. This involves homogenisation by gradual disappearance of the liquid–vapour phase boundary, rather than homogenisation by disappearance of the bubble by shrinkage. Three inclusions showed critical points between 331 and 337°C.

The significance of the wide range of the homogenisation temperatures, their homogenisation to liquid and vapour, and critical behaviour in some inclusions are discussed later in this section.

TYPE B:

Two-phase inclusions with high vapour–liquid ratios (Type B-1) homogenised to liquid in the range of 218 to 309°C (fig. 5*c*). Only "primary-looking" type B-2 fluid inclusions in quartz and calcite from veins and vugs were selected for homogenisation temperature measurements, and these ranged from 136 to 167°C (fig. 5*a* and *b*).

TYPE C:

Due to the rarity of Type C fluid inclusions (LH_2O+VH_2O +solid phase) only five homogenisation temperatures were measured; these ranged from 167 to 178°C, with homogenisation to liquid. The solid phase neither dissolved nor decreased in size upon heating (up to 400°C).

Fluid Inclusion Composition—Freezing Experiments

Salinity measurements using the ice melting method are inaccurate in CO_2-bearing inclusions (Type A-2 and A-3) due to clathrate formation (Poty *et al.*, 1978; Hollister and Burruss, 1976; Collins, 1979). However, the CO_2 hydrate melting temperatures may be utilised for salinity measurements provided no other gas species (e.g. CH_4) are present (Hollister and Burruss, 1976). This assumption appears to be valid for types A-2 and A-3 fluid inclusions, as $TmCO_2$ values are indicative of relatively pure CO_2 (-55.8–56.4°C). Measurement of clathrate melting temperatures was difficult because of the small size of fluid inclusions, the similarity of CO_2 hydrate refractive indices to those of aqueous solutions, and the isotropic character of CO_2 hydrate. Therefore the precision of measurements could vary as much as ± 2°C. A few measured melting temperatures for CO_2 hydrate ranged from +8.5 to +10°C (i.e. 0 to 2 wt% NaCl; Collins, 1979; Appendix 5).

Freezing experiments were not successful on most of the Type B-1 fluid inclusions because of their small sizes and large vapour–liquid ratios in which very small volume expansion resulted upon freezing, and in most cases was not detectable. The measurements for Type B-1 ranged from -28 to -32°C, which are lower than both H_2O–NaCl and H_2O-KCl-NaCl eutectics (-20.80°C and -22.9°C respectively; Crawford, 1981), and indicates the presence of other solute species such as $CaCl_2$ and $MgCl_2$ (Crawford, 1981). Therefore Tm ice for these inclusions may not represent the actual salinity of the fluids. The freezing points for Type B-1 range from -2 to -13°C (fig. 6). Freezing points for Type B-2 inclusions in quartz from vugs range from -0.2 to -1.1°C, and Te are close to the NaCl–H_2O entectic (-21.2 to -23°C). However the composition of type B-2 inclusions in quartz-calcite veins is distinctly different, as they are more saline (Tf = -6.9 to -7.5°C) (fig. 6), and Te measurements indicate the presence of species such as $MgCl_2$ in addition to KCl and NaCl (Te = -29.1 to -31.5°C). No freezing measurements were made on Type C inclusions.

Discussion

Despite the lack of sufficient "primary-looking" fluid inclusions in the samples, the data appear to be significant to the understanding of at least part of the evaluation of the mineralising hydrothermal fluids at the Lakeside Prospect.

The distribution of different types of CO_2-bearing fluid inclusions in quartz from quartz-sulphide veins, and their behaviour upon heating and freezing, may be explained by fluid immiscibility in the H_2O–CO_2 system (i.e. CO_2-bearing fluid inclusions are on a two phase immiscibility curve). The criteria used for this interpretation are:

(a) Co-existence of CO_2-poor and CO_2-rich fluid inclusions in the same region of the same sample.

(b) Variability in vapour–liquid ratios and/or water–CO_2 ratios (i.e. different compositions and densities).

(c) Lack of any evidence for necking down processes or leakage (Roedder, 1984).

(d) Homogenisation of the fluid inclusions to either vapour or liquid and, in some, exhibition of critical behaviour.

(e) Scattered homogenisation temperatures, most of which are towards the higher temperature end of the range. However the homogenisation temperatures are very similar for 70% of the measurements. The high and scattered homogenisation temperatures indicate the entrapment of two fluids in the same inclusion (i.e. heterogeneous trapping). This is reliable evidence for fluid immiscibility, as it clearly indicates that the two different phases (i.e. CO_2-poor and CO_2-rich fluids) were in contact with each other at the time of trapping.

Fluid immiscibility has been suggested for different geological environments (e.g. Eastoe, 1978; Wilson *et al.*, 1980; Spooner, 1980; Roedder, 1977). Fluid immiscibility was also suggested by Halley (1982) from a study of fluid inclusions in quartz from the vein-type Devonian granite-related mineralisation at Rossarden in north-eastern Tasmania.

Freezing measurements on the CO_2-bearing fluid inclusions indicate a period of very low salinity (0–2 wt%), and are also supported by the low critical temperatures of some fluid inclusions (330°C), as critical temperatures are strongly dependent on NaCl content (Sourirajan and Kennedy, 1962). The solubility of CO_2 largely decreases with increase in NaCl ("salting out" effect), and consequently causes the enlargement of the immiscibility field (Ellis and Golding, 1963; Takenouchi and Kennedy, 1965*b*; Drummond, 1981; Gehrig *et al.*, 1979). Gehrig *et al.* (1979) showed that the addition of 6 wt% NaCl to a H_2O-rich fluid (4.0% mole CO_2) increases the maximum for the two-fluid phase field by 100°C (from 367 to 467°C); they also showed that the critical point shifted from 440° to 480°C when 9.7 molc% CO_2 was added to a simple 6 wt% NaCl solution.

The CO_2-bearing fluid inclusions at the Lakeside Prospect appear to have been formed by the trapping of immiscible fluids derived from the boiling of a CO_2-bearing magmatic-dominated fluid (oxygen isotope data, see later). This may be explained as follows:

Presence of CO_2 as a common constituent of the magmatic fluid, as is shown by the fluid inclusions, allows the

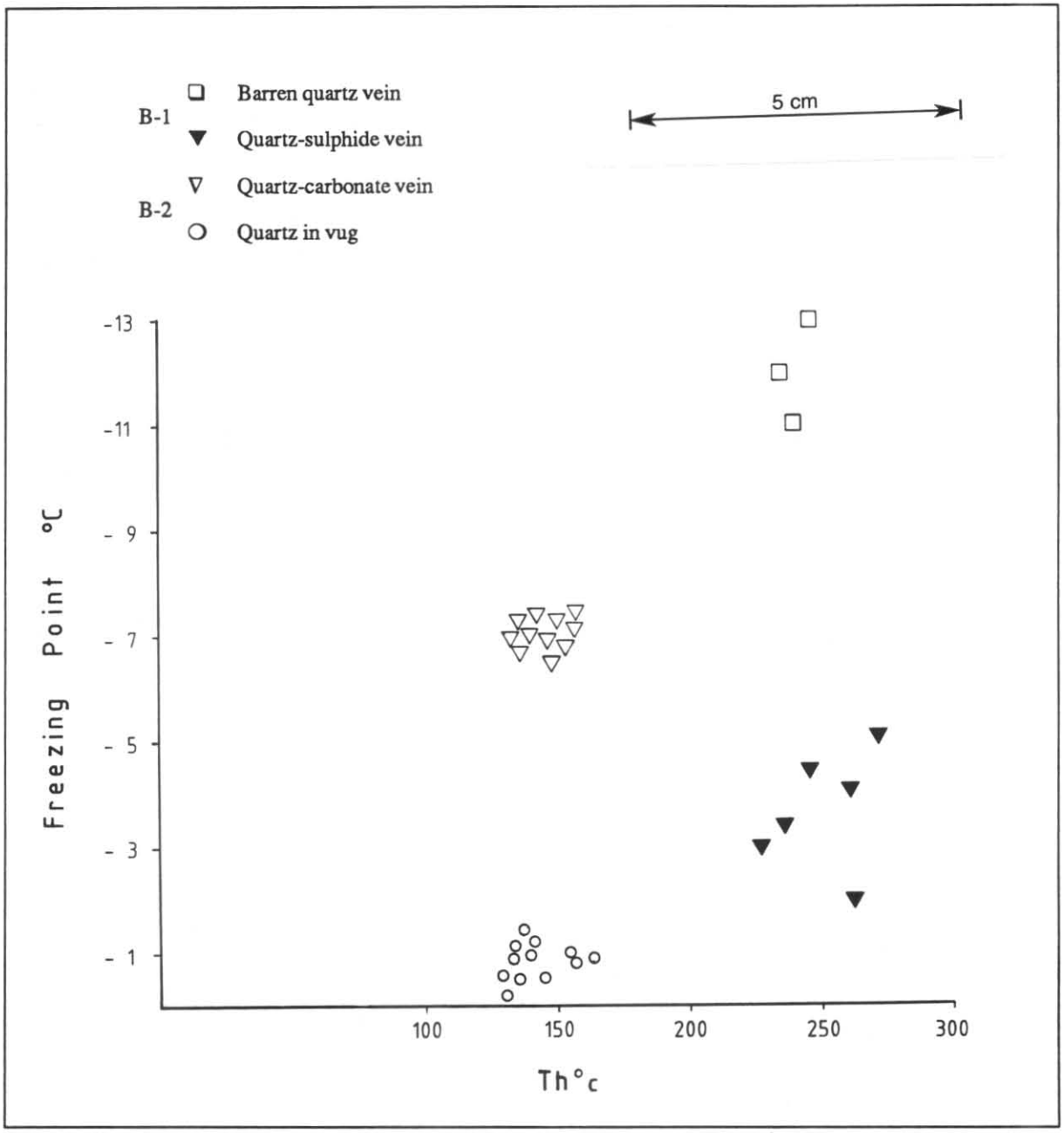

Figure 6. *Th vs freezing points for type B-1 and B-2 inclusions, Lakeside Prospect.*

magma to rise to a higher level (i.e. lower pressure) in the crust before saturation occurs (i.e. CO_2 lowers the αH2O; Holloway, 1976). The mechanical energy released by the volume expansion through the exsolution of the magmatic fluid during the emplacement and crystallisation of the Granite Tor Granite was probably sufficient to cause fracturing both within the granite and the country rocks. A magma with 2.7 wt% H_2O will expand nearly 50% at shallow depth (e.g. 2 km, Burnham and Ohmoto, 1980). However according to Berry (1989), high angle reverse movement of the Henty Fault was synchronous with the intrusion of the Granite Tor Granite. If this is the case, then the fault movement had probably a more significant effect in creating permeable ore channels than the volume expansion associated with fluid exsolution during the emplacement of the granite. A sudden drop in pressure due to fracturing initiated by either of the above mechanisms caused fluid boiling, resulting in the exsolution of a CO_2–H_2O fluid.

No fluid inclusions were found that can be related to the parent fluid from which the CO_2–H_2O immiscible fluid was derived. There is no evidence of fluid mixing, as the lower temperature fluid inclusions (i.e. types B-1 and B-2) appear to have been formed from fluids of different origins (meteoric and/or metamorphic) or times. This is indicated by completely different compositions for fluid inclusions of similar homogenisation temperatures occurring in different sample types (fig. 6).

No pressure correction is needed for fluid inclusions showing immiscibility relationships, as both fluids are saturated with respect to each other. Therefore the temperature range of 330 to 350°C is suggested for the quartz-sphalerite-arsenopyrite veins. Arsenopyrite composition is the same for different stages of mineralisation. This may indicate that temperature variation for different stages of mineralisation was insignificant, and that the main mineralising stages were probably in the range of 330 to 350°C at the Lakeside Prospect. Similar ranges of formation temperatures have been reported for the early stages of Devonian granite-related mineralisation (e.g. Patterson, 1979; Halley, 1982). Considering the critical temperatures (330–350°C), a pressure range of 320 to 400 bars is estimated for the main mineralising stage, using the

experimental work of Takenouchi and Kennedy (1964). The CO_2 content of the fluid shows a critical phenomena range from 11 to 18 mole% (fig. 7).

An estimate of pressure at the time of trapping can also be obtained by using the homogenisation temperature and CO_2 contents of a pair of coexisting inclusions using the CO_2–H_2O binary system of Takenouchi and Kennedy (1964; fig. 7). However the CO_2 contents of the CO_2-bearing fluid inclusions (types A-2 and A-3) were not calculated, because the small size of the inclusions made visual estimates of the proportion of CO_2 very difficult.

It appears that the best pressure estimates are those obtained from inclusions showing critical points.

Assuming the same range of pressure for the late quartz and quartz-carbonate veins as those for quartz-sulphide veins (i.e. 370–400 bars), and considering the measured salinities, formation temperatures ranging from 170 to 200°C are estimated for the late veins at the Lakeside Prospect (Potter and Brown, 1977). The fluids from which these late veins have been formed have distinctly different compositions (fig. 6), and this clearly indicates that they have been formed at different stages, possibly from fluids of different origins, and are not necessarily the end products of the main mineralisation event.

In summary, extensive overprinting of high temperature, presumed primary or pseudosecondary fluid inclusions by later-formed low temperature secondary inclusions did not permit the study or the complete evaluation of the hydrothermal solution at the Lakeside Prospect. However, this study shows that at least part of the mineralising fluid was of very low salinity H_2O-CO_2 mixture derived by exsolution from the primary magmatic fluid during the main mineralising period (i.e. formation of pyrite, arsenopyrite, sphalerite). A temperature range of 330 to 350°C and a pressure range of 320 to 400 bars are suggested for this period of the mineralisation.

Assuming a pressure range of 320 to 400 bars, a formation temperature of 170 to 200°C is indicated for late quartz-carbonate in veins.

Late stage veins have formed from fluids of different compositions and possibly different origins.

OXYGEN ISOTOPE DATA

Eight quartz samples from quartz-sulphide, quartz and quartz-carbonate veins were selected for oxygen isotope analysis (Table 3). The purpose of this study was to investigate the possible origin(s) of the fluids for these veins using fluid inclusion data for their formation temperatures. Samples were analysed at the University of Tasmania by Michael Power, using standard BrF5 conversion techniques.

The reproductibility of the oxygen isotope analyses was within ± 0.2 ‰ for the analysed samples.

The oxygen isotope values in quartz range from 11.3 to 14.9‰. Quartz samples from late quartz-carbonate veins and vugs are lower in $\delta^{18}O$ relative to those from quartz-sulphide veins (Table 3).

There are no $\delta^{18}O$ values available from the Granite Tor Granite. However, the oxygen isotope values of granites along the same ridge (fig. 12), including the Pine Hill Granite and the Heemskirk Granite, range from 9.3 to 10.6‰ and 9.8 to 10.9‰ respectively (Patterson, 1979;

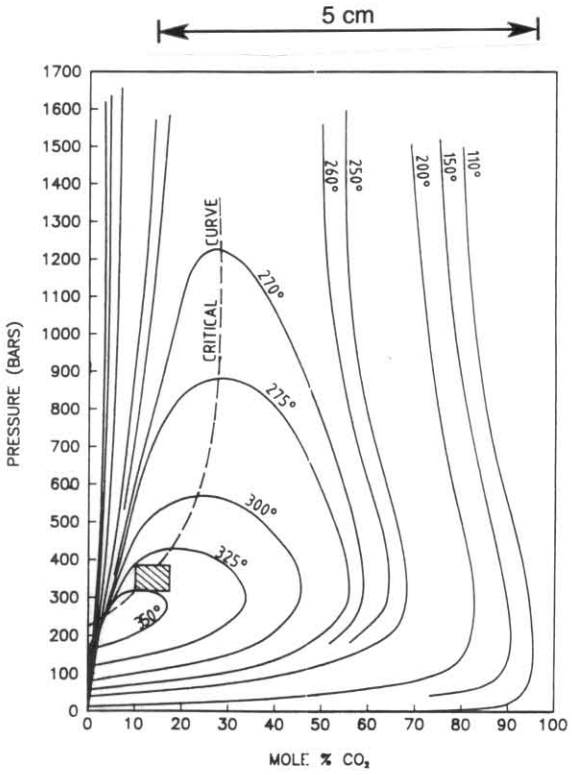

Figure 7. *P–X plot of isotherms for the system CO_2 – H_2O (adopted from Takenouchi and Kennedy, 1964) showing the range of pressure and compositions for the fluid inclusions with critical points, Lakeside Prospect.*

Taheri, 1985). Assuming a similar range of oxygen isotope values for the Granite Tor Granite, then the quartz samples from quartz-sulphide veins exhibit higher $\delta^{18}O$ values than those from the Granite Tor Granite. However taking the estimated formation temperature of 350°C into account, then the oxygen isotope composition of water in equilibrium with mineralised quartz falls in the range of +7.2 to +9.1‰ (from quartz-H_2O fractionation of Clayton *et al.*, 1972), and indicates deriviation of the fluid from a dominantly magmatic aqueous phase. A dominantly magmatic source was also indicated by $\delta^{18}O$ studies at the Renison Bell tin deposit for the early stages of cassiterite-sulphide mineralisation (Patterson *et al.*, 1981).

The calculated $\delta^{18}O$ compositions of water associated with the late-formed quartz are distinctly lower than those from the quartz-sulphide veins (Table 3), and are indicative of the involvement of externally derived fluid(s), such as meteoric water. Pure water was assumed for the estimation of the $\delta^{18}O$ values of the hydrothermal fluids derived above (i.e. the salinity effect on the oxygen isotope activity ratio of water was not considered; Truesdell, 1974). Little error is introduced by this assumption, because the salinity of fluids responsible for the formation of quartz-sulphide veins appears to be very low (0–2 wt%, fluid inclusion data), and the effect of salinity on the $\delta^{18}O$ values of low temperature fluids is neglibible (<0.5 ‰).

SULPHUR ISOTOPE DATA

$\delta^{34}S$ values have been determined for 33 sulphide minerals from mineralised sections within the Farrell Slates, and pyrite veinlets in andesites of the Mt Black Volcanics. The sulphide minerals include pyrite, sphalerite, galena, chalcopyrite and arsenopyrite. The samples were analysed according to the method of Robinson and Kusakabe (1975). These data, and those from other prospects along the Henty Fault Zone (Both *et*

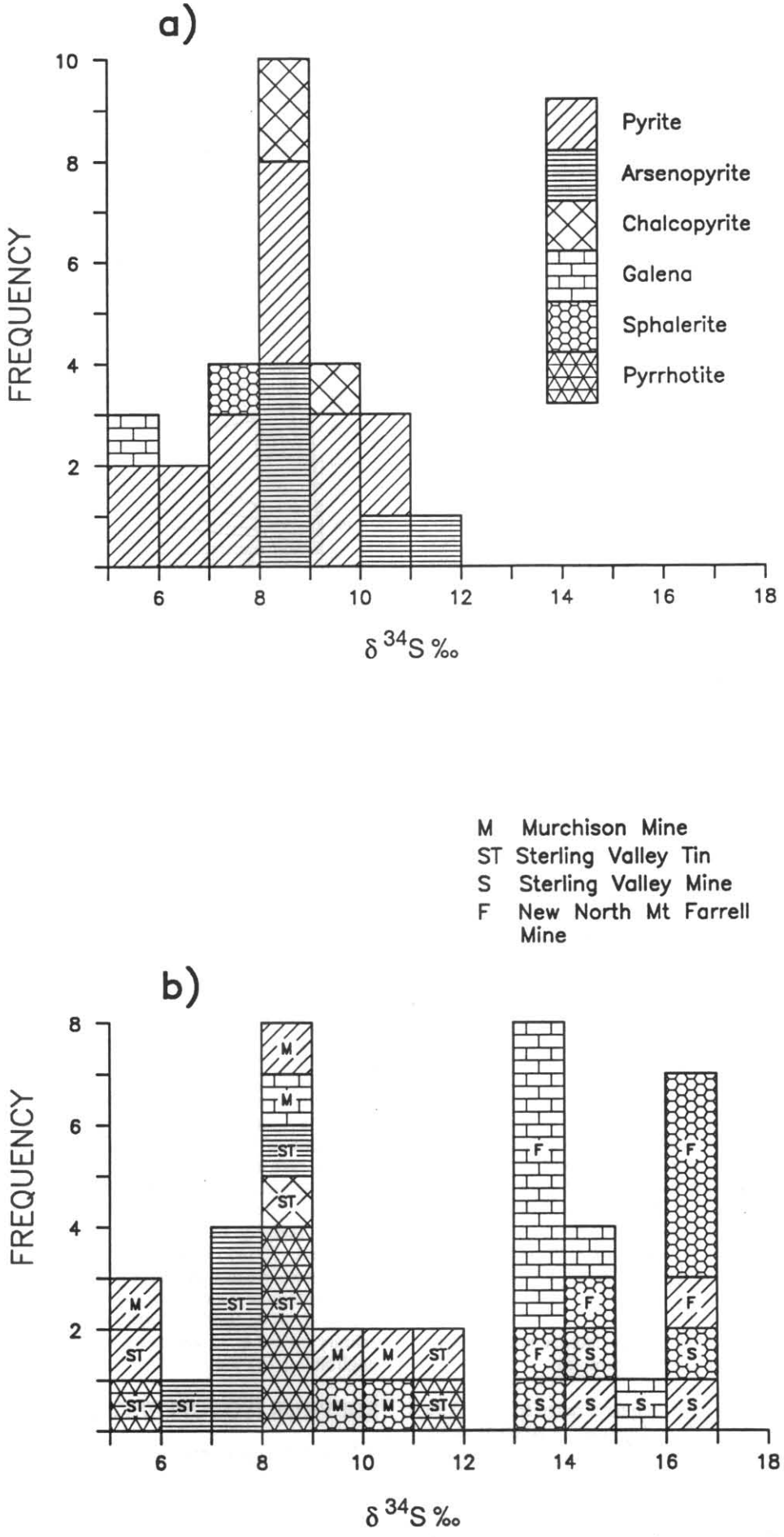

Figure 8. *Frequency distribution of sulphur isotope compositions of sulphides from: (a) Lakeside Prospect; (b) Sterling Valley Tin, Murchison Mine, New North Mt Farrell Mine, and Sterling Valley Mine (data from Table 4).*

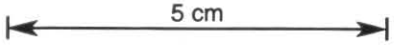

Table 3. *Oxygen isotope analyses from quartz samples and their equilibrating fluids at indicated temperatures (°C), Lakeside Prospect.*

Sample No.	Rock type	Estimated formation temp (°C) (fluid inclusion data)	$\delta^{18}O$‰ (rock) (SMOW)*	$\delta^{18}O$ ‰ (water) (SMOW)
102843	quartz-pyrite vein	350	+13.00	+7.2
102844	quartz-pyrite-sphalerite vein	350	+13.5	+7.7
102892	quartz-carbonate vein	200	+11.3	-0.9
102891	quartz in vug	180	+12.2	-1.4
102845	quartz-pyrite	350	+14.9	+9.1
102896	quartz-sphalerite, arsenopyrite	350	+13.2	+7.4
102895	quartz vein	300	+14.8	+7.4
102894	quartz-carbonate vein	200	+12.1	-0.1
102893	quartz-carbonate	200	+11.8	-0.4

* Analytical error is ± 0.2‰

al., 1969; Polya, 1986; Solomon *et al.*, 1988; and this study) are presented in Figure 8 and Table 4.

Measured $\delta^{34}S$ values for the sulphides in the Lakeside Prospect range from +5.6 to +11.4‰, with 70% of the population falling in the range of +7‰ to +10‰. The $\delta^{34}S$ values do not show any systematic variation with respect to position in the paragenetic sequence space or type of occurrences.

Appropriate pairs of sulphides (e.g. galena–sphalerite) give unreasonably high temperatures (approximately 500°C), indicating isotopic disequilibrium condition between these pairs. Sulphide minerals at the Lakeside Prospect and the Sterling Valley Tin area have similar $\delta^{34}S$ values, and are isotopically the lightest sulphides along the Henty Fault Zone (fig. 8).

The $\delta^{34}S$ values in the Sterling Valley, New North Mt Farrell and Tullah mines (Polya *et al.*, 1986; this study) are relatively high and show a narrow range of +11.9 to +16.5‰ (Table 4).

There are no $\delta^{34}S$ data from the Granite Tor Granite, however magmatic pyrite in granites closely related to that at Granite Tor (e.g. Pine Hill and Heemskirk Granites) have low $\delta^{34}S$ values of around +2.5‰ (Patterson, 1979; Taheri, 1986). Therefore it might be reasonable to assume similar light $\delta^{34}S$ values for the Granite Tor Granite. However Cambrian sulphides and/or sulphate appear to be high in $\delta^{34}S$ values (e.g. Solomon *et al.*, 1969; Green *et al.*, 1981).

There seems to be a direct relationship between the position of the subsurface granite ridge and the general distribution of sulphides and sulphur isotope values (fig. 13). Isotopically light sulphides and high-temperature sulphide minerals (e.g. pyrrhotite) occur in the Lakeside Prospect and the Sterling Valley Tin area, where the granite surface is very shallow (<1 km), and as a result it is supposed that the Devonian magmatic sulphur input was higher for the formation of these mineralised areas. The higher $\delta^{34}S$ values and lower temperature sulphides are mainly from the Mt Farrell mining field and the Sterling Valley Mine, in which the granite ridge is at greater depth (>3 km), and consequently the hydrothermal fluids circulated through a greater thickness of Cambrian rocks, thus permitting a greater contribution of Cambrian sulphur richer in $\delta^{34}S$.

In summary, a substantial source of sulphur in the Lakeside Prospect and Sterling Valley Tin area appears to have been from a Devonian magmatic fluid, whereas isotopically heavier sulphides in the Mt Farrell Mining District and Sterling Valley Mine are indicative of a greater sulphur input from dissolved Cambrian sulphides and/or sulphates.

GEOCHEMISTRY OF MINERALISED ZONES

Core samples from fourteen drill holes have been analysed for Cu, Pb, Zn, Au, As, Ag and Sn by Billiton Australia (Hall *et al.*, 1987, 1988). The results were made available for this study by Mr D. B. Hall of Billiton Australia.

Split core samples, one to two metres long, were used for the analyses. The locations of drill holes are shown in Figure 4.

In detail, the distribution of individual metals is erratic (Table 5) and varies over small intervals (e.g. 200 mm or less). This is mainly due to the style of mineralisation as fissure-fillings and replacements of early phases by later formed minerals. The relationship between base metals, gold, silver and tin are shown in Figure 9*a-h*.

In general, the close association between As, Au, Cu and Sn (Stage 2 mineralisation) is clearly indicated by most of the samples from the different drill holes (figs 9*a, c, d, e, f*). A direct relationship between Pb, Zn and Ag (Stage 3 mineralisation) is also shown in Figure 9*g* and 9*h*. Correlation coefficients between these metals (Table 6) also show similar relationships with those shown in Figure 9. Paragentically, arsenopyrite was formed mainly before the deposition of gold. However the concentration of gold appears to be directly related to the As contents in some mineralised sections (eg DDH RED87-2, RED87-4, RED87-6, fig. 9*c*). This is explained by mineralogical observations, in which much of the gold at the Lakeside Prospect occurs as fissure-fillings in arsenopyrite (Plate 10). The possibility of the minor occurrence of gold in arsenopyrite and pyrite in the Lakeside Prospect and the Sterling Valley Tin area was examined by micro-probe analyses (Model Cameca SX50 System). No gold was detected in these sulphide minerals (detection limit ≡ 130 ppm).

Table 4. *Sulphur isotope data*

Sample No.	Location	Mineral	Paragenetic stage	$\delta^{34}S‰$	Data source
Lakeside Prospect					
102803	RED87-3, 108.6 m	Arsenopyrite	1	8.5	(1)
102806	RED87-3, 112.9 m	Pyrite	1	8.4	(1)
102801	RED87-3, 102.8 m	Arsenopyrite	1	10.1	(1)
102807	RED87-3, 114.5 m	Pyrite	1	7.6	(1)
103702	RED87-3, 79.4 m	Pyrite	1	9.7	(1)
102808	RED87-2, 209.1 m	Pyrite	1	10.6	(1)
102900	RED87-2, 230.1 m	Arsenopyrite	1	8.7	(1)
102810	RED87-2, 230.9 m	Pyrite	3	9.1	(1)
103703	RED87-5, 52.9 m	Pyrite	1	9.6	(1)
103713	RED87-5, 52.8 m	Arsenopyrite	1	11.4	(1)
103704	RED87-6, 41.8 m	Pyrite	-	8.3	(1)
103705	RED87-6, 118.8 m	Pyrite	-	8.1	(1)
102818	RED87-6, 113.3 m	Pyrite	-	7.5	(1)
102826	RED87-1, 224.8 m	Sphalerite	3	7.2	(1)
102826	RED87-7, 224.8 m	Pyrite	1	5.6	(1)
102829	RED87-7, 245.4 m	Arsenopyrite	1	8.4	(1)
103707	RED87-8, 112.0 m	Pyrite	1	6.9	(1)
102831	RED87-7, 253.0 m	Pyrite	-	7.5	(1)
103708	RED87-2, 217.0 m	Pyrite	1	6.4	(1)
103709	RED87-9, 49.6 m	Pyrite	-	6.0	(1)
103710	RED87-10, 148.0 m	Galena	-	5.9	(1)
103711	RED87-10, 150.0 m	Pyrite	1	10.1	(1)
103712	RED87-7, 161 m	Arsenopyrite	1	8.1	(1)
103710	RED87-10, 148 m	Pyrite	1	8.5	(1)
102807	RED87-3, 114.5 m	Chalcopyrite	2a	8.05	(1)
102834	RED87-3, 113 m	Chalcopyrite	2a	10.0	(1)
102805	RED87-3, 112.4 m	Chalcopyrite	2a	8.9	(1)
Murchison Mine					
103715		Pyrite	?	5.9	(1)
103714		Galena	?	8.9	(1)
103714		Sphalerite	?	11.0	(1)
102528	No. 2 Level	Sphalerite	?	10.0	(2)
11198	Open Cut	Pyrite	?	9.6	(2)
11199	Open Cut	Pyrite	?	10.2	(2)
61618	Open Cut	Pyrite	?	8.7	(2)
Sterling Valley Tin					
102868	STP221, 37.9 m	Pyrrhotite	2	8.1	(1)
102865	STP221, 36.9 m	Pyrite	1	5.2	(1)
102865	STP221, 36.9 m	Arsenopyrite	2	7.4	(1)
102869	STP218, 99.2 m	Pyrrhotite	2	5.3	(1)
102866	STP217, 98 m	Arsenopyrite	2	6.43	(1)
102866	STP217, 98 m	Chalcopyrite	3	8.35	(1)
102866	STP217, 98 m	Pyrrhotite	2	8.9	(1)
102871	STP217, 29.1 m	Arsenopyrite	2	7.1	(1)
102862	STP217, 98.7 m	Pyrrhotite	2	8.7	(1)
102861	STP217, 99.5 m	Pyrrhotite	2	11.5	(1)
102861	STP217, 99.5 m	Arsenopyrite	2	7.29	(1)
102864	STP217, 85.0 m	Arsenopyrite	2	7.28	(1)
102872	STP218, 38.8 m	Pyrite	1	12.00	(1)

Sample No.	Location	Mineral	Paragenetic stage	$\delta^{34}S‰$	Data source
102867	STP217, 98.9 m	Pyrrhotite	2	8.7	(1)
102867	STP217, 98.9 m	Arsenopyrite	2	8.3	(1)
Sterling Valley Mine					
102870		Pyrite	?	16.4	(1)
103716		Galena	?	15.2	(1)
103716		Sphalerite	?	16.6	(1)
61669		Pyrite	?	14.6	(3)
10526		Sphalerite	?	13.8	(2)
10527		Sphalerite	?	14.2	(2)
New North Mt Farrell Mine					
10430	9 Level	Pyrite	?	16.5	(2)
10430	9 Level	Sphalerite	?	16.2	(2)
10434	9 Level	Galena	?	13.2	(2)
10431	8 Level	Galena	?	13.2	(2)
10432	8 Level	Galena	?	13.2	(2)
10436	7 Level	Galena	?	13.4	(2)
10438	9 Level	Galena	?	13.8	(2)
10522	4 Level	Sphalerite	?	14.0	(2)
10438	9 Level	Sphalerite	?	15.4	(2)
101066	9 Level	Sphalerite	?	17.0	(2)
101067	9 Level	Galena	?	14.2	(2)
101066	9 Level	Galena	?	13.7	(2)
101067	9 Level	Sphalerite	?	16.6	(2)

(1)=This study; (2)=Solomon *et al.* (1969); (3)=Polya *et al.* (1986)

All values are in ‰ relative to Canyon Diablo Troilite

Analytical precision ± 0.05 ‰. Analyses for this study by R. N. Woolley.

Table 5. *Average and standard deviation of Au and Sn contents of mineralised rocks from analysed drill core, Lakeside Prospect.*

Drill Hole*	Total depth (m)	Mineralised zone (m)	Au (ppm) X ± S, N**	Sn (ppm) X ± S, N	Au, Sn rich min. zones	Au (ppm) X ± S, N	Sn (ppm) X ± S, N
RED88-4	325	246–277	0.4 ± 0.6, 32	1083 ± 1011, 32	254-275	0.8 ± 0.6,16	2135 ± 1003, 9
RED88-3	178.5	82–98	<0.03, 7	5 ± 2, 7	None	<0.04 ppm	<9 ppm
RED88-2	289.3	210–252	0.6 ± 1, 30	742 ± 1172, 30	211-228	1.1 ± 1.2, 14	1851 ± 1306,10
RED88-1	322	255–301	0.1 ± 0.2, 45	769 ± 3034, 45	256-262	0.4 ± 0.23 , 5	
					290-293		9720 ± 8824, 3
RED87-10	169.2	None			None		
RED87-8	280	210–259	<0.04, 24	28 ± 33, 24	224-229	<0.03	<20 ppm
RED87-7	277	217–254	0.4 ± 1, 21	188 ± 248, 21	235-248	1.2 ± 1.7, 6	403 ± 312,7
RED87-6	157	100–127	0.7 ± 1, 21	408 ± 891, 21	112-120	1.5 ± 1.2, 9	1572 ± 1402, 5
RED87-5	145.5	29–139	0.3 ± 0.5, 38	567 ± 1122, 38	30-36	0.2 ± 0.1, 5	1603 ± 67, 2
RED87-4	328	192–270	<0.05, 51	13 ± 16, 51	247-250	0.2 ± 0.04, 6	<100 ppm
					258-261	0.2 ± 0.04, 6	<100 ppm
RED87-3	153.4	100–130	1.6 ± 3, 27	726 ± 975, 27	108-116	4.8 ± 4.6, 7	1631 ± 1195, 8
RED87-2	260	199–234	2 ± 3, 12	756 ± 987, 12	199-234	1.9 ± 1.6, 4	2063 ± 1048, 9

* See Figure 4 for location
** X Average
S Standard deviation
N Number of analyses

Figure 9 (a–h). *Variation diagrams for As, Sn, Au, Pb, Zn, Ag and Cu from mineralised sections of drill core from the Lakeside Prospect. For drill hole locations and depth and/or thickness of mineralised section see Figure 4 and Table 5 respectively (data from Hall et al., 1987; Hall et al., 1988).*

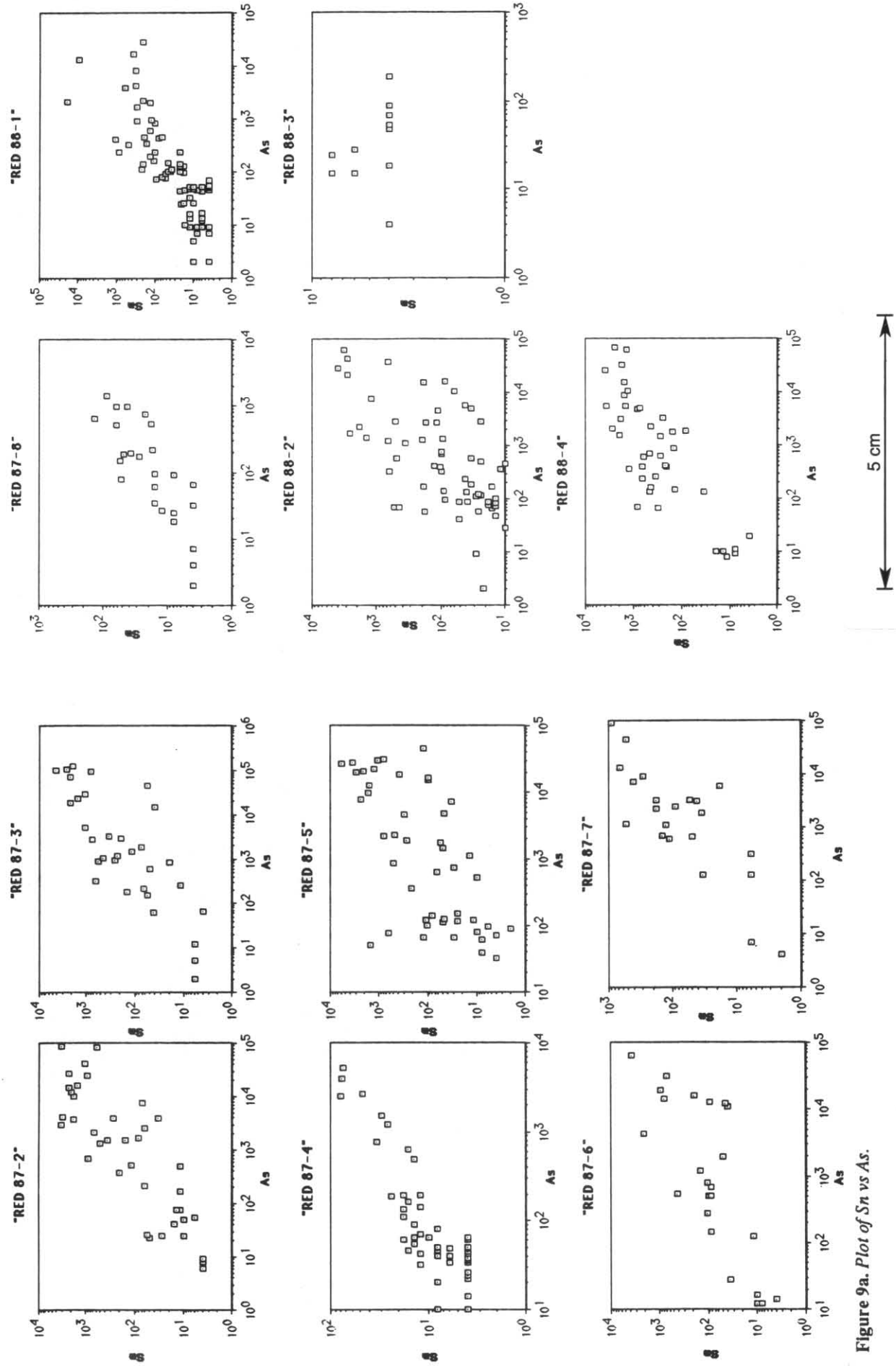

Figure 9a. *Plot of Sn vs As.*

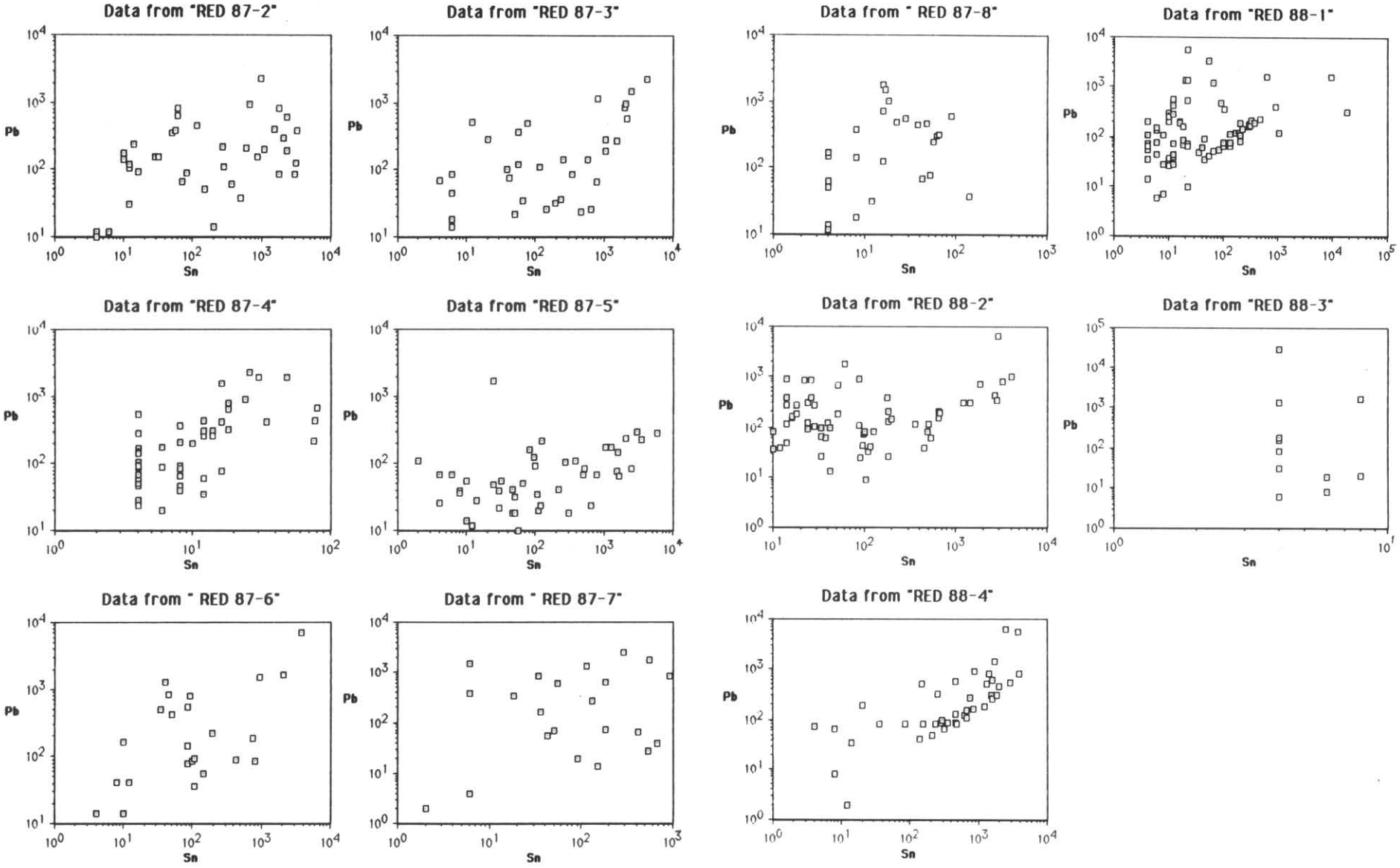

Figure 9b. *Plot of Pb vs Sn.*

5 cm

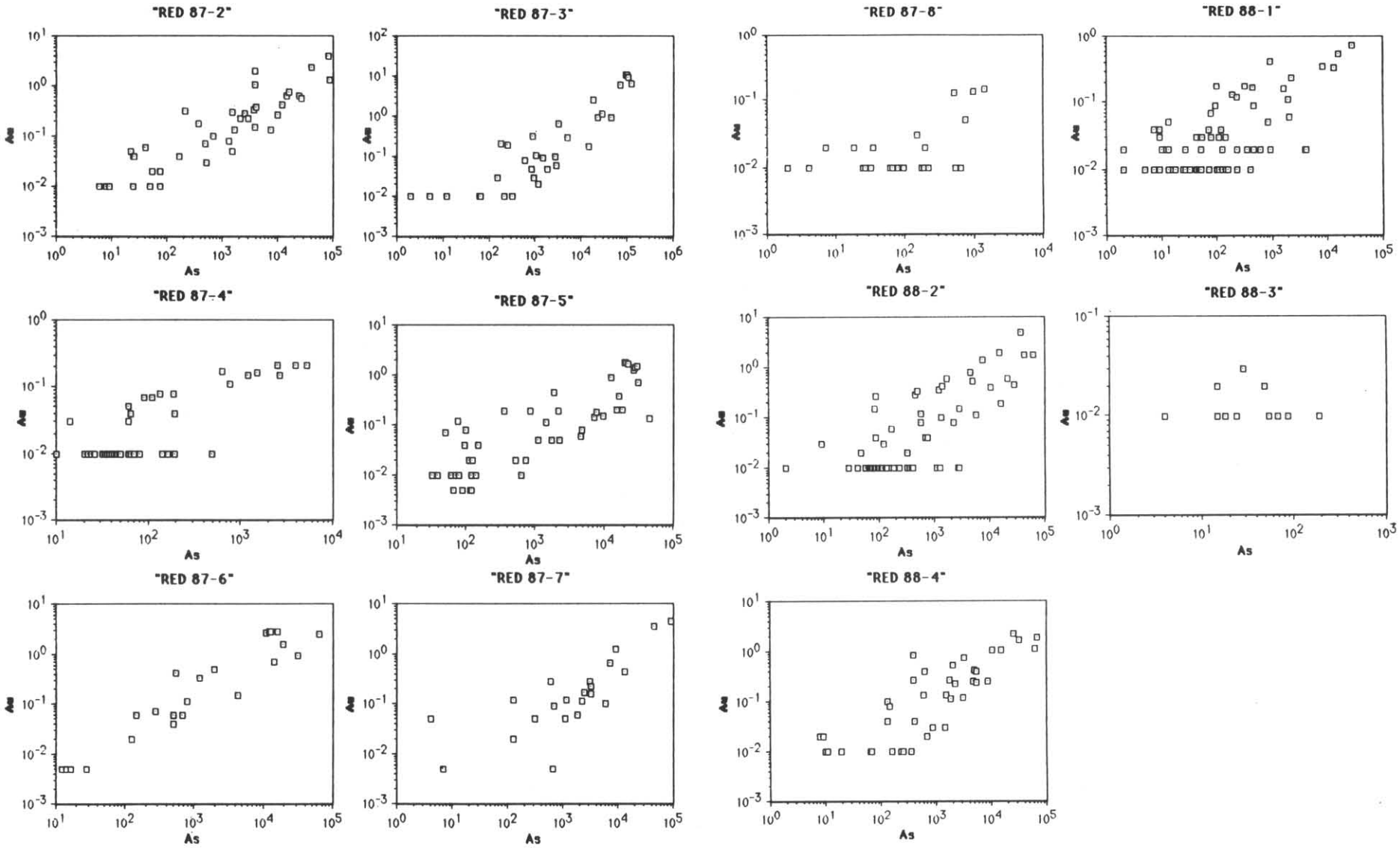

Figure 9c. *Plot of Au vs As.*

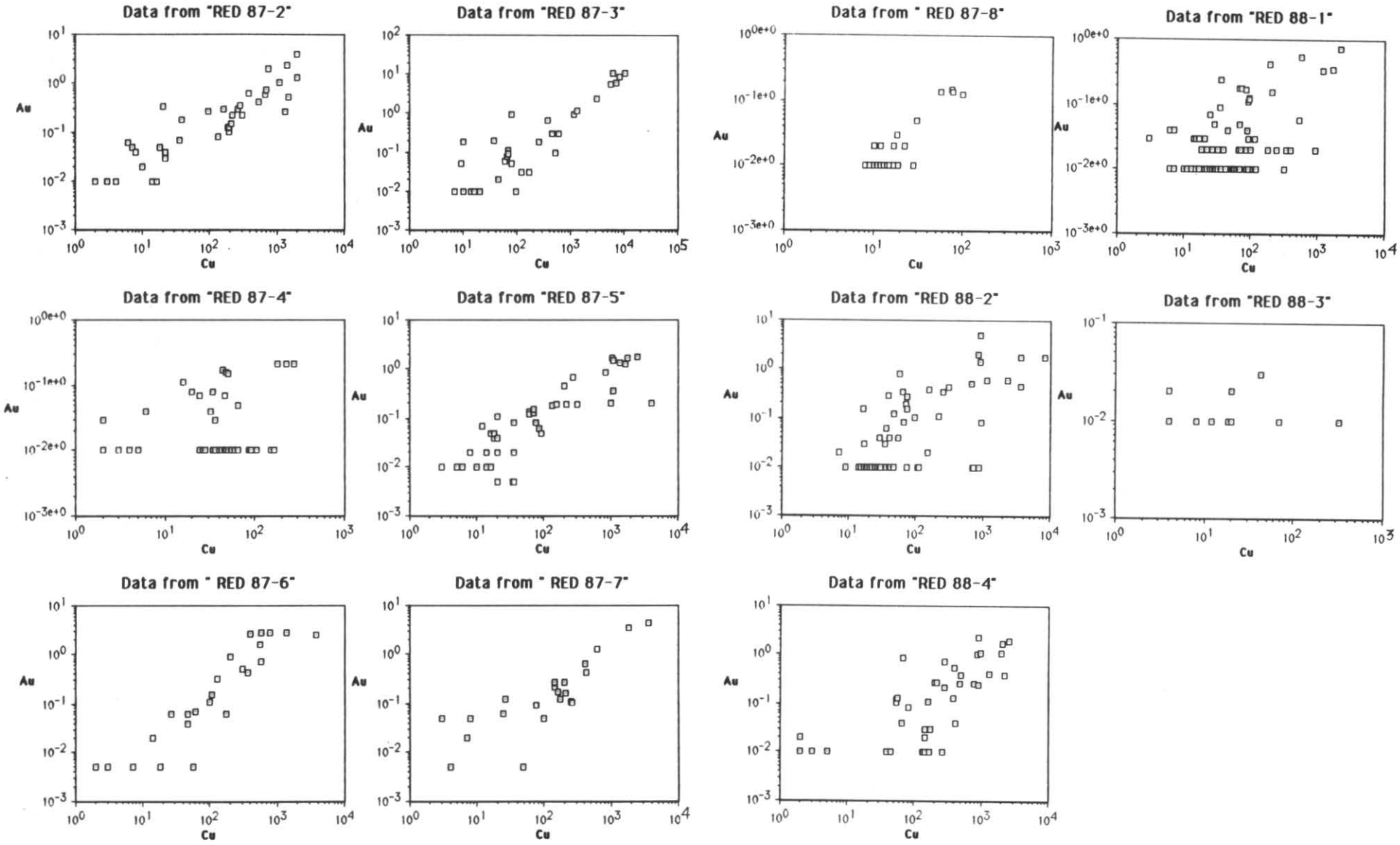

Figure 9d. *Plot of Au vs Cu.*

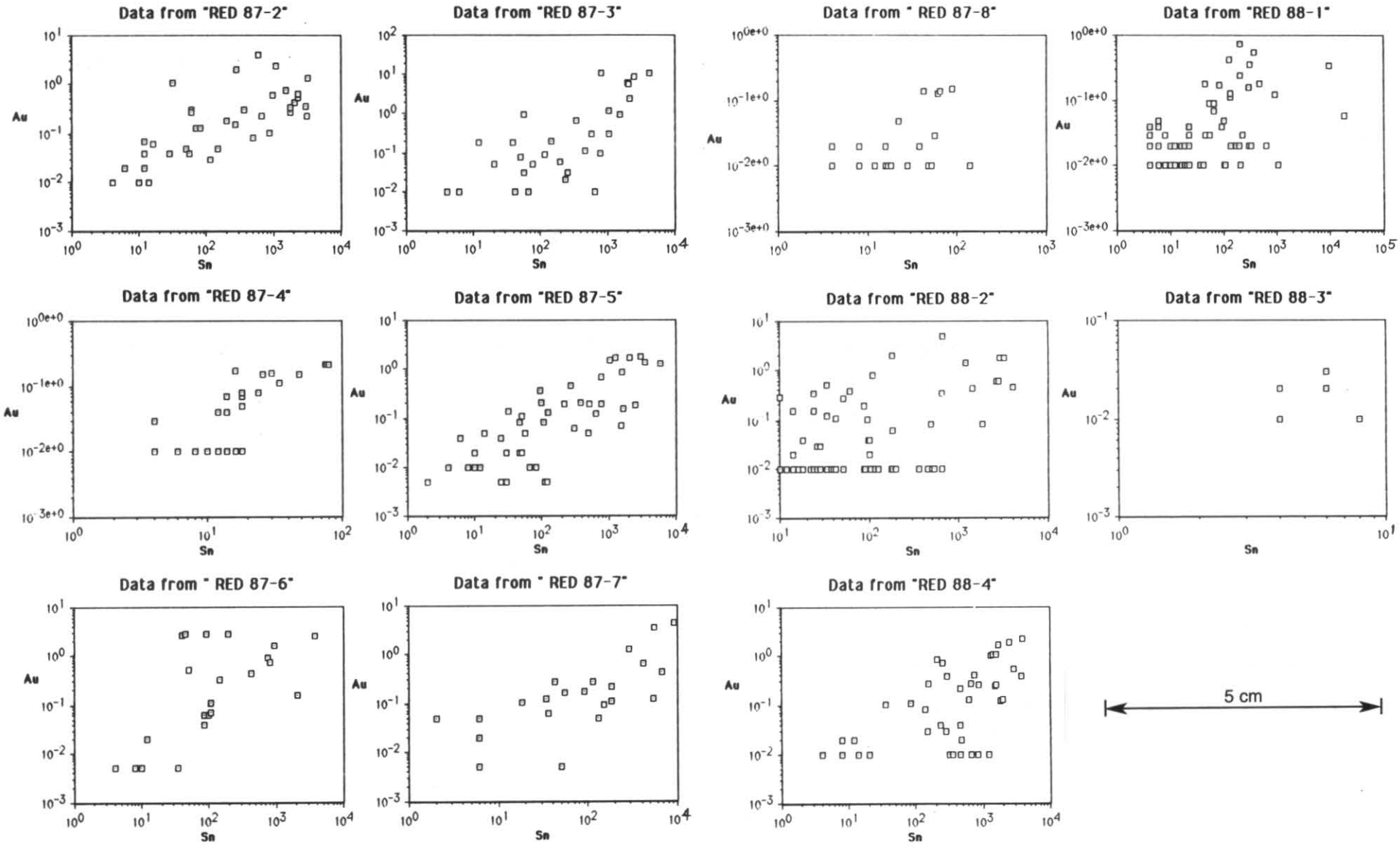

Figure 9e. *Plot of Au vs Sn.*

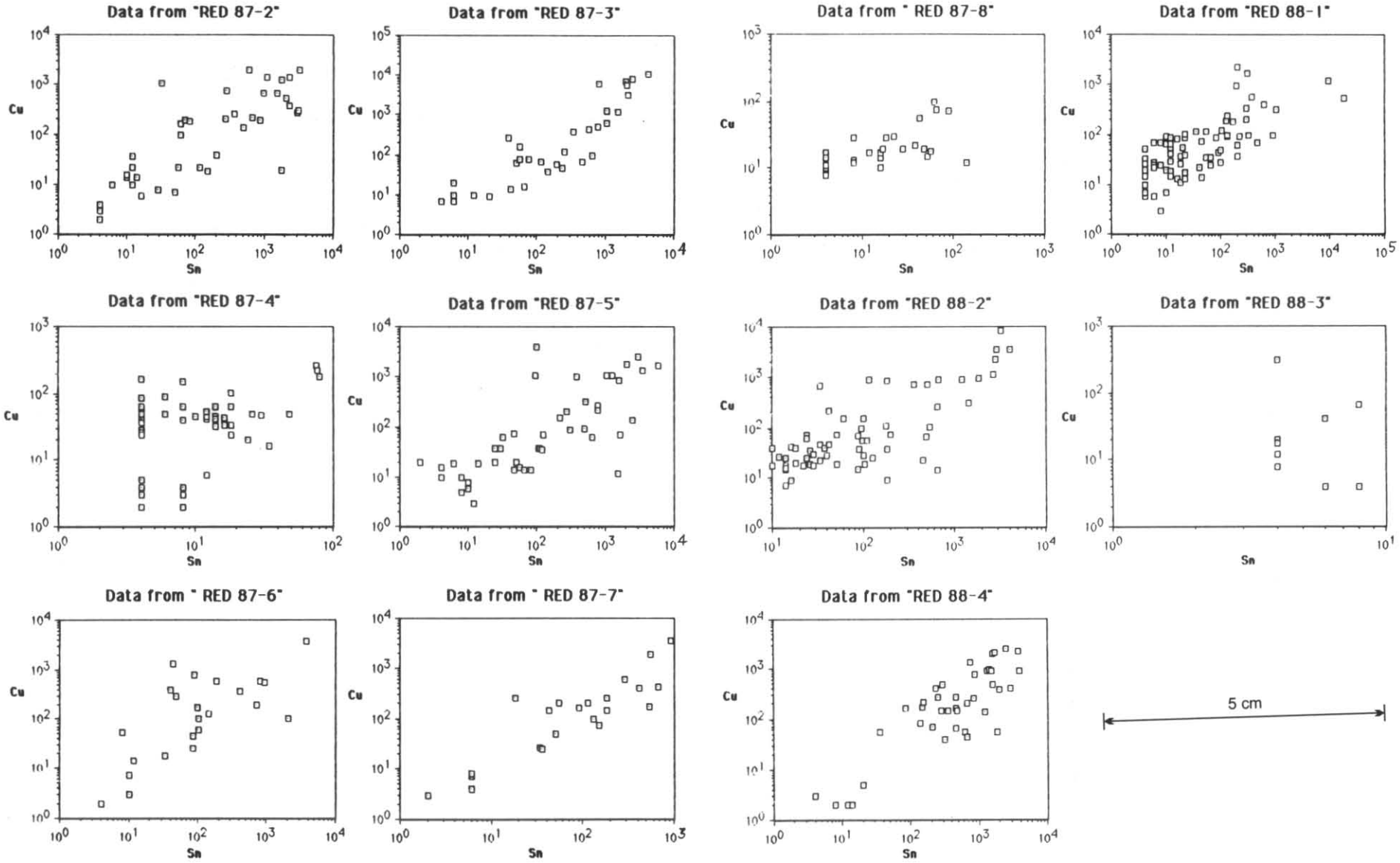

Figure 9f. *Plot of Cu vs Sn.*

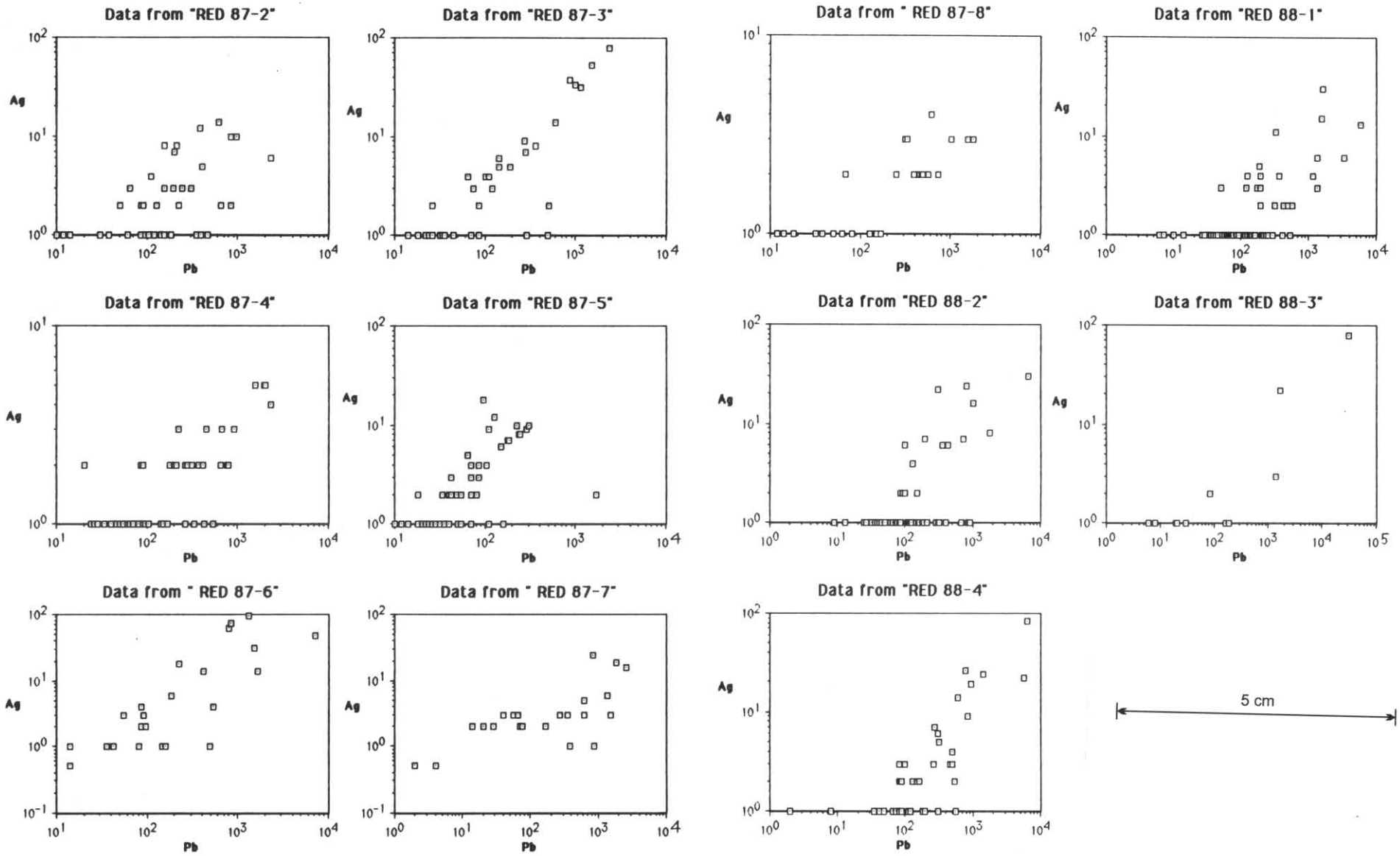

Figure 9g. *Plot of Ag vs Pb.*

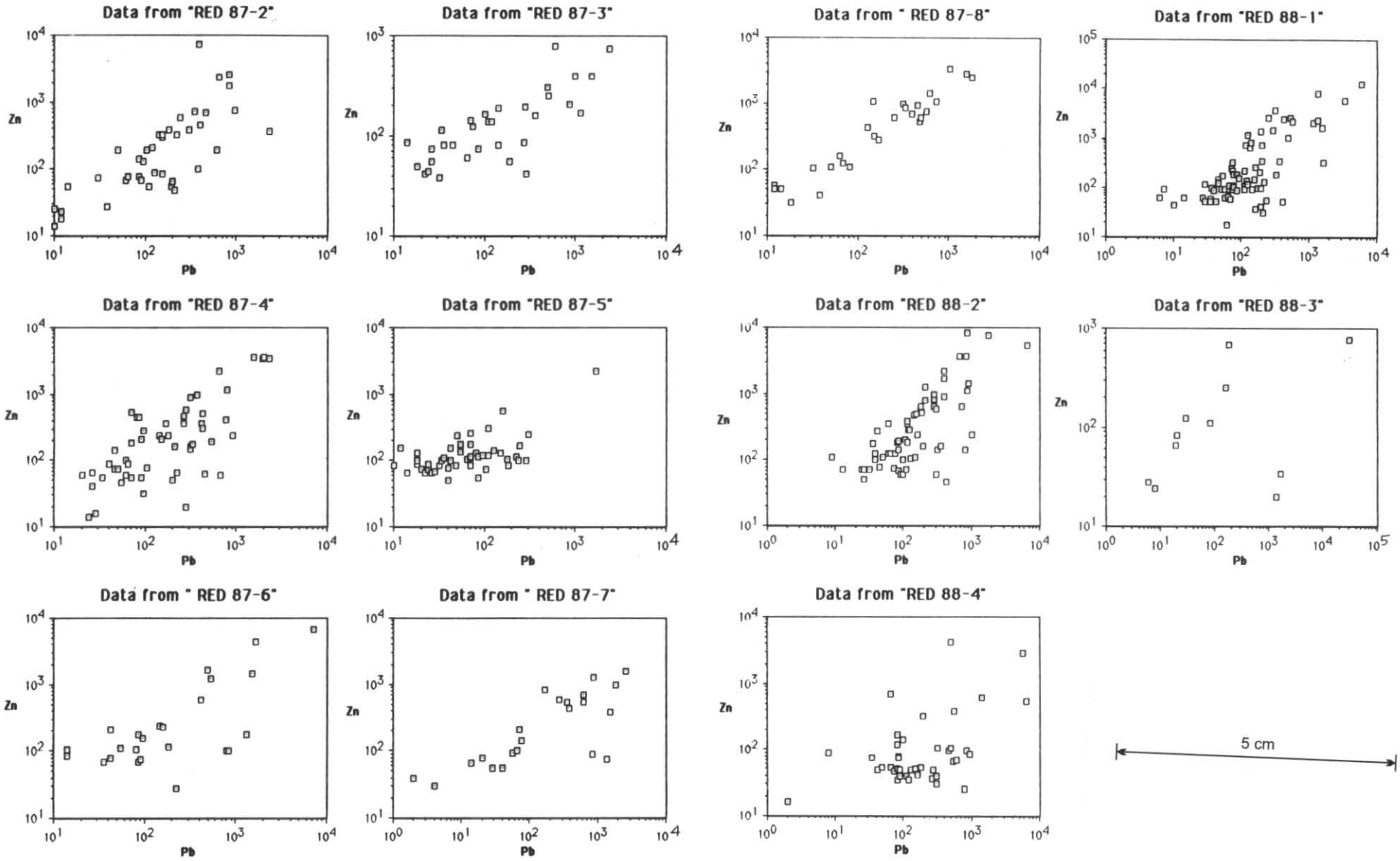

Figure 9h. *Plot of Zn vs Pb.*

Table 6. *Correlation coefficient between Cu, As, Ag, Au, Pb, Zn, Sn obtained from mineralised core samples.*

*	Cu	As	Ag	Au	Pb	Zn	Sn
Cu	-	0.74	0.77	0.77	0.37	0.30	0.78
As		-	0.67	0.78	0.23	0.24	0.60
Ag		0.67	-	0.73	0.44	0.47	0.56
Au		0.78	0.73	-	0.26	0.22	0.69
Pb		0.23	0.44	0.26	-	0.67	0.29
Zn		0.24	0.47	0.22	0.67	-	0.27
Sn		0.60	0.56	0.69	0.29	0.27	-

	Cu	As	Ag	Au	Pb	Zn	Sn
Cu	-	0.76	0.63	0.84	0.18	0.12	0.41
As	0.76	-	0.51	0.82	0.16	0.04	0.03
Ag	0.63	0.51	-	0.64	0.27	0.47	0.36
Au	0.84	0.82	0.64	-	0.15	0.05	0.73
Pb	0.18	0.16	0.27	0.15	-	0.35	0.06
Zn	0.12	0.04	0.47	0.05	0.35	-	0.16
Sn	0.41	0.03	0.36	0.23	0.06	0.16	-

* Log values

ORIGIN AND PHYSICOCHEMICAL CONDITIONS OF HYDROTHERMAL FLUIDS AT THE LAKESIDE PROSPECT

The polymetallic mineralisation at the Lakeside Prospect is unusual because of the metallogenetically rare association of gold and tin. Therefore any information regarding the physicochemical conditions of hydrothermal solutions in a gold–tin-bearing system may be useful in understanding the conditions under which these elements originated, were transported, and eventually deposited. This also assists assessment of the relative importance of Cambrian and/or Devonian processes in the formation of this and other similar deposits along the Henty Fault.

The physicochemical conditions of ore-forming solutions for the Lakeside Prospect could not be quantitatively determined. This is because of the lack of appropriate mineral assemblages and the paucity of good fluid inclusion material.

Thermal History

A formation termperature of about 350°C is suggested for the main stage of mineralisation (Stage 2) in the Lakeside Prospect (fluid inclusion data). Arsenopyrite is the most common mineral over different stages of mineralisation, however its composition remained constant. This may indicate that the temperature of mineralisation stayed the same over the metallogenetically more significant Stages 1 and 2.

Exsolution of fluid from the crystallising magma may have provided sufficient mechanical energy to cause the fracturing of the granite and the country rocks. The sudden drop in pressure due to the fracturing resulted in boiling of the hydrothermal solutions, and consequent precipitation of the ore-forming minerals. Fluid access was possibly controlled by the combination of major structures (e.g. faults) and local permeable zones produced by hydraulic fracturing of the country rocks. Boiling is considered to be the most effective mechanism for ore deposition in many hydrothermal deposits, and has been discussed in detail by Drummond and Ohmoto (1985).

The boiling episode at the Lakeside Prospect was likely to be isoenthalpic rather than isothermal (i.e. the solution lost heat to the vapour phase and cooled as boiling proceeded). According to Barton and Toulmin (1961) an isoenthalpic drop in pressure from 2000 bars to 100 bars can lower the temperature of the fluid from 700 to 400°C.

A further drop in temperature resulted as the magmatic-dominated fluid mixed with meteoric water and/or conducted heat to the wall rocks. Oxygen isotope data suggest that the former was an effective mechanism in the Lakeside Prospect. Continuous cooling of the hydrothermal solution reduced the solubility of silica (Fournier, 1983) and probably caused the deposition of vein quartz and silicification of the wall rocks. The low temperature quartz-carbonate and/or carbonate veins could have been derived from a separate stage of meteoric water circulation.

Transport, deposition and origin of gold

There are two ionic forms of gold in nature (Au^{+} and Au^{+3}). However Au^{+3} solubility appears to be negligible at the temperature and oxygen fugacity conditions of hydrothermal fluids, and is not further considered.

In recent years the solubility and deposition of gold in hydrothermal solutions have attracted much attention (e.g. Romberger, 1986; Seward, 1984*b*, Crerar *et al.*, 1985; Wood *et al.*, 1987; Huston and Large, 1987). However the speciation of gold is still less understood than those of Fe, Ag, Zn and Pb. Consequently many different complexes including chlorite, chloride-hydroxide, bisulphides, hydroxides, etc. have been proposed for gold transport. Most of the calculations are based on insufficient available thermodynamic data from Seward (1973), Helgeson (1969), and Shenberger and Barnes (1989), and in some cases the thermodynamic data may not agree with the experimental work. For example the stability constants given by Helgeson (1969) for $AuCl_2^-$ appear to be 5 to 10 orders of magnitude lower than those estimated by Cole and Drummond (1986) and Wood *et al.* (1987). This indicates either the importance of species other than $AuCl_2^-$ or simply inaccurate thermodynamic data.

Seward (1984*b*) proposed that Au $(HS)^0$, Au $(HS)_2^-$ and $Au_2(HS)_2S^{-2}$ are significant species in acidic to basic chloride-free solutions.

However Wood *et al.* (1987) suggested species $HAu(HS)_2^0$ as being the dominant gold bisulphide complex at a pH equal to 5 or less. Gold transport has also been considered as atomic gold (Au^0) or antimony and tellurium species (Wood *et al.*, 1987; Seward, 1984*b*). In general, bisulphide complexes appear to be more acceptable as dominant gold species (e.g. Au $(HS)^{-2}$, $HAu(HS)_2^{0)}$ in chloride-free solutions. The dependence of gold solubility on chloride concentration has been shown experimentally by Henley (1973) and Wood *et al.* (1987), and gold species such as Au_2Cl_6, $AuCl^0$, and $AuCl_2$ have been suggested.

The occurrence of pyrite and pyrrhotite, and lack of magnetite or hematite in the Lakeside Prospect indicates a reducing condition for the hydrothermal solution. Therefore ligands such as SO_4^{-2} and HSO_4^- are insignificant in transporting any metals. Complexes containing S_2^- and OH^- are only important at high concentration in very alkaline solutions, and cannot play a major role in the Lakeside deposit.

Antimony and tellurium species are probably not significant, as antimony sulphides or tellurides have not been observed.

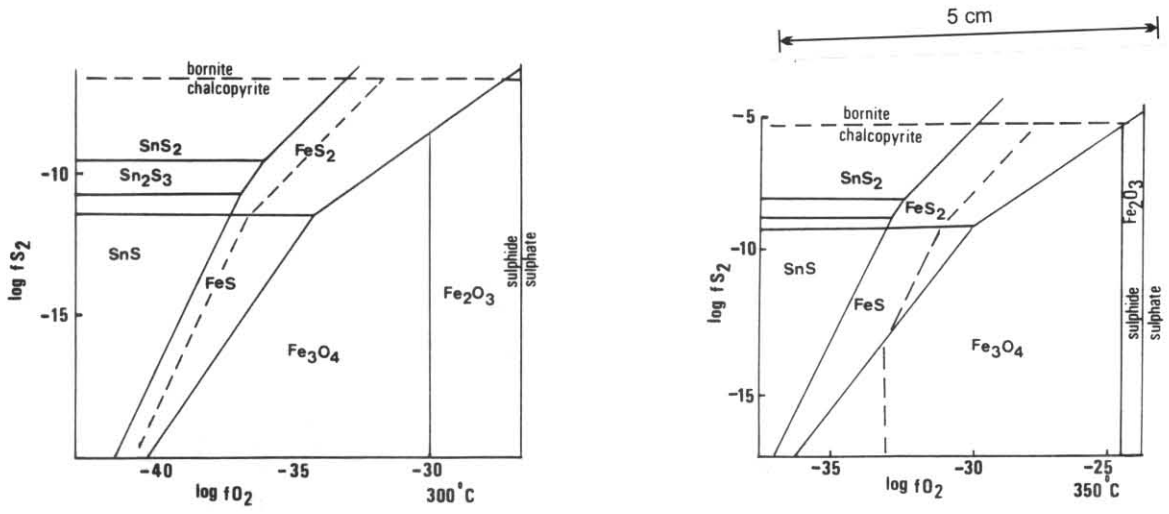

Figure 10. *Log fS_2–log fO_2 diagrams at 350 and 300°C for the Fe–O–S and Sn–O–S systems (pH=3). Dashed lines represent the stability field for reaction cassiterite + chalcopyrite = stannite + iron sulphides. Lines of different total sulphur in the H_2S stability field are shown by dashed-dotted lines.*

Carbonate and bicarbonate complexes do not appear to be important in gold transport as Au^+ is one of the softest metal ions and carbonate ions are very hard (Pearson, 1963; Crerar *et al.*, 1985). Therefore only chloride and bisulphide complexes appear to be contenders as the gold complexing agents for the Lakeside mineralisation.

pH-fO_2 diagrams with $Au(HS)_2^-$ and $AuCl_2^-$ solubility contours have been used to evaluate the chloride versus bisulphide complexes (e.g. Porter and Ripley, 1985; Phillips and Groves, 1983; Huston and Large, 1987). These diagrams indicate that gold chloride complexing is favoured by acidic oxidising conditions. A drop in temperature and/or fO_2, and an increase in pH causes the deposition of gold. However a decrease in pH or increase in fO_2 favours the deposition of gold from bisulphide complexes.

Because muscovite is ubiquitous in the Farrell Slates at the Lakeside Prospect, the fluid must have been neutral to moderately acid. Reducing conditions are implied by the mineral assemblage pyrite-pyrrhotite-arsenopyrite-stannite. Pyrite and pyrrhotite appear to be in equilibrium which gives a $\log fS_2$=-9.6 at 350°C. A $\log fO_2$ of -30.7 is indicated from the equilibrium between arsenopyrite, as the most common sulphide mineral, and pyrrhotite. The pyrite, stannite, cassiterite and chalcopyrite assemblage also gives a similar $\log fO_2$ of -31 at $\log fS_2$ of -9.6, (fig. 10; Appendix 6).

The occurrence of sericite in the Farrell Slates may suggest a pH of <-5. However there are no appropriate mineral assemblages to tightly define the pH of the mineralising fluid, and the solubility of gold in both chloride and bisulphide solutions (as $AuCl_2^-$ and $Au(HS)_2^-$) is strongly pH dependent. Considering the likely depositional conditions of the main stage of mineralisation at the Lakeside Prospect (i.e. T=350°C, $fO_2=10^{-31}$, $aH_2S=10^{-2}$ and assuming $aCl^-=0.3$; Appendix 6), a change in pH of the fluid from 3 to 5 decreases the solubility of gold as the chloride complex from 5 to 5×10^{-2} ppb, whereas the gold solubility in a bisulphide complex increases from 2×10^{-1} to 2×10^{-3} ppb. If gold was transported dominantly as a chloride complex prior to boiling, boiling of the mineralising solution would have provided an effective mechanism to precipitate gold as the temperature dropped and/or pH increased.

Tin transport and deposition

Tin is likely to be transported in its lower valency state (Sn^{+2}) in the aqueous phase, similar to copper and iron as described by Crerar and Barnes (1976).

Different complexes and/or physicochemical conditions have been suggested for transport of tin in hydrothermal solutions (Mulligan, 1975; Klintsova *et al.*, 1975; Patterson *et al.*, 1981; Eadington and Gilbin, 1979; Wilson and Eugster, 1984; Bloom and Wall, 1984). However hydroxyl, fluoro and chloro complexes appear to be more important in the transport of tin in hydrothermal solutions.

At the Lakeside deposit, sulphate complexing is negligible as ore deposition occurred under conditions in which reduced sulphur species predominated. Sulphide complexes are also insignificant, as they become unstable at elevated temperatures. Patterson *et al.* (1981) showed that hydroxyl complexing becomes important at very low fO_2 or very alkaline conditions, and is unlikely to play a major role in hydrothermal tin transport. Fluoride complexes are only significant at low pH and high fluorine concentration. Chloride complexing appears to be the most effective mechanism of tin transport under conditions of low pH and low fO_2 (Eadington and Gilbin, 1979; Patterson *et al.*, 1981), similar to the conditions under which the main stage of mineralisation was formed at the Lakeside Prospect. $SnCl_2^0$ is likely to be the most significant complex in solution in equilibrium with cassiterite. The boiling of the fluid during the main stage of mineralisation (fluid inclusion data) resulted in a drop in temperature, increase in pH and fO_2, and consequently deposited cassiterite in the Lakeside prospect (i.e. $SnCl_2+H_2O+\frac{1}{2}O_2 \Rightarrow SnO_2+2HCl$).

Stannite is stable with increasing ΣS and fS_2 at a given temperature. The field of stannite stability increases more relative to cassiterite within the pyrite-pyrrhotite field (fig. 10). Stannite becomes less stable with decreasing temperature (fig. 10), and below 300°C tin is likely to be present as tin sulphide and/or cassiterite (e.g. DC Orefield China, Zhengen and Xilin, 1982).

At the Lakeside Prospect, cassiterite precipitation predates the formation of stannite. This indicates:

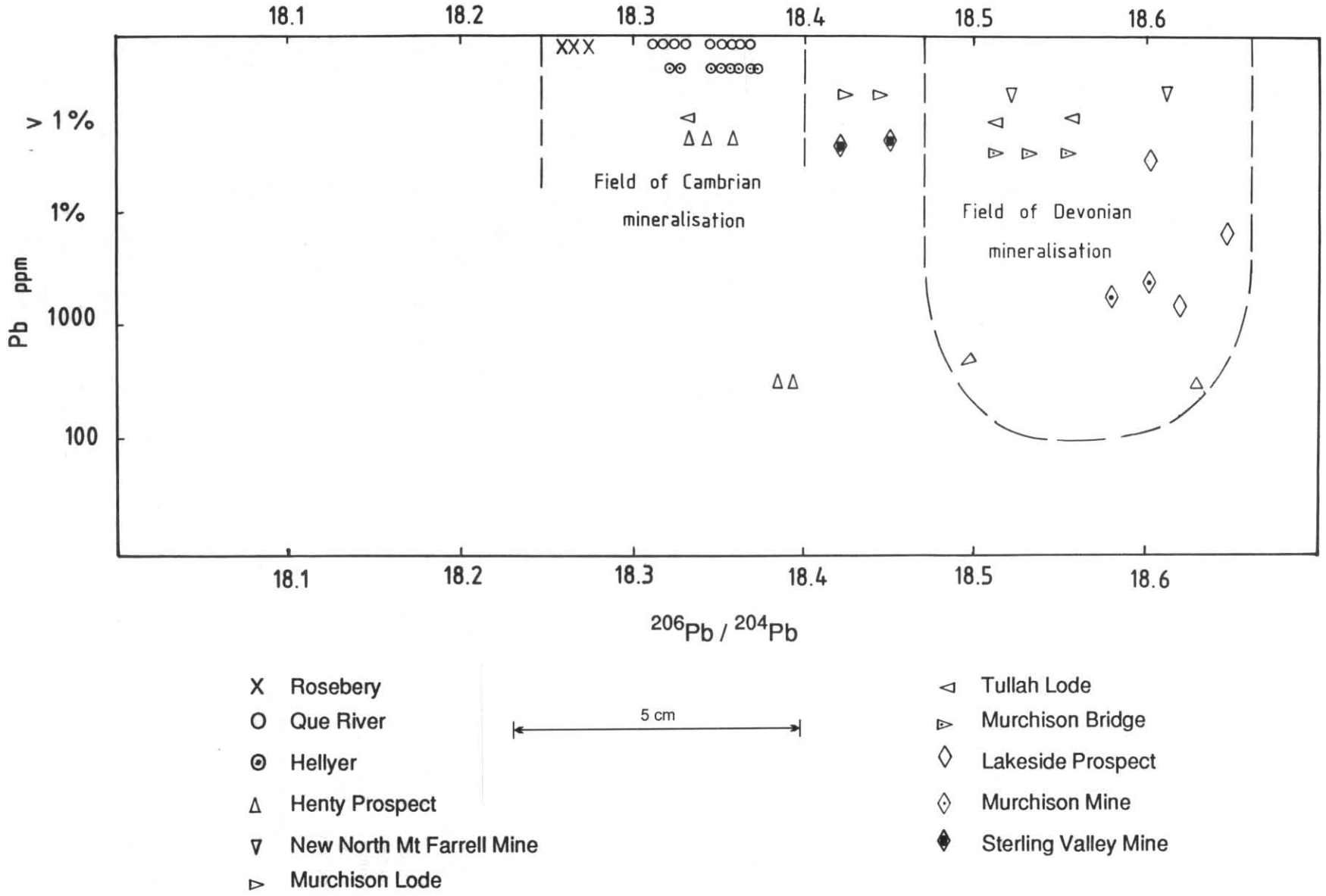

Figure 11. *$^{206}Pb/^{204}Pb$ vs lead concentration (ppm) for the Lakeside Prospect, Sterling Valley, and Murchison mines (Carr, 1988), together with representative data from Cambrian massive sulphide deposits and vein type post-Cambrian mineralisation (Gulson and Porritt, 1987), western Tasmania.*

(a) an increase in fS_2 and ΣS_2 of the fluids, and

(b) that the temperature probably stayed the same at this stage of mineralisation.

A temperature range of 300 to 350°C appears to be common for the deposition of tin minerals in most of the hydrothermal tin mineralisation in Tasmania (Patterson, 1981; Halley, 1982, 1987; this study).

Low salinity, CO_2-rich fluid and fluid immiscibility have also been described by Collins (1981) and Halley (1982, 1987) from the Cleveland tin deposit, and the Lutwyche Vein System and Mt Bischoff tin deposit respectively. An immiscibility relationship may be inferred from the description of the fluid inclusions in Stage 1 mineralisation at the Cleveland tin deposit, but was not recognised by Collins (1981). Consequently, a pressure correction of ~150°C was added to the actual homogenisation temperatures of these inclusions. Based on the description of the fluid inclusions, their behaviour upon heating, and homogenisation temperatures, the authors believe that temperatures of around 310°C represent the true formation temperature, as a pressure correction is not required for trapped immiscible fluids. If this is true, then formation temperatures for the Cleveland tin deposit will be in a good agreement with other tin deposits of Tasmania. Boiling appears to have been one of the most effective mechanisms for the deposition of tin minerals in a hydrothermal tin system, because the drop in temperature, increase in fO_2 and pH all favour the deposition of tin in hydrothermal solutions (Patterson *et al.*, 1981).

Lead isotope data.

Lead isotopes are informative in differentiating the ore deposits of different origins (Cannon *et al.*, 1961, 1971; Doe *et al.*, 1979; Gulson, 1984*b*; Gulson *et al.*, 1987; Gulson and Porritt, 1987). Gulson and Porritt (1987) showed that Cambrian volcanogenic-associated deposits (e.g. Rosebery, Que River, Hellyer) have relatively uniform isotope compositions throughout the deposits, and are different in $^{206}Pb/^{204}Pb$ by one percent from deposits which are related to the Devonian to Carboniferous granites and/or Tabberabberan metamorphism.

Recent lead isotope data (Carr, 1988) from the Sterling Valley Mine, Lakeside Prospect, Murchison and New North Farrell mines (Appendix 7) are in good agreement with the mineralogical studies and sulphur isotope data along the Henty Fault. In general, the lead isotope compositions for mineral deposits associated with the Henty Fault are more radiogenic (i.e. higher $^{206}Pb/^{204}Pb$) than Cambrian mineralisation, and plot in the Devonian mineralisation field of Gulson and Porritt (1987) (fig. 11, Appendix 7). The lead isotope composition of deposits such as the Sterling Valley Mine, in which the sulphur was partially derived from dissolved Cambrian sulphide and/or sulphate, plot between the Cambrian and Devonian mineralisation fields, whereas the lead isotope composition at the Lakeside Prospect, with a magmatic-dominated sulphur source, is most radiogenic along the Henty Fault Zone (fig. 11).

Granite Tor and its bearing on the mineralisation along the Henty Fault Zone

Recent gravity data (Leaman, 1986; Leaman and Richardson, 1989; Archer, 1989) revealed that the Granite Tor Granite is a large body at shallow depth, and that only a small part of the granite is exposed at Granite Tor. No detailed geological and/or petrochemical studies have been undertaken on this granite. Two shallow ridges of the granite extend to the WSW from Granite Tor, and NE from Mt Pelion to the Dolcoath Granite (fig. 12). Minor Cu, Sn, and W mineralisation is associated with the NE-trending granite spine (MacLeod *et al.*, 1961) where the body is irregular or offset, possibly reflecting pre-existing or Devonian faults.

The WSW-trending granite ridge extends from the Granite Tor Granite to the Pine Hill Granite, and possibly as far west as the Heemskirk Granite.

Prior to the gravity interpretations, the possible involvement of a Devonian granite in the formation of mineralised areas extending from Tullah to the Heemskirk Granite had been suggested (e.g. Solomon, 1965; Polya *et al.*, 1986). This was based on the occurrence of a number of tin and tourmaline-bearing deposits, as well as the Pb-Zn-Ag vein deposits within the zone of the WSW-trending granite ridge (fig. 12). Some of these deposits are closely associated with major faults (e.g. Henty Fault and Rosebery Fault), indicating the direct involvement of the granite ridge in the formation and/or remobilisation of the deposits along the pre-existing and/or Devonian faults.

The mineralisation and the $\delta^{34}S$ values of sulphide minerals associated with the Henty Fault are spatially zoned relative to the granite ridge (fig. 13). Polymetallic mineralisation with high temperature minerals (i.e. type 1 mineralisation) occurs right above the Granite Tor ridge, and is less than one kilometre from the ridge surface. These minerals are characterised by relatively low sulphur isotope values, which indicates the deriviation from a magmatic-dominated sulphur source. However Pb-Ag–dominated mineralised areas (i.e. type 2 mineralisation) are located away from the ridge at a greater height above the surface of the granite (e.g. > 3 km). The sulphur isotope composition of sulphides are relatively high (Table 4), and the involvement of a sedimentary Cambrian sulphur source is indicated in these deposits.

Mineralisation at the Henty Prospect may be genetically different to other deposits along the Henty Fault. It is unlikely to be related to the Granite Tor intrusion, as the granite is located at depths of more than 7 km in this area (Leaman and Richardson, 1989; fig. 13), and the lead isotope compositions (Gulson and Porritt, 1987) are very similar to most of the volcanic-associated deposits in western Tasmania (fig. 11). No detailed geological or petrochemical information is available for this gold deposit.

IMPLICATIONS FOR EXPLORATION

The association of the Lakeside and Sterling Valley Tin styles of mineralisation with the crest of the buried granite ridge connecting the Granite Tor and Pine Hill granites, together with the evidence described in this paper that the mineralisation was related to Devonian magmatism, effectively places constraints on the potential extent of Lakeside-type mineralisation along the Henty Fault Zone.

Although little information has been published on the Henty Prospect, the gravity modelling of Leaman and Richardson (1989) suggests that the granite lies at a depth of around 8 km, and the generally Cambrian lead isotope signatures at this prospect (Gulson and Porritt, 1987) suggest that Cambrian ore-forming processes may have been predominant. This indicates that there may be a number of distinctive mineralisation processes, and

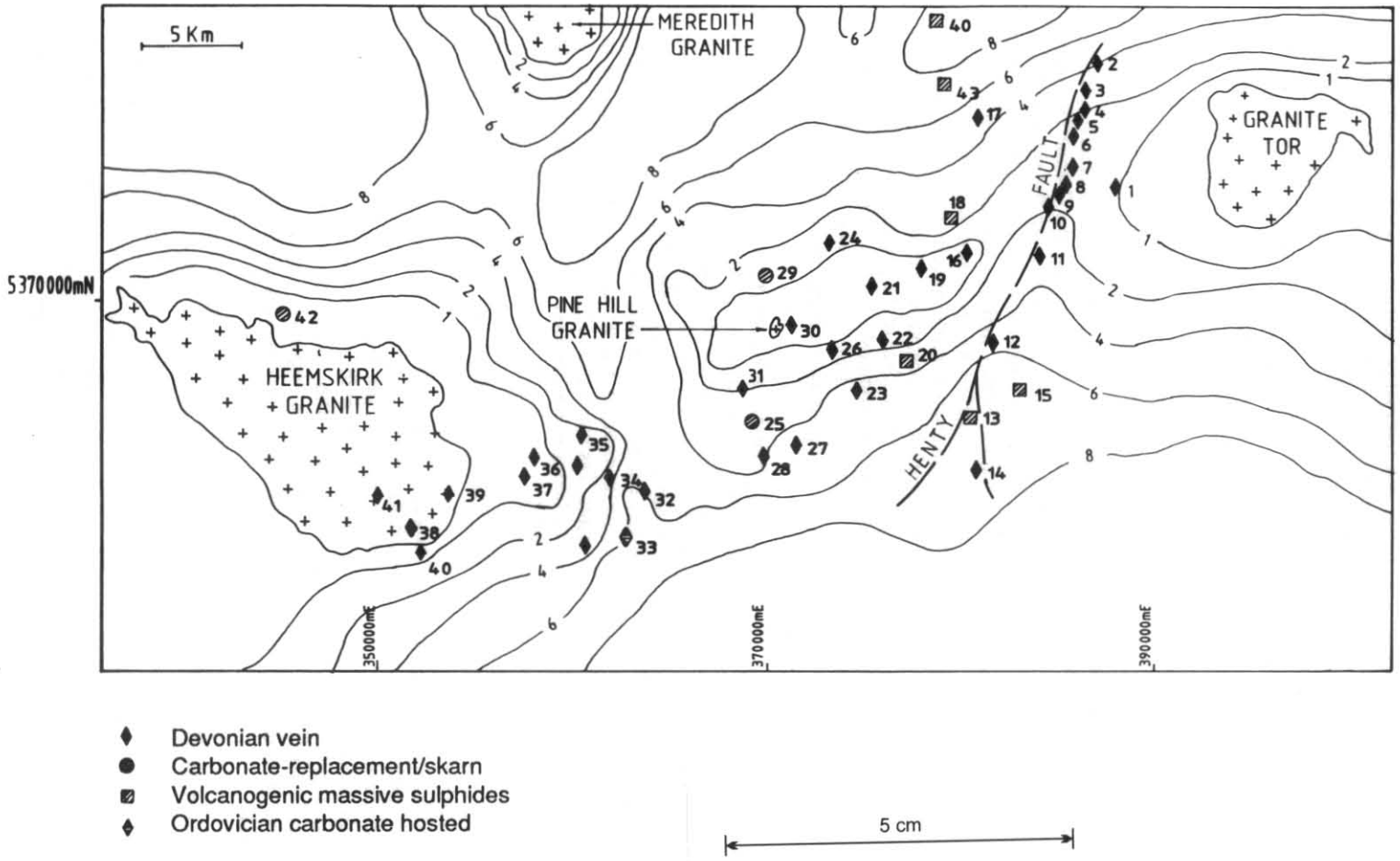

1 Osborne Copper (Cu, Pb, Ag)
2 Farrell Blocks (Pb, Cu)
3 Mackintosh Mine (Cu, Ag)
4 New North Mt Farrell (Pb, Ag, Zn)
5 North Mt Farrell (Pb, Ag)
6 Mt Farrell Mine (Pb, Ag, Zn)
7 Murchison River (Pb, Zn, Ag)
8 Murchison River Gold (Au, As, Pb, Zn)
9 Lakeside Prospect (As, Au, Sn, Pb, Zn)
10 Sterling Valley Tin (Sn, As, Zn)
11 Sterling Valley Mine (Pb, Ag)
12 Henty Fault Zone Copper (Cu)
13 Henty Fault Zone Gold (Zn, Pb, Au, Ag, Cu)
14 Tyndall Mine (Pb, Zn, Cu, Ag, As)
15 Red Hills (Zn, Pb, Ag, Au)
16 Great South Rosebery (Au, Cu, W)
17 Langdons Mine (Pb, Zn)
18 Rosebery (Zn, Pb, Cu, Ag, Au, Ba)
19 Chamberlain (Pb, Zn, Cu, Au)
20 Hercules (Zn, Pb, Cu, Ag, Au)
21 Olympic (Sn)
22 Hamilton Mine (Pb, Zn, Sn)
23 Moores Pimple (Ag, Cu)
24 Fenton (Sn)
25 Razorback (Sn)
26 Curtain Davis (Ag, Cu)
27 Comet (Pb, Zn, Ag)
28 Severn (Sn, Ag, Cu, Pb, Zn)
29 Renison Bell (Sn)
30 Pine Hill Tin (Sn)
31 Grand Prize (Sn, W)
32 Zeehan Bell (Pb, Ag)
33 Oceana (Pb, Ag)
34 Florence (Pb, Ag)
35 Zeehan Montana (Pb, Ag)
36 Sylvester (Pb, Zn, Ag)
37 Comstock (Pb, Zn, Ag)
38 Sweeney (Sn, Pb, Zn, Ag)
39 Globe (Pb, Zn, Sn, Ag)
40 Maynes (Sn)
41 Federation (Sn)
42 St Dizier (Sn)
43 Chester (Ba)
44 Pinnacles (Pb, Zn, Cu)

Figure 12. *Relationship between locations of Devonian veins and replacement deposits to subsurface granite ridge connecting the Heemskirk and Granite Tor granites. Contours are the inferred depth to the upper surface of the granite in kilometres. Compiled from Leaman and Richardson (1989), Green and Bamford (1986), McKibben (1968), Brooks (1962), and Blissett 1962).*

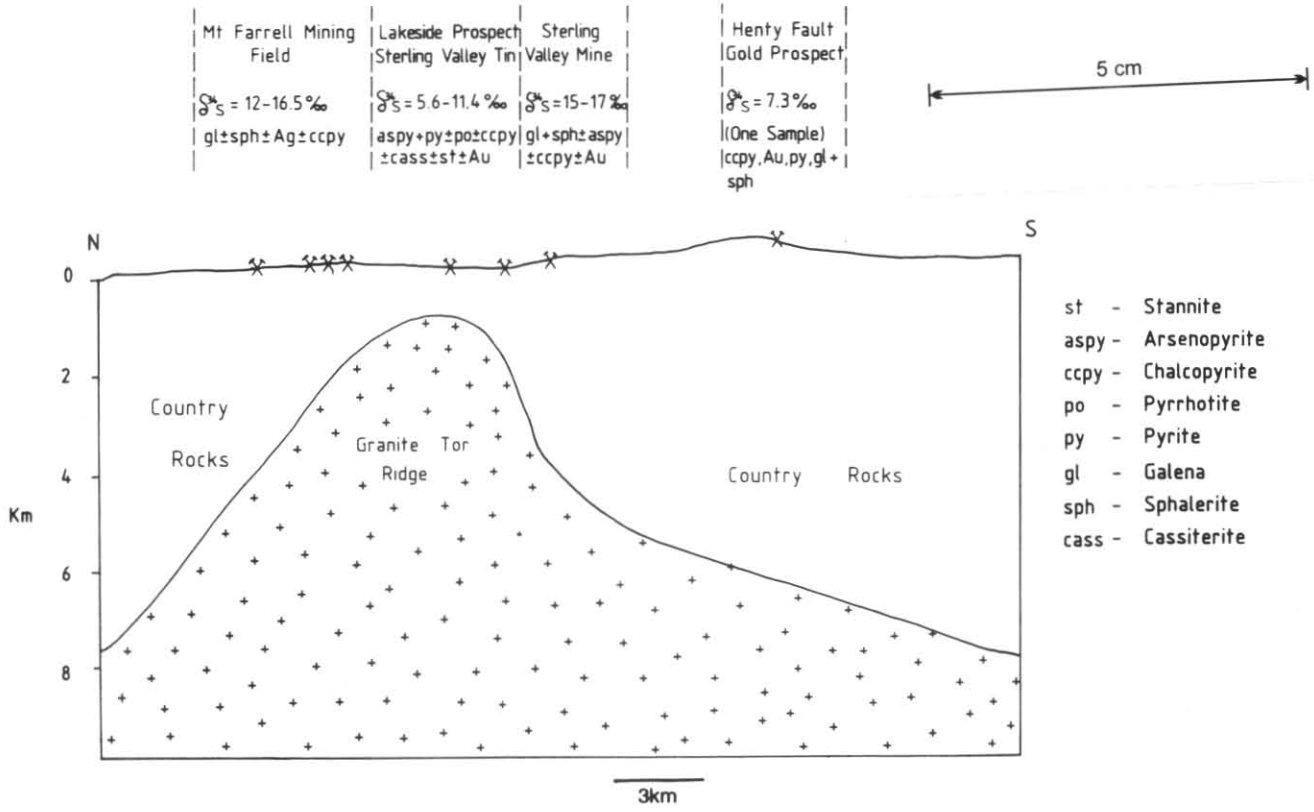

Figure 13. *Spatial relationships between $\delta^{34}S$ values and mineral assemblages, and the intrusion of the Granite Tor Granite along the Henty Fault, western Tasmania.*

consequently types of gold deposits, along the Henty Fault Zone.

Although the gold-tin association is rare in western Tasmania, it is also found in the Tin Spur area near Cethana (Bamford and Green, 1988), and other Devonian vein deposits hosted by, or in rocks overlying, the Mt Read Volcanics (e.g. Round Hill) contain significant gold credits (Green, *in press*). This is in contrast to the majority of Sn or Pb-Ag deposits in the Dundas Trough which are poor in gold. Similar mineralisation to the Lakeside deposit might be expected where the granite ridge is intersected by major faults, and there are similarities between Lakeside and some of the old prospects along the Rosebery Fault (e.g. Green and Bamford, 1986).

In the Tullah area, Berry (1989) suggested that the two major Devonian movements along the Henty Fault Zone were syn-mineralisation reverse dip-slip faulting and a later sinistral transcurrent movement, but he was unable to assess the magnitude of these displacements.

The metal zoning at the Lakeside Prospect and the Sterling Valley Tin Prospect may offer an important clue to the solution of this problem. At the Lakeside Prospect the highest gold values are found in pyrite-arsenopyrite-stannite-chalcopyrite veins which overlie, and possibly flank, a zone of pyrite-arsenopyrite-pyrrhotite-cassiterite mineralisation with lower gold values (i.e. higher temperature mineral assemblage). The Sterling Valley Tin Prospect contains even lower gold grades but has a higher As content, and pyrrhotite is a major mineral, consistent with a still deeper level of emplacement. The higher temperature of mineralisation at the Sterling Valley Tin area is also indicated by higher As contents of the arsenopyrite compared with those at the Lakeside Prospect (Appendix 2). The known strike length of mineralisation at both prospects is similar. It is therefore highly possible that the two sites of mineralisation were initially juxtaposed, and were later displaced relative to one another (fig. 14). Such a proposal is entirely consistent with Berry's (1989) reconstruction of the deformation history of the fault zone.

The extent of syn- and post-granite movement on the fault is limited by the lack of observable offset on the granite depth contours of Leaman and Richardson (1989) and Archer (1989), but their interpretations were imprecise because of lack of detail of the regional gravity survey (nominally one station per square kilometre). If our model is correct, the mineralogical evidence might suggest left-lateral movement of about 1100 m, and a more poorly constrained west-side up vertical movement of at least 250 metres. The fact that silver-lead vein deposits closer to Lakeside (e.g. Murchison River Mine) contain a high proportion of chalcopyrite and arsenopyrite, and also have anomalous gold values compared with more distal deposits (New North Mount Farrell), further supports our model.

Although the Lakeside Prospect contains sub-economic mineralisation, it is clear that the potential exists for further discoveries. On the western side of the fault the best targets for drilling for gold would be lateral to the Sterling Valley Tin Prospect. On the eastern side of the fault deeper areas adjacent to Lakeside might also be prospective. Any future exploration should use the Sterling Valley Tin and Lakeside data as constraints, bearing the following questions in mind:

(1) Is the depth to granite the prime factor governing the nature of the mineralisation? Do local granite cupolas play any role?

(2) Are cross structures important in focussing fluid flow during ore formation? If so, are there other potential sites for mineralisation along the segment of the Henty Fault underlain by the granite ridge?

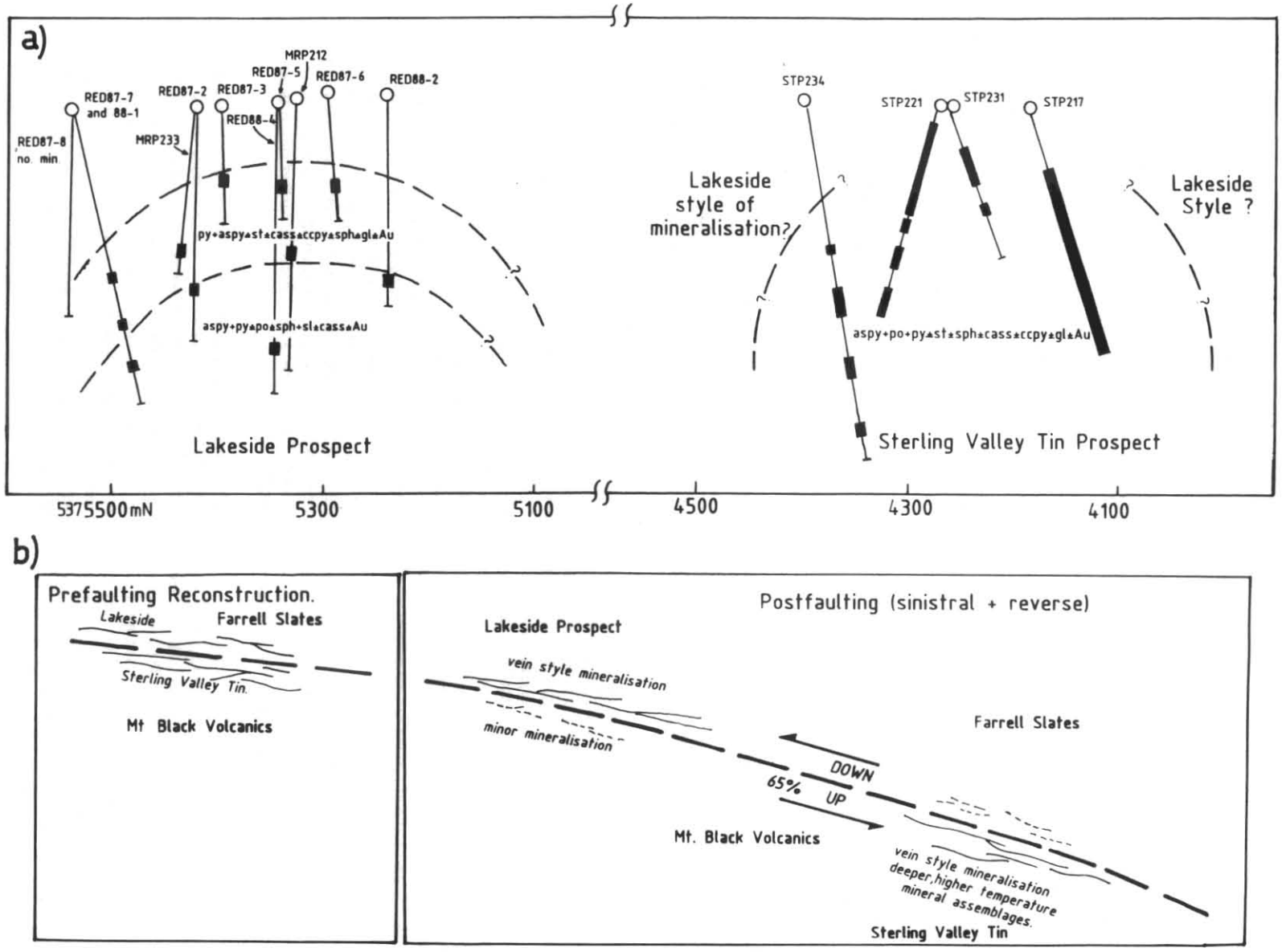

Figure 14. *Metal zoning (14a) and suggested pre-faulting construction (14b) for the Lakeside Prospect and Sterling Valley Tin Prospect.*

5 cm

In conclusion, we would suggest that more detailed geophysical surveys combined with structural, and possibly remote sensing interpretations, should assist in the definition of drilling targets. Detailed mineralogical and fluid inclusion studies of drill core should further guide exploration.

CONCLUSIONS

1. The mineralisation is related to the Granite Tor Granite, although lithological input for S (and Au?) might be important (textural, mineralogical, Pb, S, O isotope and fluid inclusion data).

2. The mineralisation was formed from boiling of reduced magmatic-dominated fluids at a temperature of about 340°C. The Au-Sn association is a result of temperatures sufficiently high for Cl complexes to have played a significant (and possibly major) role in Au transport.

3. More than one style of Au mineralisation may exist along the Henty Fault.

4. The Sterling Valley Sn and Lakeside systems may have originally occupied adjacent areas on either side of the fault. The latter represents a shallower part of the system. This is consistent with the independent structural interpretation of the Henty Fault Zone by Berry (1989). Lithological control in the form of favourable source rocks (Mt Read Volcanics) may also have been important.

   However under the low oxygen fugacity conditions of the mineralisation gold transport is not particularly favoured. Because of the high temperatures involved gold transport was probably mainly effected by chloride complexes. Boiling would have provided a very effective depositional mechanism under these conditions, and concentration of gold was probably optimised at the Lakeside Prospect. Therefore we consider it unlikely that an economically significant gold-only deposit might be found in the area.

ACKNOWLEDGEMENTS

We would like to express our appreciation for the support and co-operation of Billiton and Pasminco, particularly the Regional Exploration Manager David Hall, and geologists Jeff Randell, Geoff Iliff, Steve Hunns and, in particular, Ian Gordon for making core and some thin sections available for this study.

Our appreciation is also extended to colleagues in the Department of Mines; Janine Triffett and Jane Mackey (Lapidary); David Ferguson and Robert Turvey (Drafting); Richie Woolley (sulphur isotope determinations); and Michael Power (oxygen isotope determinations), for their support and cheerful and co-operative assistance.

We wish to thank Ralph Bottrill for the valuable discussions, and David Duncan for his support throughout the project.

We also thank Lisa Doran, Jan Howie, Michael Dix and James Nye for typing and editing the manuscript.

Finally, this research would not have been possible without the insight and imaginative management of those who conceived the MRV project, particularly M. R. Hargreaves and the present and past Governments of Tasmania, who have recognised the importance of this richly-endowed terrain.

REFERENCES

ADAMS, C. J.; BLACK, L. P.; CORBETT, K. D.; GREEN, G. R. 1985. Reconnaissance isotope studies bearing on the tectonothermal history of early Palaeozoic and late Proterozoic sequences in western Tasmania. *Aust. J. Earth Science* 32:7–36.

ARCHER, D. 1989. *Geophysical interpretation of the Devonian granite complex and its relationship to mineralisation in western Tasmania.* B.Sc. (Hons) thesis, University of Tasmania : Hobart.

BAMFORD, A. L.; GREEN, G. R. 1988. Mt Read Volcanics Project 1:50 000 Metallic Mineral deposits map series. Sheet 8114-IV. Cethana. *Department of Mines, Tasmania.*

BARTON, P. B. 1984. Redox reactions in hydrothermal fluids, *in:* HENLEY, R. W.; TRUSEDELL, A. H.; BARTON, P. B.; WHITNEY, J. A. (ed.). Fluid-mineral equilibria in hydrothermal systems. *Rev. Econ. Geol.* 1:99–114.

BARTON, P. B.; TOULMIN, P. 1961. Some mechanisms for cooling hydrothermal fluids. *Prof. Pap. U.S. geol. Survey* 424-D:348–352.

BERRY, R. F. 1989. The history of movement on the Henty Fault Zone, western Tasmania: An analysis of fault striations. *Aust. J. Earth Science* 36:189–205.

BLOOM, M. S.; WALL, V. J. 1984. Aqueous chemistry of tin at 300°C, with applications to tin transport and cassiterite deposition in alumino-silicate host rocks. *Abstr. geol. Soc. Aust.* 12:64–65.

BOTH, R. A.; RAFTER; T. A.; SOLOMON, M.; JENSEN, M. L. 1969. Sulfur isotopes and zoning of the Zeehan mineral field, Tasmania. *Econ. Geol.* 64:618–628.

BOWERS, T. S.; JACKSON, K. J.; HELGESON, H. C. 1984. *Equilibrium activity diagrams for coexisting minerals and aqueous solutions at pressures and temperatures to 5 kb and 600 °C.* Springer Verlag : Berlin.

BOYLE, R. W. 1979. The geochemistry of gold and its deposits. *Bull. geol. Surv. Can.* 280

BROOKS, C. 1962. *Geology of the Tullah area.* B.Sc. (Hons) thesis, University of Tasmania : Hobart.

BURNHAM, C. W.; OHMOTO, H. 1980. Late-stage processes of felsic magmatism, *in:* ISHIHARA, S.; TAKENOUCHI, S. (ed.). Granitic magmatism and related mineralization. *Spec. Issue min. Geol. (Japan)* 8:1–11.

CANNON, R. S.; PIERCE, A. P.; ANTWEILER, J. C.; BUCK, K. L. 1961. The data of lead isotope geology related to problems of ore gensis. *Econ. Geol.* 56:1–38.

CANNON, R. S.; PIERCE, A. P.; ANTWEILER, J. C. 1971. Suggested uses of lead isotopes in exploration. *Spec. Vol. Can. Inst. Min. Metall.* 11:457–463.

CARR, G. R. 1988. *Isotope compositions of exploration samples from the Mt. Read Volcanics, northwest Tasmania.* Unpublished Report to Billiton Aust., Burnie, Tasmania.

CATHELINEAU, M.; NIEVA, D. 1985. A chlorite solid solution geothermometer; the Los Azufres (Mexico) geothermal system. *Contrib. Mineral. Petrol.* 91:235–244.

CLARK, L. A. 1960. The Fe-As-S system phase relations and applications. *Econ. Geol.* 55:1345–1381, 1631–1652.

CLAYTON, R. N.; O'NEIL, J. R.; MAYEDA, T. K. 1972. Oxygen isotope exchange between quartz and water. *J. Geophys. Res.* 77:3057–3067.

COLE, D. R.; DRUMMOND, S. E. 1986. The effect of transport and boiling on Ag/Au ratios in hydrothermal solutions: A preliminary assessment and possible implications for the formation of epithermal precious-metal ore deposits. *J. Geochem. Explor.* 25:45–80.

COLLINS, P. L. F. 1979. Gas hydrates in CO_2-bearing fluid inclusions and the use of freezing data estimation of salinity. *Econ. Geol.* 74:1435–1444.

COLLINS, P. L. F. 1981. The geology and genesis of the Cleveland tin deposit, western Tasmania: Fluid inclusion and stable isotope studies. *Econ. Geol.* 76:365–392.

COLLINS, P. L. F.; GULLINE, A. B.; WILLIAMS, E. 1981. Geological atlas 1 mile series. Sheet 44 (8014N). Mackintosh. *Explan. Rep. geol. Surv. Tasm.*

CORBETT, K. D. 1981. Stratigraphy and mineralisation in the Mt Read Volcanics, western Tasmania. *Econ. Geol.* 76:209–230.

CORBETT, K. D.; KOMYSHAN, P. 1989. Geology of the Hellyer–Mt Charter area. *Geol. Rep. Mt Read Volc. Proj. Tasm.* 1.

CORBETT, K. D.; LEES, T. C. 1987. Stratigraphic and structural relationships and evidence for Cambrian deformation at the western margin of the Mt Read Volcanics, Tasmania. *Aust. J. Earth Science* 34:45–67.

CORBETT, K. D.; McNEILL, A. W. 1986. Mt Read Volcanics Project 1:25 000 Series. Map 2. Geology of the Rosebery—Mt Block area. *Department of Mines, Tasmania.*

CRAWFORD, M. L. 1981. Phase equilibria in aqueous fluid inclusions, *in:* HOLLISTER, L. S.; CRAWFORD M. L. (ed.). *Short course in fluid inclusions: Applications to petrology.* 75–100. Mineralogical Association of Canada : Calgary.

CRERAR, D. A.; BARNES, H. L. 1976. Ore solution chemistry v. solubilities of chalcopyrite and chalcocite assemblages in hydrothermal solution at 200° to 350°C. *Econ. Geol.* 71:772–794.

CRERAR, D. A.; WOOD, S. A.; BRANTLEY, S. L.; BOCARSLY, A. 1985. Chemical controls on solubility of ore-forming minerals in hydrothermal solutions. *Can. Mineral.* 23:333–352.

DOE, B. R.; STEVENS, T. A.; DELEVAUX, M. H.; STACEY, J. S.; LIPMAN, P. W.; FISHER, F. S. 1979. Genesis of ore deposits in the San Juan volcanic field, southwestern Colorado—lead isotope evidence. *Econ. Geol.* 74:1–26.

DRUMMOND, S. E. 1981. *Boiling and mixing of hydrothermal fluids: Chemical effects on mineral precipitation.* Ph.D. thesis, Pennsylvania State University.

DRUMMOND, S. E.; OHMOTO, H. 1985. Chemical evolution and mineral deposition in boiling hydrothermal systems. *Econ. Geol.* 80:126–147.

EADINGTON, P. J.; GIBLIN, A. 1979. Alteration minerals and the precipitation of tin in granitic rocks. *Tech. Comm. CSIRO Inst. Earth Res.* 68.

EASTOE, C. J. 1978. A fluid inclusion study of the Panguna Porphyry copper deposit, Bougainville, Papua New Guinea. *Econ. Geol.* 73:721–748.

ELLIS, A. J.; GOLDING, R. M. 1963. The solubility of carbon dioxide above 100°C in water and in sodium chloride solutions. *Am. J. Sci.* 261:47–60.

FLEET, M. E.; MACLEAN, P. J.; BARBIER, J. 1988. Oscillatory-zoned As-bearing pyrite from stratabound gold deposits: Evidence for primary mineralisation. *Abstr. geol. Soc. Aust.* 22.

FOURNIER, R. O. 1983. Self-sealing and brecciation resulting from quartz deposition within hydrothermal systems. *International Conference on Water-Rock interaction, Tokyo, Japan. Extended Abstracts.* 137–140.

GEHRIG, M. H.; LENTZ and FRANK, E. U. 1979. Thermodynamic properties of water carbon dioxide - sodium chlorite mixture at high temperatures and pressures, *in:* TIMMERHAUS, K. D.; BARBER, M. S. (ed.). *International conference on high pressure science and technology (6th, 1977 Univ. of Colorado): Vol. 1 physical properties and material synthesis.* 539–542. Plenum Press : New York.

GREEN, G. R.; BAMFORD, A. L. 1986*a*. Mt Read Volcanics Project. 1:50 000 Metallic Mineral Deposits map series. Sheet 8014-III. Rosebery. *Department of Mines, Tasmania.*

GREEN, G. R.; BAMFORD, A. L. 1986*b*. Mt Read Volcanics Project. 1:50 000 Metallic Mineral Deposits map series. Sheet 8014-IV. Tullah. *Department of Mines, Tasmania.*

GREEN, G. R.; SOLOMON, M.; WALSHE, J. L. 1981. The formation of the volcanic-hosted massive sulfide ore deposit at Rosebery, Tasmania. *Econ. Geol.* 76:304–338.

GULSON, B. L. 1984. Assessment of massive sulfide base metal targets using lead isotopes in soils. *J. Geochem. Explor.* 24:291–313.

GULSON, B. L.; LARGE, R. R.; PORRITT, P. M. 1987. Base metal exploration of the Mount Read Volcanics, western Tasmania: Pt. III. Application of lead isotopes at Elliott Bay. *Econ. Geol.* 82:308–327.

GULSON, B. L.; PORRITT, P. M. 1987. Base metal exploration of the Mount Read Volcanics, western Tasmania: Pt II. Lead isotope signatures and genetic implications. *Econ. Geol.* 82:291–307.

HALL, G.; COTTLE, V. M.; ROSENHAIN, P. B.; McGHIE, R. R. 1953. The lead-zinc deposits of Read-Rosebery and Mount Farrell. *Publs. 5th emp. min. metall. Cong.* 1:1145–1159.

HALL, D. B.; CREAGH, C. J.; HUNGERFORD, N. 1988. *Exploration Licence 1/62, annual report to 22 January 1989.* Billiton Australia Ltd [TCR 88-2895].

HALL, D. B.; RANDELL, J. P.; HUNGERFORD, N. 1987. *Exploration Licence 1/62. Annual report on work completed 23 January 1987 to 22 January 1988.* Billiton Australia Ltd [TCR 85-2751].

HALL, D. B. 1988. *Exploration Licence 1/62. Relinquishment report.* Billiton Australia Ltd [TCR 88-2899].

HALL, G.; SOLOMON, M. 1962. Metallic mineral deposits, *in:* SPRY, A. H.; BANKS, M. R. The geology of Tasmania. *J. geol. Soc. Aust.* 9(2):285–309.

HALLEY, S. W. 1982. *A fluid inclusion study of the Lutwyche vein system, Rossarden.* B.Sc.(Hons) Thesis, University of Tasmania : Hobart.

HALLEY, S. W. 1987. *Genesis of Mt Bischoff tin deposit* Ph.D. Thesis, Australian National University : Canberra.

HEINRICH, C. A.; EADINGTON, P. J. 1986. Thermodynamic predictions of the hydrothermal chemistry of arsenic, and their significance for the paragenetic sequence of some cassiterite-arsenopyrite base metal sulfide deposits. *Econ. Geol.* 81:511–529.

HELGESON, H. C. 1969. Thermodynamics of hydrothermal systems at elevated temperatures and pressures. *Am. J. Sci.* 267:729–804.

HENLEY, R. W. 1973. Solubility of gold in hydrothermal chloride solutions. *Chem. Geol.* 11:73–87.

HIDDEN, W. E., 1882. A phenomenal find of fluid-bearing quartz crystals. New York. *Trans. Acad. Sci.* 1881–1882 (1):131–136.

HOLLISTER, L. S.; BURRUSS, R. C. 1976. Phase equilibria in fluid inclusions from the Khtada Lake metamorphic complex. *Geochim. Cosmochim. Acta.* 40:163–175.

HOLLISTER, L. S.; CRAWFORD, M. L. (ed.). 1981. *Short course in fluid inclusions: Applications to petrology.* Mineralogical Association of Canada : Calgary.

HOLLOWAY, J. R. 1976. Fluids in the evolution of granitic magmas: Consequences of finite CO_2 solubility. *Bull. geol. Soc. Am.* 87:1513–1518.

HUSTON, D. L.; LARGE, R. R. 1987. *A chemical model for the concentration of gold in volcanogenic massive sulphide deposits.* University of Tasmania, Hobart.

JENSEN, H. E. 1959. *Examination of Farrell Mining Company's properties at Tullah, Tasmania.* Rio Tinto Australia Exploration Pty Ltd. 20/1959 [TCR 59-299].

KLINSTOVA, A. P.; BARSUKOV, V. L.; SHEMARYKINA, T. P.; KHODAKOVSKIY, I. L. 1975. Measurement of the stability constants for Sn(IV) hydroxofluoride complexes. *Geochem. Internat.* 12:207–215.

KRETSCHMAR, U.; SCOTT, S. D. 1976. Phase relations involving arsenopyrite in the system Fe-As-S and their application. *Can. Miner.* 14:364–386.

KRANIDIOTIS, P.; MACLEAN, W. H. 1987. Systematics of chlorite alteration at the Phelps Dodge massive sulfide deposit, Matagami, Quebec. *Econ. Geol.* 82:1898–1911.

LEAMAN, D. E. 1986. Gravity interpretation, west and north west Tasmania. *Geophys. Rep. Mt Read Volcanics Project Dep. Mines. Tasm.* 3.

LEAMAN, D. E.; RICHARDSON, R. G. 1989. The granites of west and north-west Tasmania—a geophysical interpretation. *Bull. geol. Surv. Tasm.* 66.

MacLEOD, W. N.; JACK, R. H.; THREADER, V. M. 1961. One mile geological map series. K55-11-52. Du Cane. *Explan. Rep. geol. Surv. Tasm.*

MALININ, S. D. 1959. The system water–carbon dioxide at high temperatures and pressures. *Geochemistry* 3:292–305.

McDONALD, I. R. 1985. *Exploration Licence 4/73–Sterling Valley. Annual report on exploration activity 2 May 1984 to 6 March 1985.* Electrolytic Zinc Company of Australia Ltd T202 [TCR 85-2347].

McNEILL, A. W. 1987. Mt Read Volcanics Project 1:25 000 Series. Map 4. Geology of the Mt Murchison area. *Department of Mines, Tasmania.*

MEYER, M.; SAAGER, R. 1985. The origin of gold in Archaean epigenetic gold deposits. *Inf. Circ. Uni. Witwatersrand Econ. Geol. Res. Unit* 172.

MILL, J. H. A.; McDONALD, I. R.; WEEDEN, R. J. 1980. *Mt Black Exploration Licence 1/62. Report on work undertaken 30 June 1979 to 30 June 1980.* Electrolytic Zinc Company, Geology Department Report 134 [TCR 80-1468].

MULLIGAN, R. 1975. Geology of Canadian tin occurrences. *Econ. Geol. Rep. geol. Surv. Can.* 28.

MURRAY, R. C.; CUBICIOTTI, D. 1983. Thermodynamics of aqueous sulphur species to 300°C and potential-pH diagrams. *J. Electrochem. Soc.* 130:866–869.

NIKOLAEVA, N. M.; YERENBURG, A. M.; ANTIPINA, V. A. 1972. Temperature dependence of the standard potential of halide complexes of gold. *Isvest. Sib. Otd. Akad. Nauk SSR. Ser. Khim.* 4:126–129.

OSTIC, R. G.; RUSSELL, R. D.; STANTON, R. L. 1967. Additional measurements of the isotopic composition of lead from stratiform deposits. *Can. J. Earth Sci.* 4:245–269.

PATTERSON, D. J. 1979. *Geology and mineralisation at Renison Bell, Western Tasmania.* Ph.D. thesis, University of Tasmania : Hobart.

PATTERSON, J. D.; OHMOTO, H.; SOLOMON, M. 1981. Geologic setting and genesis of cassiterite-sulfide mineralization at Renison Bell, western Tasmania. *Econ. Geol.* 76:393–438.

PEARSON, R. G. 1963. Hard and soft acids and bases. *J. Am. Chem. Soc.* 85:3533–3539.

PHILLIPS, G. N.; GROVES, D. I. 1983. The nature of Archaean gold-bearing fluids as deduced from gold deposits of Western Australia. *J. geol. Soc. Aust.* 30:25–39.

PICHAVANT, M.; RAMBOZ, C.; WEISBROD, A. 1982. Fluid immiscibility in natural processes: Use and misuse of fluid inclusion data. Phase equilibria analysis—a theoretical and geometrical approach. *Chem. Geol.* 37:1–27.

POLYA, D. A.; SOLOMON, M.; EASTOE, C. J.; WALSHE, J. L. 1986. The Murchison Gorge, Tasmania—A possible cross-section through a Cambrian massive sulfide system. *Econ. Geol.* 81:1341–1355.

PORTER, E. W.; RIPLEY, E. 1985. Petrologic and stable isotope study of the gold-bearing breccia pipe at the Golden Sunlight deposit, Montana. *Econ. Geol.* 80:1689–1706.

POTTER, R. W.; BROWN, D. L. 1977. The volumetric properties of aqueous sodium chloride solutions from 0° to 500°C at pressures up to 2000 bars based on a regression of available data in the literature. *Bull. U.S. geol. Surv.* 1421-C.

POTY, B.; STALDER, H. A.; WEISBROD, A. M. 1974. Fluid inclusion studies in quartz from fissures of Western and Central Alps. *Schweiz. Mineral. Petrogr. Mitt.* 54:717–752.

PRIKAZCHIKOV, L. A. 1959. On tube canals in morion crystals of pegmatites from Volhynia. *Vses. Mineral Obshch. Zapiski.* 88:99–102 (in Russian).

RAMDOHR, P. 1969. *The ore minerals and their intergrowths.* Pergamon Press : London.

RANDELL, J. P.; PURVIS, J. G.; HUNGERFORD, N. 1986. *Rosebery East Joint Venture, Exploration Licence 1/62, west Tasmania. Progress report on exploration for the period ending 22 December 1986.* Billiton Australia, Electrolytic Zinc Company and Little River Pty Ltd [TCR 86-2622].

RANKIN, A. H.; GREENAWAY, F. 1978. Macroscopic inclusions of fluid in British fluorites from the mineral collection of the British Museum (Natural History). *Br. Mus. (Nat. Hist.) Bull. Geol.* 30:295–325.

RICHARDSON, L. A. 1951. *Geophysical survey of Mackintosh area, Tullah.* Electrolytic Zinc Co. Aust. Ltd.

RIPLEY, E. M. 1976. *Mineralogic, stable isotope, and fluid inclusion studies of the stratabound copper deposits at the Raul mine, Peru, South America*. Ph.D. thesis, Pennsylvania State University.

RIPLEY, E. M.; OHMOTO, H. 1977. Mineralogic, sulfur isotope, and fluid inclusion studies of the stratabound copper deposits at the Raul mine, Peru. *Econ. Geol.* 72:1017–1041.

ROBIE, R. A.; WALDBAUM, D. R. 1968. Thermodynamic properties of minerals and related substances at 298.15°K (25°C) and one atmosphere (1.013 Bars) pressure and at higher temperatures. *Bull. U.S. geol. Surv.* 1259.

ROBINSON, B. R.; KUSAKABE, M. 1975. Quantitative preparation of sulphur dioxide for $^{34}S/^{32}S$ analyses from sulphides by combustion with cuprous oxide. *Anal. Chem.* 47:1179–1181.

ROEDDER, E. 1977. Fluid inclusion studies of ore deposits in Viburnum Trend, southeast Missouri. *Econ. Geol.* 72:474–479.

ROEDDER, E. 1984. Fluid inclusions. *Reviews in Mineralogy* 12.

ROMBERGER, S. B. 1986. Mechanisms of deposition of gold in low-temperature hydrothermal systems (abstract). *J. Geochem. Explor.* 25:1237.

SAINTY, R. A.; MILL, J. H. A. 1982. *Exploration Licence 4/73. Progress report on activity 5 May to 24 August 1982*. Electrolytic Zinc Company, Geology Department Report 154MD [TCR 82-1844].

SEWARD, T. M. 1973. Thiocomplexes of gold and the transport of gold in hydrothermal ore deposits. *Geochim. Cosmochim. Acta*. 37:379–399.

SEWARD, T. M. 1984. The transport and deposition of gold in hydrothermal systems, *in:* FOSTER, R. P. (ed.). *Gold '82*. A. A. Bulkama Publications : Rotterdam.

SHERNBERGER, D. M.; BARNES, H. L. 1989. Solubility of gold in aqueous sulphide solutions from 150°C to 300°C. *Geochim. Cosmoch. Acta* 53:269–278.

SOLOMON, M. 1965. Lead-silver-zinc ore deposits at Mt Farrell. *Publs. 8th common. min. metall. Cong.* 1:490

SOLOMON, M. 1977. Metallic mineral deposits of the Pieman-Gordon region and the likelihood of new discoveries, *in:* BANKS, M. R.; KIRKPATRICK, J. B. (ed.). *Landscape and Man*. Royal Society of Tasmania : Hobart.

SOLOMON, M. 1981. An introduction to the geology and metallic ore deposits of Tasmania. *Econ. Geol.* 76:194–208.

SOLOMON, M.; EASTOE, C. J.; WALSHE, J. L.; GREEN, G. R. 1988. Mineral deposits and sulphur isotope abundances in the Mount Read Volcanics between Que River and Mount Darwin, Tasmania. *Econ. Geol.* 83:1307–1328.

SOLOMON, M.; RAFTER, T. A.; JENSEN, M. L. 1969. Isotope studies on the Rosebery, Mt Farrell and Mt Lyell ores, Tasmania. *Mineralium Deposita* 4:172–199.

SORBY, H. C. 1858. On the microscopic structure of crystals, indicating the origin of minerals and rocks. *Quart. J. geol. Soc. London*. 14 (1):453–500.

SOURIRAJAN, S. J.; KENNEDY, G. C. 1962. The system H_2O-NaCl at elevated temperatures and pressures. *Am. J. Sci.* 260:115–141.

SPOONER, E. T. C. 1980. Cu-pyrite mineralization and sea water convection in economic crust; the ophiolitic ore deposits of Cyprus, *in:* STRANGWAY, D. W. (ed.). The continental crust and its mineral deposits. *Spec. Pap. Geol. Assoc. Can.* 20:685–704.

TAHERI, J. 1985. *Origin of mineralisation in south Heemskirk Granite*. Ph.D. thesis, University of Tasmania : Hobart.

TAKENOUCHI, S.; KENNEDY, G. C.; 1965. The solubility of carbon dioxide in NaCl solutions at high temperatures and pressures. *Am. J. Sci.* 263:445–454.

TAKENOUCHI, S.; KENNEDY, G. C. 1964. The binary system H_2O-CO_2 at high temperatures and pressures. *Am. J. Sci.* 262:1055–1074.

TRUESDELL, A. H. 1974. Oxygen isotope activities and concentrations in aqueous salt solutions at the elevated temperatures: consequenceS for isotope geochemistry. *Earth Planet. Sci. Lett.* 23:387–396.

VAUGHAN, D. J.; CRAIG, J. R. 1978. *Mineral chemistry of metal sulfides*. Cambridge University Press : Cambridge.

WALSHE, J. 1986. A six-component chlorite solid solution model and the conditions of chlorite formation in hydrothermal and geothermal systems. *Econ. Geol.* 81:681–703.

WALSHE, J. L.; HEDGES, M. M.; HARROLD, B. P. 1986. Evaluating the conditions of chlorite formation in hydrothermal and geothermal systems (abstract). *Fifth international symposium on water-rock interaction, Int. Assoc. Geoch. and Cosmoch.* 5:605–609.

WILLIAMS, E. 1978. Tasman Fold Belt System in Tasmania. *Tectonophysics* 48:159–206.

WILLIAMS, E.; SOLOMON, M.; GREEN, G. R. 1976. The geological setting of metalliferous ore deposits in Tasmania. *Monogr. Ser. australas. Inst. Min. Metall.* 5:567–581.

WILSON, J. W. J.; KESLER, S. E.; CLOKE, P. L.; KELLY, W. C. 1980. Fluid inclusion geochemistry Granisle and Bell porphyry copper deposits, British Columbia. *Econ. Geol.* 75:45–61.

WILSON, G. A.; EUGSTER, H. P. 1984. Cassiterite solubility and tin-chlorite speciation in supercritical solutions. *Geol. Soc. Am. Abstr. with Prog.* 16:696.

WOOD, S. A.; CRERAR, D. A.; BORCSIK, M. P. 1987. Solubility of the assemblage pyrite-pyrrhotite-magnetite-sphalerite-galena-gold-stibnite-bismuthinite-argentite-molybdenite in H_2O-NaCl-CO_2 solutions from 200° to 350°C. *Econ. Geol.* 82:1864–1887.

ZHANG, Z.; LI, X. 1982. The mineralisation and composition of the DC mining region, Guangxi. *China. Geoch.* 1:355–368.

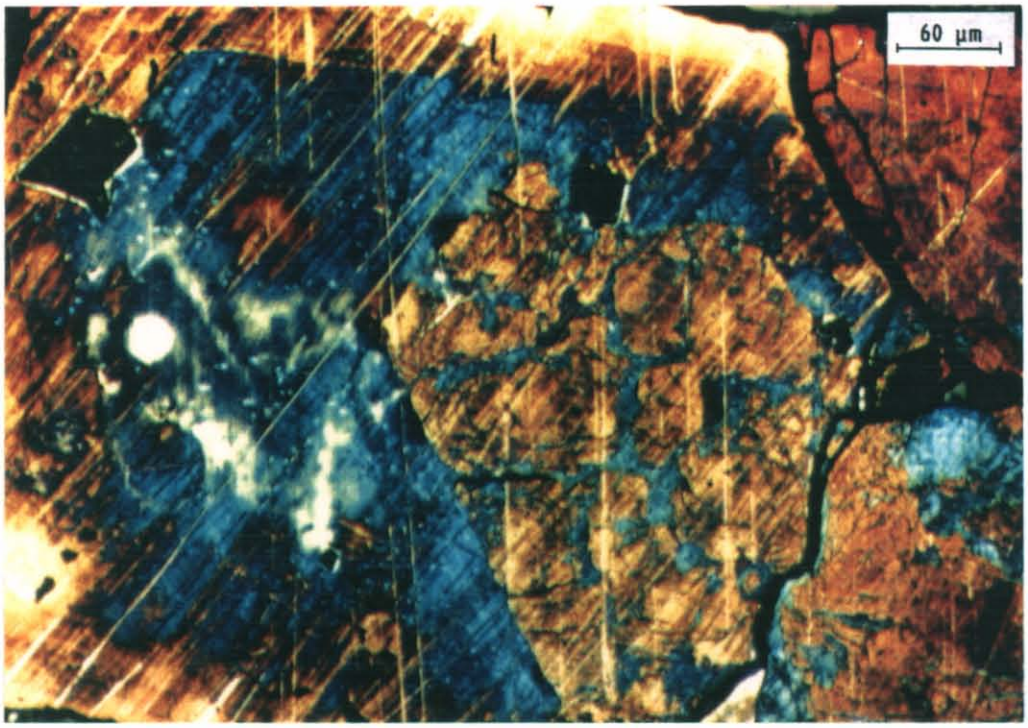

Plate 1. *Early-formed As-poor pyrite (yellow) is partially replaced and overgrown by As-rich pyrite (blue). Note the overgrowth of the second generation of low-As content pyrite (yellow) on high-As content pyrite (blue).*

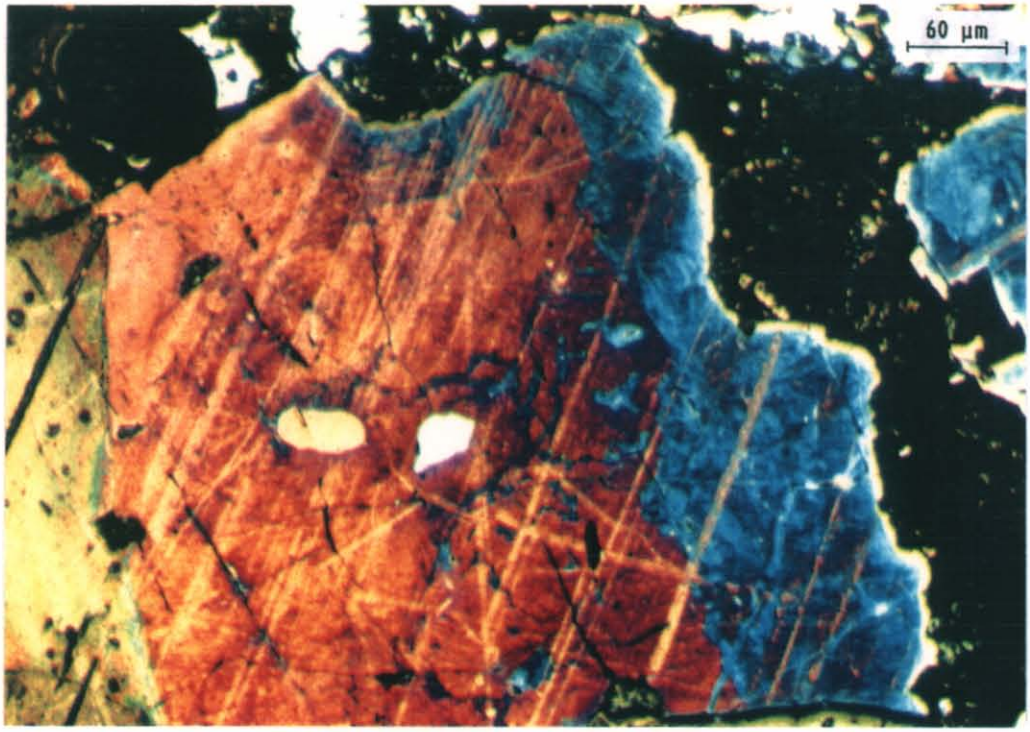

Plate 2. *Late-forming As-rich pyrite (blue) along fractures and on the surface of the As-poor pyrite (yellow-brown).*

5 cm

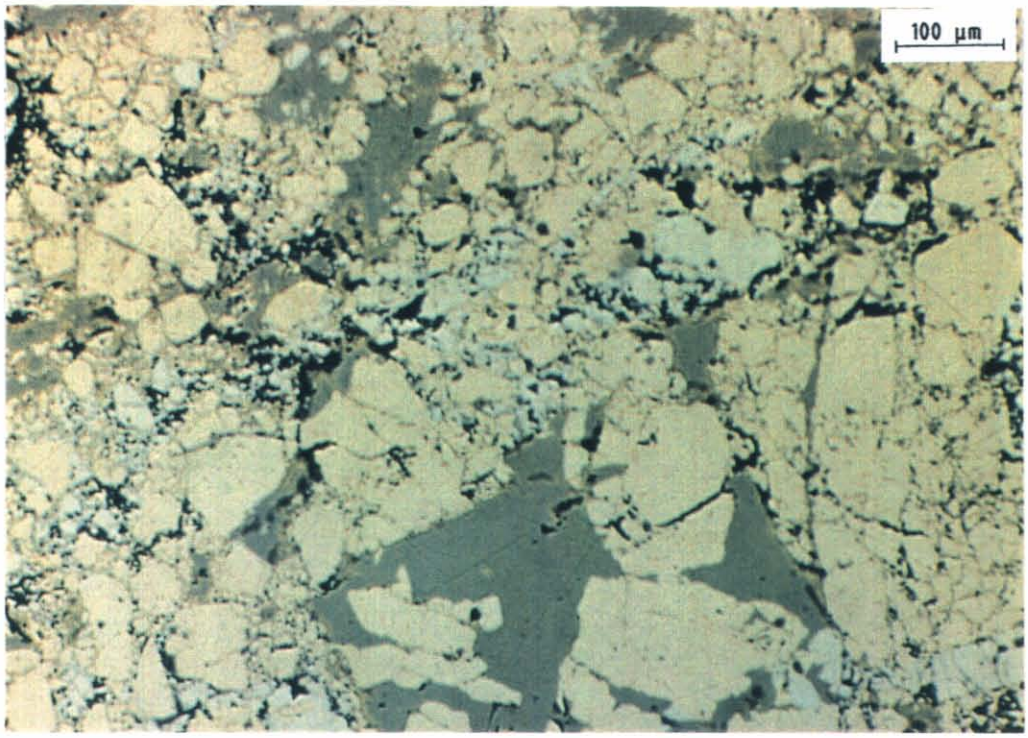

Plate 3. *Finely brecciated pyrite (cream) and arsenopyrite (white) healed by quartz and carbonate infillings.*

Plate 4. *Partial replacement of pyrrohtite (po) by pyrite (py) and carbonates (carb).*

5 cm

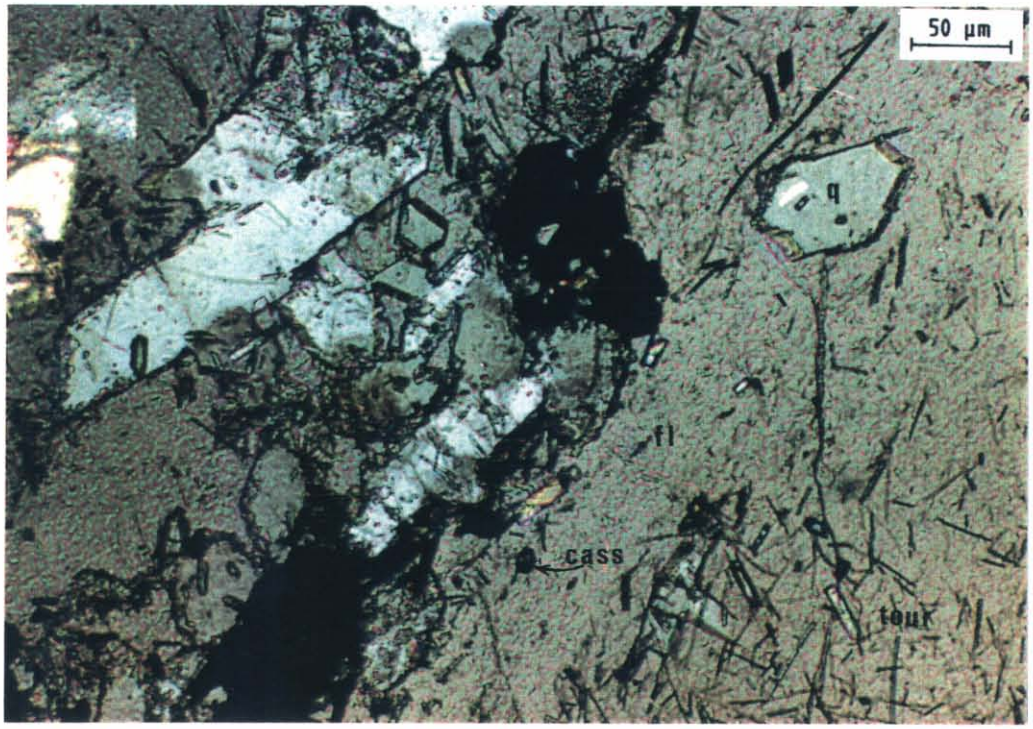

Plate 5. *Quartz (q), fluorite (fl), tourmaline (tour), arsenopyrite (black), and cassiterite (cass) assemblage.*

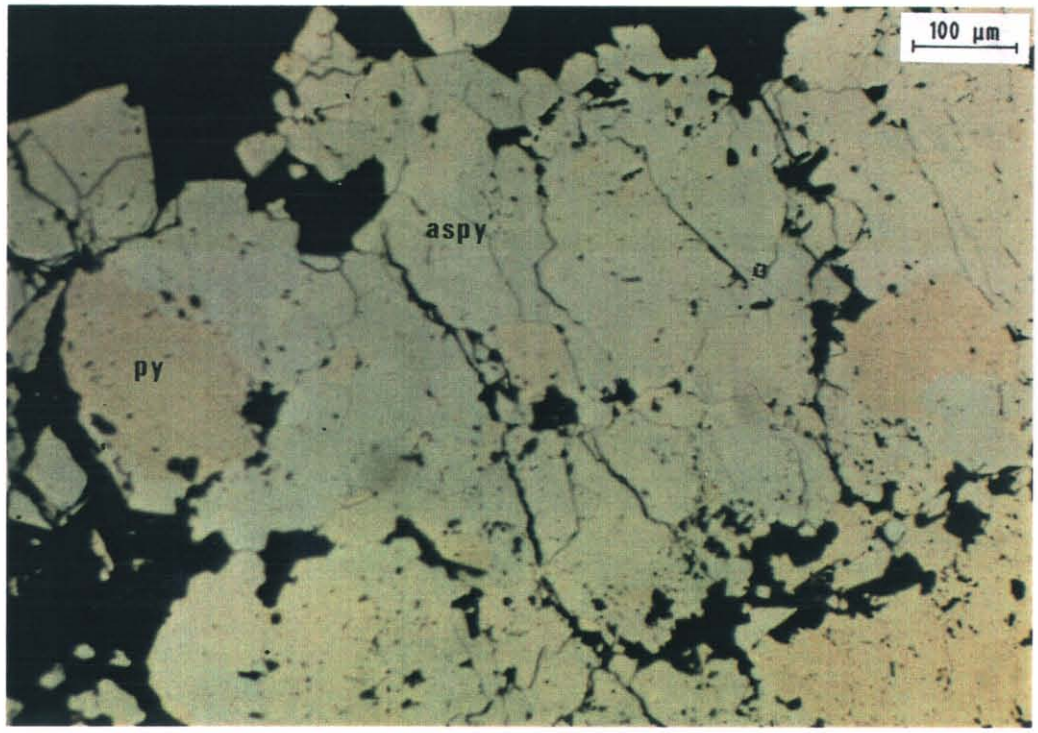

Plate 6. *Partial replacement of pyrite (py) by arsenopyrite (aspy).*

5 cm

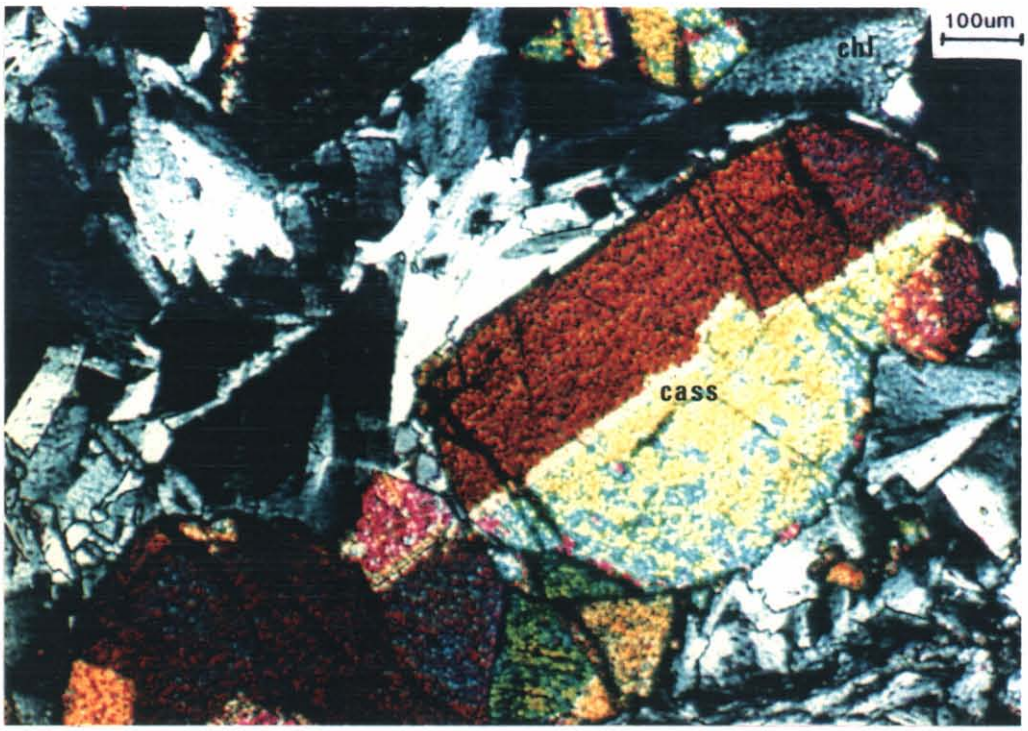

Plate 7. *Occurrence of twinned cassiterite crystals (cass) in close association with chlorite.*

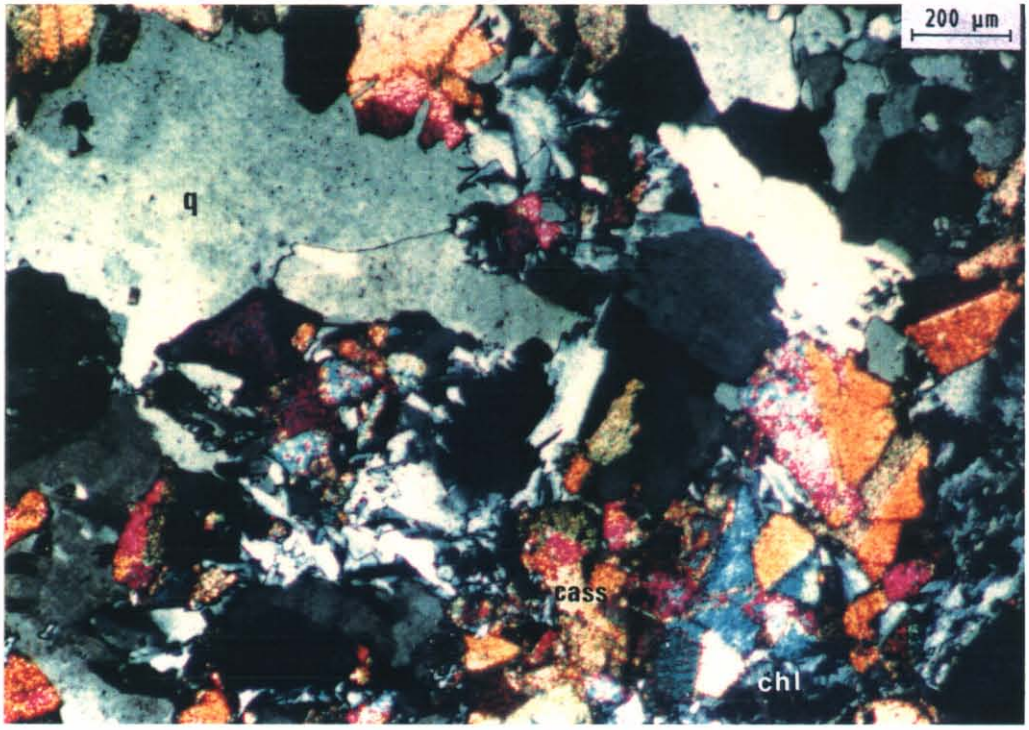

Plate 8. *Cassiterite (cass), quartz (q), chlorite (chl), and arsenopyrite (black) assemblage.*

5 cm

Plate 9. *Occurrence of chalcopyrite (ccpy) along fractures in arsenopyrite (aspy) and as patches. Note the close association of gold (Au) and chalcopyrite, and the late-formed galena (gl) and sphalerite (sph) in brecciated arsenopyrite.*

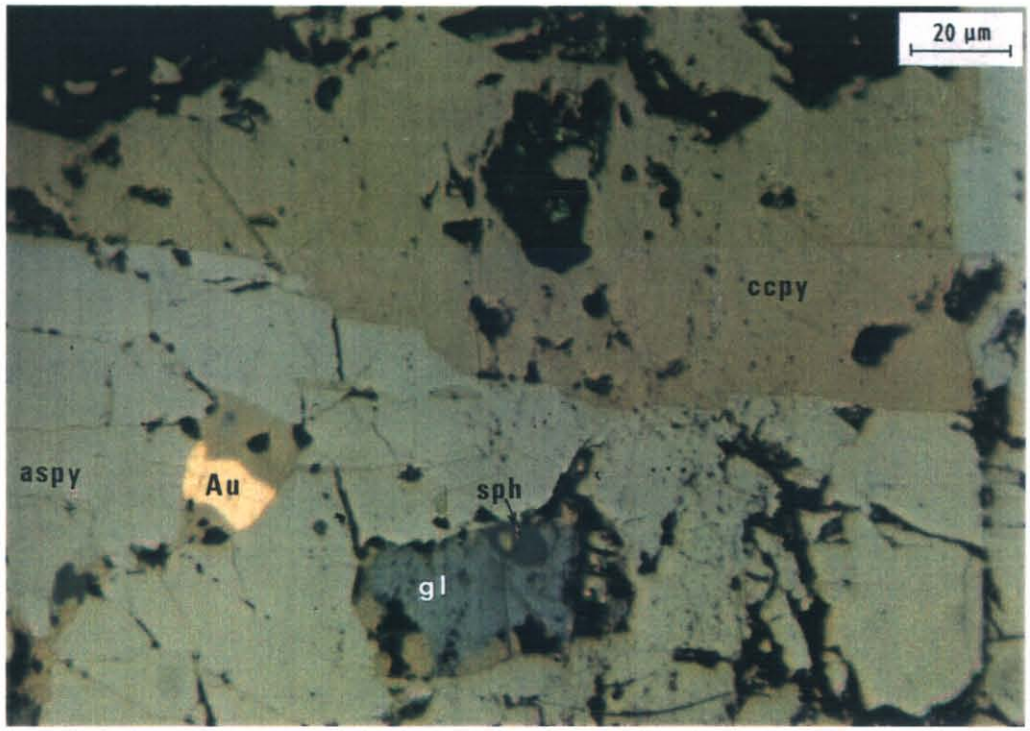

Plate 10. *Occurrence of chalcopyrite (ccpy) and gold (Au) as fissure-filling within brecciated arsenopyrite (aspy). Chalcopyrite is also closely associated with galena (gl) and sphalerite (sph).*

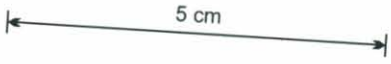

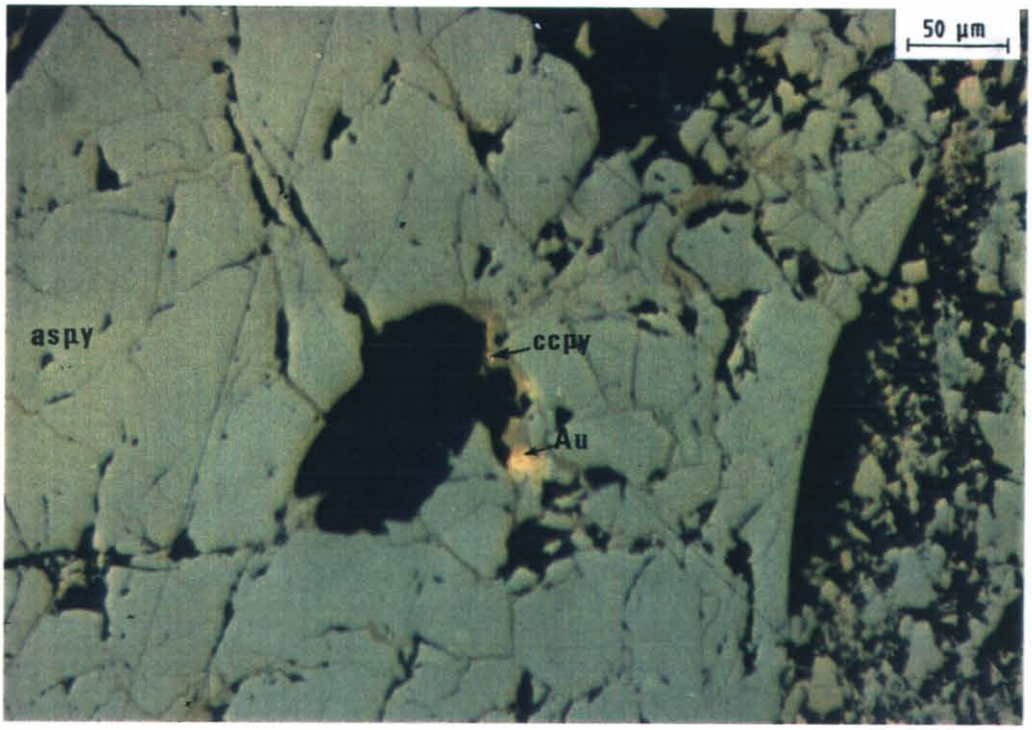

Plate 11. *Occurrence of chalcopyrite (ccpy) and gold (Au) along the microfractures in brecciated arsenopyrite (aspy).*

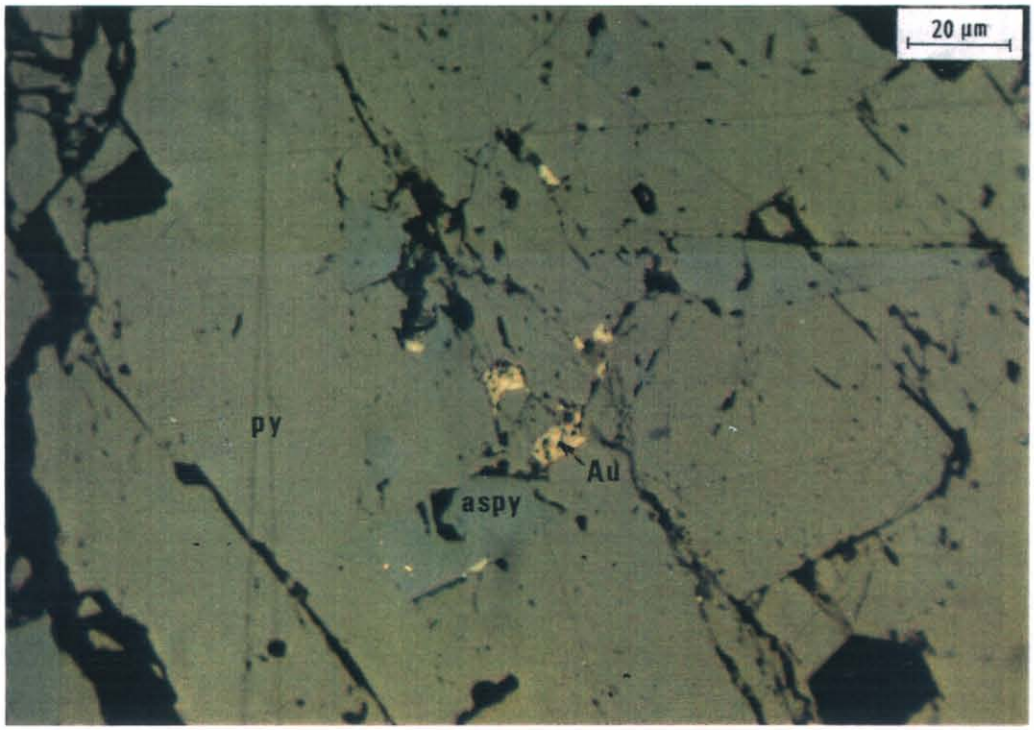

Plate 12. *Occurrence of gold (Au) in microfractures in pyrite (py) or at the arsenopyrite (aspy)–pyrite boundary.*

5 cm

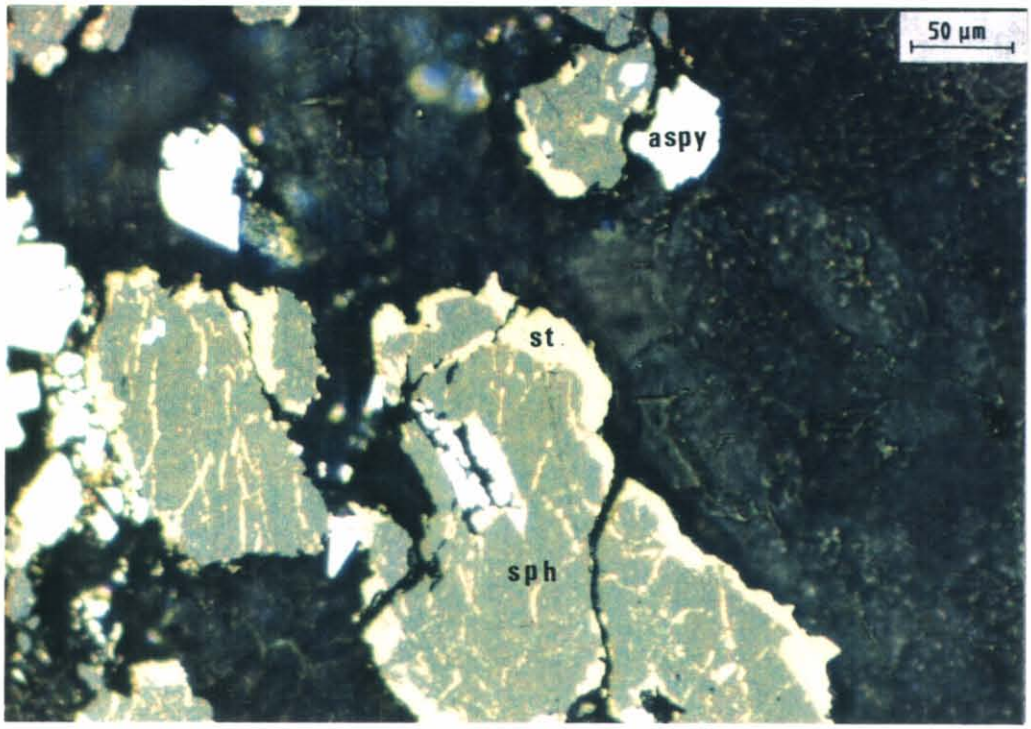

Plate 13. *Replacement of sphalerite (sph) by stannite (st). Note the stannite veinlets in sphalerite. White minerals are arsenopyrite.*

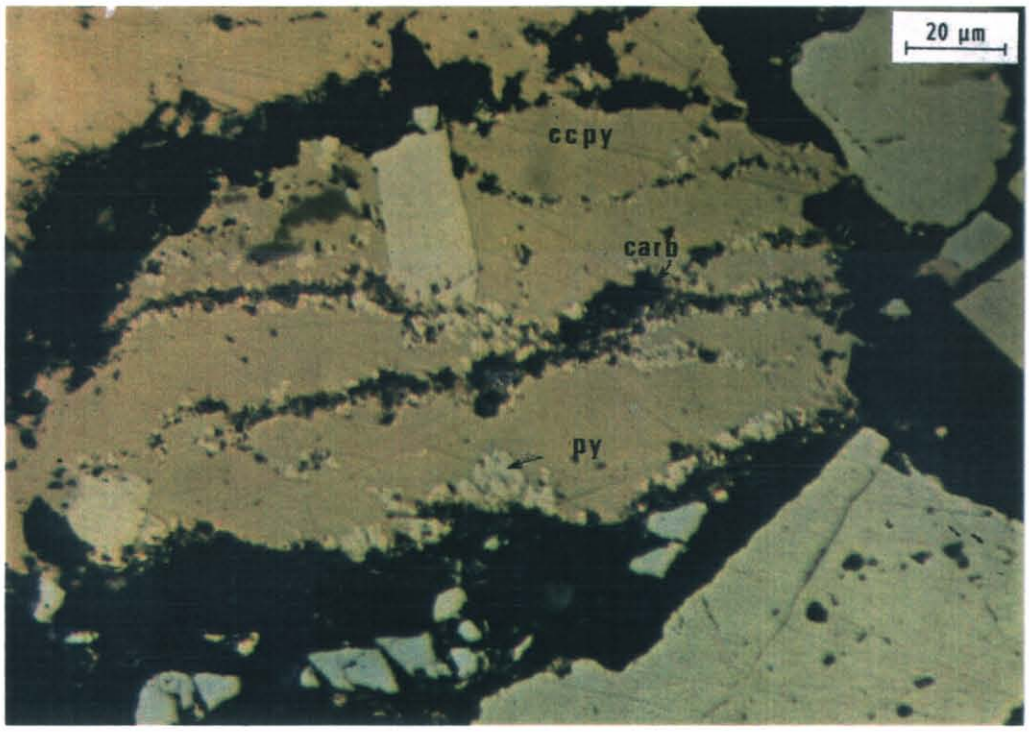

Plate 14. *Occurrence of late pyrite (py) on margins and both sides of carbonate (carb) veinlets in chalcopyrite (ccpy).*

5 cm

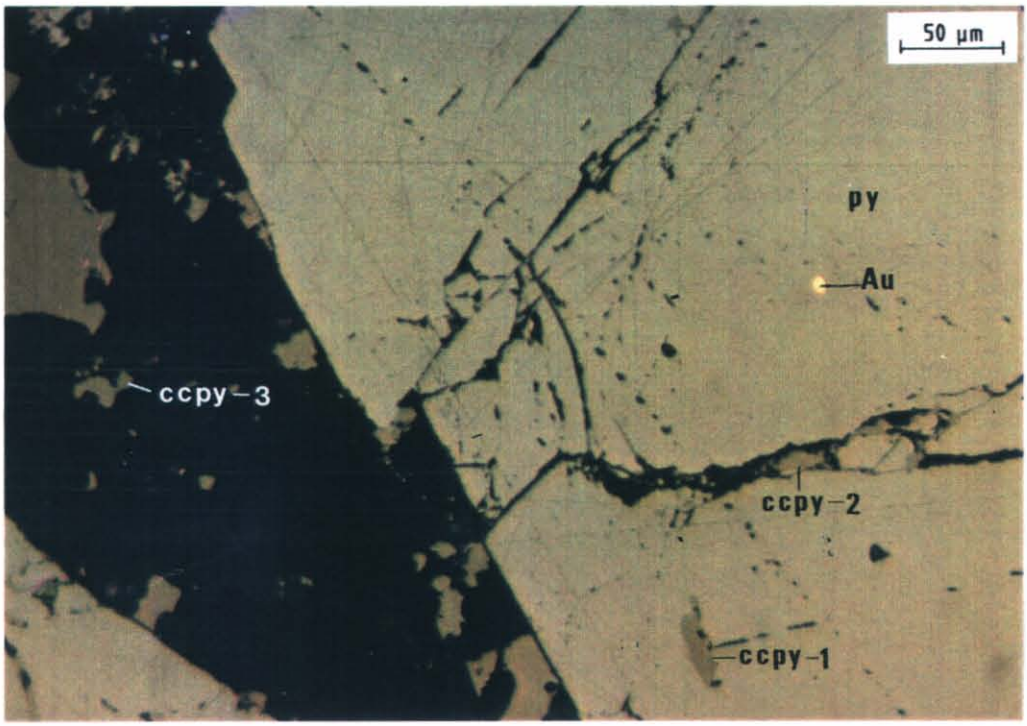

Plate 15. *Occurrence of gold (Au) as inclusions in pyrite (py). Note the occurrence of chalcopyrite as: (a) inclusion (ccpy-1); (b) in microfractures (ccpy-2); and (c) in quartz-tourmaline veinlet (ccpy-3).*

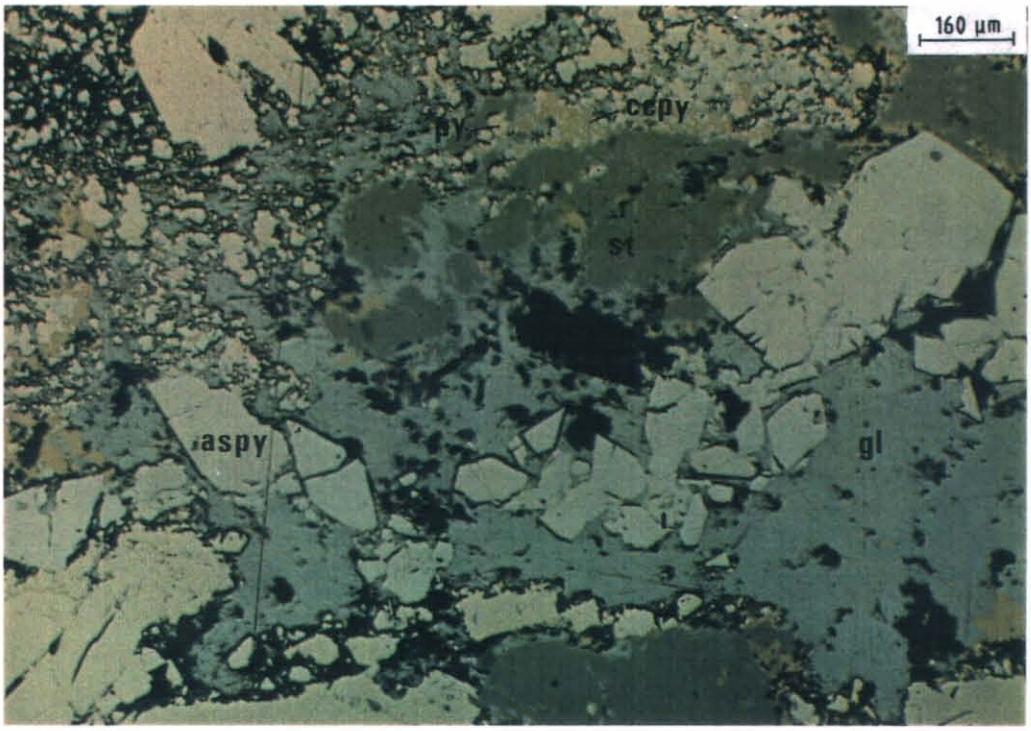

Plate 16. *Galena (gl) enclosing and partially replacing stannite (st), arsenopyrite (aspy), pyrite (py) and chalcopyrite (ccpy).*

5 cm

(a) Type A-2 inclusion (L_{H_2O}(1) + L_{CO_2}(2) + V_{CO_2}(3)) in quartz.

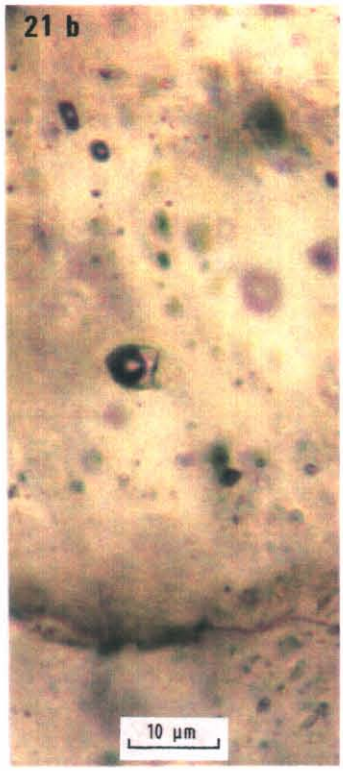

(b) Type A-3 inclusions (L_{H_2O} + V_{H_2O} + CO_2) in quartz.

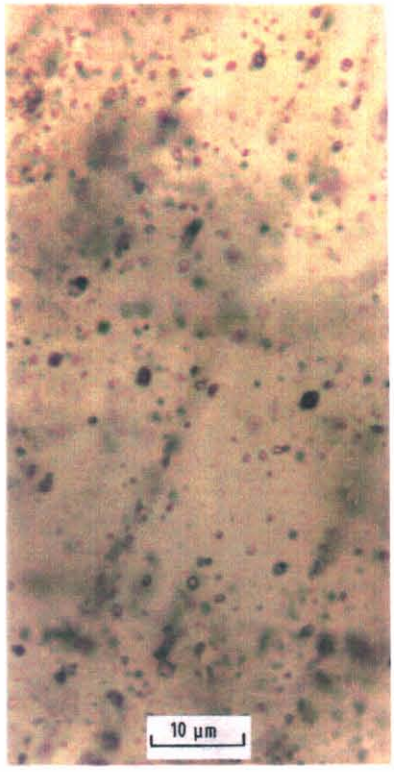

(c) Type B-1 inclusions (L_{H_2O} + V_{H_2O}) in quartz. Note the small size of B-1 inclusions and the abundance of secondary fluid inclusions along the microfractures.

(d) Type B-2 inclusions (L_{H_2O} + V_{H_2O}) in calcite.

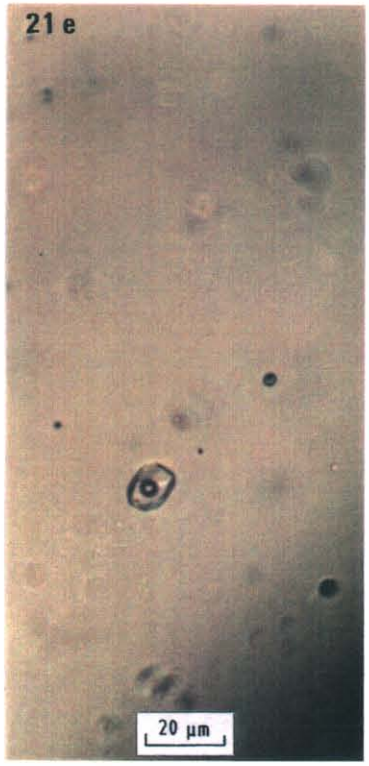

(e) Type C inclusions (L_{H_2O} + V_{H_2O} + solid phase) in quartz.

Plate 17. *Fluid inclusion types from the Lakeside Prospect.*

5 cm

APPENDIX 1

Chemical composition of pyrite, Lakeside Prospect

Sample No. 13939

Elements (wt%)					
S	53.43	53.80	53.89	53.87	53.86
Mn	0.11	0.11	0.11	0.11	<0.11
Fe	45.94	46.20	45.49	45.49	46.14
Co	0.00	0.00	0.00	0.00	<0.00
Ni	0.14	0.13	0.14	0.13	<0.13
Cu	0.17	0.16	0.35	0.16	<0.19
Zn	0.19	0.19	0.25	0.64	<0.19
As	0.41	0.20	0.19	0.20	0.41

Atoms				
S	0.67	0.67	0.67	0.67
Mn	0.00	0.00	0.00	0.00
Fe	0.33	0.33	0.33	0.33
Co	0.00	0.00	0.00	0.00
Ni	0.00	0.00	0.00	0.00
Cu	0.00	0.00	0.00	0.00
Zn	0.00	0.00	0.00	0.00
As	0.00	0.00	0.00	0.00

Sample No. 102817

Elements (wt%)								
S	53.83	54.05	52.34	53.42	52.73	52.84	49.87	52.61
Mn	0.13	0.10	0.11	0.11	0.11	0.11	0.11	0.11
Fe	43.24	46.00	47.66	45.90	45.60	45.77	44.18	44.15
Co	0.00	0.23	0.22	0.21	0.41	0.21	0.20	0.35
Ni	0.15	0.14	0.14	0.13	0.33	0.16	0.14	0.20
Cu	0.1	0.00	0.17	0.20	0.16	0.16	0.20	0.16
Zn	0.21	0.28	0.19	0.18	0.19	0.19	0.19	0.18
As	2.74	0.21	0.23	0.48	0.92	1.23	5.75	1.7

Atoms							
S	0.67	0.66	0.67	0.665	0.670	0.641	0.668
Mn	0.00	0.00	0.00	0.000	0.000	0.000	0.000
Fe	0.33	0.34	0.33	0.327	0.327	0.326	0.328
Co	0.00	0.00	0.00	0.003	0.000	0.000	0.002
Ni	0.00	0.00	0.00	0.002	0.001	0.000	0.001
Cu	0.00	0.00	0.00	0.000	0.000	0.001	0.000
Zn	0.00	0.00	0.00	0.000	0.000	0.000	0.000
As	0.00	0.00	0.00	0.002	0.001	0.032	0.000

Sample No. 102828

Elements (wt%)						
S	53.63	53.01	53.28	53.70	53.88	53.43
Mn	0.11	0.10	0.10	0.11	0.10	0.11
Fe	45.83	45.96	45.75	45.87	45.71	45.70
Co	0.35	0.32	0.21	0.21	0.22	0.21
Ni	0.20	0.23	0.13	0.13	0.13	0.13
Cu	0.16	0.23	0.16	0.16	0.16	0.20
Zn	0.18	0.28	0.19	0.18	0.18	0.19
As	0.20	0.21	0.77	0.44	0.41	0.20

Atoms						
S	0.663	0.666	0.669	0.671	0.663	0.669
Mn	0.000	0.000	0.000	0.000	0.000	0.000
Fe	0.330	0.329	0.328	0.327	0.334	0.329
Co	0.002	0.000	0.000	0.000	0.000	0.000
Ni	0.002	0.000	0.000	0.000	0.000	0.000
Cu	0.001	0.000	0.000	0.000	0.000	0.001
Zn	0.002	0.001	0.000	0.000	0.000	0.001
As	0.000	0.004	0.002	0.002	0.003	0.000

APPENDIX 2

Chemical composition of arsenopyrite, Lakeside Prospect

Sample No. 102801

Element (%)

S	22.05	22.07	21.15	21.74	21.90	22.31	21.96	22.05	23.66	22.53	22.80
Fe	35.55	35.19	35.91	35.43	35.56	35.66	35.64	35.51	35.52	35.87	35.73
As	42.68	42.74	41.95	42.82	42.75	42.03	42.40	42.44	41.62	41.72	41.29

Atom%

S	0.363	0.364	0.365	0.361	0.361	0.367	0.363	0.364	0.372	0.368	0.373
Fe	0.336	0.334	0.341	0.337	0.337	0.337	0.339	0.337	0.335	0.339	0.336
As	0.301	0.302	0.296	0.303	0.302	0.296	0.311	0.311	0.292	0.293	0.283

Element (%)

S	22.29	21.80	22.06	22.01	22.28	22.73	22.51	23.24	21.82	22.89	20.83	22.06
Fe	35.46	35.67	35.70	35.76	35.78	35.75	35.81	35.77	36.03	35.53	40.10	35.81
As	42.06	42.57	42.25	42.23	42.32	41.52	41.75	41.11	42.04	41.67	39.08	42.13

Atom (%)

S	0.367	0.360	0.364	0.633	0.367	0.373	0.369	0.379	0.362	0.375	0.344	0.364
Fe	0.335	0.339	0.338	0.339	0.337	0.336	0.337	0.335	0.341	0.334	0.380	0.339
As	0.296	0.301	0.298	0.298	0.297	0.291	0.293	0.286	0.297	0.291	0.276	0.297

Sample No. 13939

Element (%)

S	22.55	22.21	21.75	22.01	22.18
Fe	35.54	35.51	35.75	35.76	35.57
As	41.70	42.28	41.99	42.23	42.10

Atom (%)

S	0.370	0.366	0.360	0.363	0.364
Fe	0.335	0.336	0.341	0.341	0.335
As	0.293	0.298	0.297	0.298	0.296

Sample No. 102807

Element (%)

S	21.87	22.46	21.91	22.13	21.53	22.11	21.10
Fe	35.69	36.07	35.23	35.65	35.60	35.81	35.46
As	42.44	41.46	42.04	41.89	42.75	41.87	43.52

Atom (%)

S	0.361	0.369	0.362	0.366	0.357	0.365	0.351
Fe	0.339	0.340	0.334	0.338	0.339	0.339	0.339
As	0.300	0.291	0.297	0.296	0.303	0.296	0.310

Sample No. 13937

Element (%)

S	22.45	22.47
Fe	35.80	35.62
As	42.02	42.30

Atom (%)

S	0.368	0.368
Fe	0.337	0.335
As	0.294	0.297

Sample No. 87-2, 209.1

Element (%)

S	22.95	22.84
Fe	36.19	35.85
As	40.53	40.69

Atom (%)

S	0.37	0.37
Fe	0.34	0.34
As	0.28	0.28

APPENDIX 2 (continued)

Chemical composition of arsenopyrite, Sterling Valley Tin

Sample No. STV 290

Element (%)								
S	22.12	21.72	21.73	21.53	21.21	20.60	20.71	21.51
Fe	35.65	35.35	35.35	35.64	35.34	35.32	34.75	35.03
As	42.16	42.14	42.41	43.25	43.20	43.60	44.02	43.20
Atom (%)								
S	0.365	0.360	0.360	0.360	0.353	0.346	0.348	0.358
Fe	0.338	0.336	0.336	0.338	0.338	0.341	0.335	0.334
As	0.298	0.301	0.301	0.306	0.308	0.313	0.316	0.307

APPENDIX 3

Chlorite analyses (mean values for each grain) and geothermometry, Lakeside Prospect

Sample No. 102877 (chlorite associated with cassiterite and sulphides)

Chemical composition

SiO_2	22.8	22.8	23.0	22.9	23.5	23.0	23.4	23.4	23.21
Al_2O_3	21.60	21.85	21.39	21.02	21.13	21.00	21.12	21.19	21.88
FeO	37.88	37.94	37.32	37.23	37.50	37.01	37.61	38.02	38.33
MnO	0.48	0.47	0.46	0.37	0.34	0.49	0.44	0.41	0.42
MgO	5.46	5.09	5.30	5.44	5.79	5.48	5.93	5.47	5.29

No. of ions

Si	5.15	5.18	5.22	5.23	5.28	5.25	5.25	5.26	5.18
Al	5.745	5.208	5.276	5.666	5.590	5.653	5.587	5.611	5.758
Fe	7.149	7.256	7.089	7.120	7.041	7.069	7.060	7.144	7.157
Mn	0.091	0.03	0.088	0.071	0.065	0.094	0.083	0.077	0.079
Mg	1.835	1.610	1.793	1.853	1.939	1.865	1.984	1.833	1.761
Al IV	2.847	2.895	2.78	2.772	2.715	2.754	2.753	2.735	2.817
Vac.	0.026	0.04	0.084	0.062	0.080	0.073	0.040	0.07	0.062
Fe/Fe + Mg	0.79	0.81	0.79	0.79	0.78	0.79	0.78	0.79	0.80

Geothermometry data

fO_2(L-V) -	-	-	-	-	-	-	-	-	-
T°C(L-V) -	-	-	-	-	-	-	-	-	-
fO_2 (1 kbar)	31.2	31.6	-	32.9	-	33.2	33.2	33.5	32.1
T°C (1 kbar)	325.5	321.5	-	309.5	-	306.5	306.5	304.5	316.5
T°C catal.	317.7	-	312.6	311.7	305.7	309.9	309.8	307.9	316.6
T°C cat. vac.	275.3	-	265.6	269.3	266.1	267.4	272.4	267.8	269.2
T°C K & M	378.8	-	371.9	370.6	363.9	368.6	367.8	367.0	376.2

Sample No. 102877 (chlorite vein in Farrell Slates)

Chemical composition

SiO_2	25.52	24.45	27.77	32.45	27.80
Al_2O_3	21.19	20.89	20.25	19.27	19.90
FeO	29.18	31.55	30.49	26.64	30.55
MnO	0.55	0.43	0.38	-	0.36
MgO	11.83	9.84	9.59	11.15	9.23

No. of ions

Si	5.455	5.381	5.915	6.591	5.969
Al	5.338	5.417	5.084	4.612	5.037
Fe	5.217	5.806	5.432	5.524	5.486
Mn	0.099	0.080	0.068	-	0.66
Mg	3.768	3.227	3.044	3.375	2.955
Al IV	2.545	2.619	2.085	1.409	2.031
Vac.	0.124	0.089	0.457	0.987	0.488
Fe/Fe + Mg	0.581	0.643	0.641	0.573	0.650

Geothermometry data

fO_2 (L-V)	-	29.91	48.83	64.83	50.36
T°C (L-V)	-	368.00	182.0	95.0	172.00
fO_2 (1kbar)	34.61	34.44	14.17	61.70	47.68
T°C (1kbar)	280.5	287.5	197.5	104.5	187.5
*T°C Catal.	287.71	295.6	238.9	167.1	233
T°C Catal. vac.	258.7	264.5	202.5	128.1	197.3
**T°C K & M	330.8	343.3	286.6	209.8	281.5

* M. Cathelineau and D. Nieva (1985).
** P. Kranidiotis and W. H. MacLean (1987).

APPENDIX 4

Chemical composition of gold (mean values for each grain), Lakeside Prospect

Sample No.	102807			102808	
Elements (wt%)					
Au	66.47	66.60	63.90	65.6	66.5
Ag	33.53	33.40	36.10	34.4	33.5
Total	100.00	100.00	100.00	100.00	100.00
Atoms					
Au	0.522	0.523	0.508	0.509	0.522
Ag	0.478	0.477	0.492	0.491	0.478
Total	1.00	1.00	1.00	1.00	1.00

APPENDIX 5

Fluid Inclusion Data

Thermometric measurements were made using USGS gas-flow heating/freezing system. A set of synthetic fluid inclusion standards* at temperatures -56.6°C, -21.2°C, -10.7°C, 0.0°C, 374.1°C and 573°C were used for calibration. The measured temperatures were -56.5°C, -21.2°C, -10.5°C, 0.0°C, 373.9°C and 571°C respectively.

* Standards were obtained from FLUID INC, PO Box 6873, Denver, CO 80206.

Sample No.	*Fluid inclusion type*	Th_L	Th_V	*Tm*	*Te*
103702 (quartz in vug)	B-2	132.4	-	0.8	-21.9
		167.0	-	0.9	-
		145.2	-	-0.4	-21.2
		140.0	-	0.9	-
		132.6	-	-1.0	-22.2
		135.7	-	-1.3	-
		154.5	-	-0.9	-23.0
		138.3	-	-0.9	-
		154.1	-	-0.8	-22.8
		135.2	-	-	-
		154.5	-	-0.8	-
		149.6	-	-	-
		148.2	-	-	-
102850 (quartz in vug)	B-2	134.3	-	-	-
		139.6	-	-	-21.9
		155.8	-	-0.8	-
		151.9	-	-	-23.0
		162.3	-	-0.9	-
		130.5	-	-0.2	-
		139.9	-	-1.1	-22.3
		130.2	-	0.4	-
		160.3	-	-	-
		158.8	-	-	-
		151.9	-	-	-
102892 (quartz-carbonate)	B-2	135.7	-	-7.06	-30.1
		139.3	-	-7.3	-
		140.1	-	-7.2	-29.1
		139	-	-7.1	-
		138	-	-6.8	-29.5
		145	-	-7.1	-31.5
		146.0	-	-7.2	-
		141	-	-7.8	-
		159.0	-	-7.1	-30.2
		147.5	-	-6.9	-
		156.0	-	-7.2	-
		149.0	-	-7.8	-
		156.2	-	-7.1	-29.9
		149.0	-	-7.2	-
		152.2	-	-6.8	-
		149.3	-	-6.9	-29.8
		149.0	-	-6.8	-
		146.0	-	-	-
		146.2	-	-	-
		153.3	-	-	-
		156.2	-	-	-
		142.1	-	-	-
		153.9	-	-	-
		160.0	-	-	-
		159.8	-	-	-
102895	B-1	249.5	-	-13	-28.9
		240.1	-	-	-
		242.3	-	-12	-32.0
		241.8	-	-11	-

Sample No.	*Fluid inclusion type*	Th_L	Th_V	*Tm*	*Te*
102896	B-1	227	-	-2.0	-28.0
		266	-	-4.5	-
		265	-	-4.0	-
		266.2	-	-5.0	-29.5
		235	-	-3.5	-
		245	-	-4.6	-
		269.2	-	-	-
		273.9	-	-	-
		295.0	-	-	-
		309.0	-	-	-29.5
		265.9	-	-	-
		308.9	-	-	-
		290.1	-	-	-31.8
		299.5	-	-	-
		296.2	-	-	-
		297.0	-	-	-
		301.0	-	-	-

		Tm		*Th*	
Sample No.	*Inclusion Type*	CO_2	*Clathrate*	CO_2	CO_2+H_2O
102896	A-2	-55.9	-	27.8(L)	401
		-56.1	9	-	-
		-55.9	8	25.8(L)	-
	A-3	-	-	-	305(L)
		-56.2	-	-	331(L)
		-56.1	-	-	339(L)
		-	8.5	-	333(L)
		-55.8	-	-	336(C.P.)
	A-2	-56.3	-	26.0(V)	331(C.P.)
	A-3	-	9	-	338(L)
		-55.8	-	-	336(C.P.)
		-56.1	8.5?	-	335(V)
		-55.8	-	-	381(V)
		-56.2	9	-	338(V)
	A-2	-56.1	-	25.9(L)	332(L)
		-	-	27.2?	333(L)
	A-3	-55.9	-	-	362(V)
		-56.1	-	-	368(V?)
		-56.2	-	-	343(L)
	A-2	-	-	28.2(V?)	382(V)
	A-3	-	-	-	336(L)
		-	-	-	331(L)
		-	-	-	333(L)
	A-2	56.2	8.5?	27.9(V?)	336(V)
		-	-	26(L)	331(L)
	A-3	-55.9	-	25.8(L?)	332(L)
	A-1	-	-	24.5(L)	-
		-56.2	-	13.7(L)	-
		-	-	25.6(L)	-
		-	-	28.5(V)	-
		-	-	28.9(V)	-
		-56.2	-	25.9(L)	-
		-56.3	-	26.5(L)	-

APPENDIX 6

Thermochemical data used in construction of diagrams

Reactions	*Log Keq (T °K)*	*Source*
$FeS_2 = FeS + \frac{1}{2}S_2$	$7.1628 - 0.7617 \times (10^4/T) + 0.00103 \times (10^4/T)^2$	1
$3FeS_2 + 2O_2 = Fe_3O_4 + 3S_2$	$14.8401 + 1.0443 \times (10^4/T) - 0.00176 \times (10^4/T)^2$	1
$FeS_2 + 3\frac{1}{2}O_2 = Fe_2O_3 + 2S_2$	$5.5042 + 1.3466 \times (10^4/T) - 0.00376 \times (10^4/T)^2$	1
$3FeS + 2O_2 = Fe_3O_4 + 3\frac{1}{2}S_2$	$-7.6752 + 3.3988 \times (10^4/T) - 0.00192 \times (10^4/T)^2$	1
$6Fe_2O_3 = 4Fe_3O_4 + O_2$	$14.8948 - 2.6110 \times (10^4/T) - 0.00175 \times (10^4/T)^2$	1
$SnO_2 + \frac{1}{2}S_2 = SnS + O_2$	$6.2119 - 2.1606 \times (10^4/T) + 0.00022 \times (10^4/T)^2$	1
$2Sn + S_2 = 2SnS$	$-10.1004 + 1.84481 \times (10^4/T)$	4
$4Sn_2S_3 + S_2 = 4SnS_2$	$-10.7232 + 1.16626 \times (10^4/T)$	4
$4SnS + S_2 = 2Sn_2S_3$	$-10.4413 + 1.2238 \times (10^4/T)$	4

Reactions	*Log Keq (T °C)* 350	*Source*
$H_2S = H^+ + HS^-$	-8.81	5
$H_2O = H_2 + \frac{1}{2}O_2$	-15.79	5
$Au + 2Cl^- + H^+ = AuCl_2^- + \frac{1}{2}H_2$	-3.65	6
$Au + H_2S + HS^- = Au(Hs)_2^- + \frac{1}{2}H_2$	-1.22	7
$4FeAsS + 6H_2O + 3O_2 = 4FeS + 4H_3AsO_3^0$	80.2	2
$SnO_2 + 2CuFeS_2 + S_2 = Cu_2FeSnS_4 + FeS_2 + O_2$	-21.75	3, 4

1: Ripley (1976) and Ripley and Ohmoto (1977)
2: Calculated from Barton (1984), Heinrich and Eadington (1986), and Bowers *et al.* (1984)
3: Calculated from Robie and Waldbaum (1968)
4: Calculated from Vaughan and Craig (1978)
5: Murray and Cubiciotti (1983)
6: Nikolaeva *et al.* (1972)
7: Shenberger and Barnes (1989)

APPENDIX 7

$^{206}Pb/^{204}Pb$ data

Deposit/ Sample No.	Mineral	$^{206}Pb/^{204}Pb$	Pb (ppm)
Mt Farrell mine (1)			
102784	gl	18.610	-
61617	gl	18.522	-
Murchison lode (1)			
61618	gl	18.441	-
61657	gl	18.425	-
Tullah lode (1)			
61624	gl	18.558	-
61625	gl	18.512	-
61652	gl	18.334	-
Murchison Bridge (1)			
70391	gl	18.550	-
70392	gl	18.528	-
70393	gl	18.511	-
Henty Prospect			
HFZ3, 102.1 m	)	18.493	530
HFZ4, 144.8 m	)	18.631	290
HFZ10, 209 m	)	18.361	13,000
HFZ10, 241.9 m	) Bulk	18.375	300
HFZ10, 242 m B	) Sulphides	18.388	300
HFZ9, 262.1 m	)	18.344	10,060
49N, trench	)	18.336	17,000
Tasman and Crown Lyell Extended			
P5	gl	18.273	-
P6	gl	18.273	-
P7	gl	18.261	-
Prince Lyell			
P445	banded ore	18.359	-
P167	fine py	18.548	180
P168	coarse py	18.616	68
P170	py	18.478	203
P171	py	19.098	37
P173	ccpy	18.576	81
P174	py	18.433	604
P185	py	18.647	754
P187	gl	18.370	-
P190	ccpy	18.354	1,330
Crown Lyell			
P177	py	18.386	478
P178	py	19.106	272
P179	ccpy	19.074	100
Que River main sulphide lenses			
QR8, 369.5 m	)	18.348)	all
QR28, 68.7 m	)Bulk	18.321)	>1%
QR218, 27.0 m	)Sulphides	18.332)	galena
QR92, 91.6 m	)	18.311)	
Que River main sulphide lenses (continued)			
QR92, 11.0 m	)	18.318)	
QR92, 85.0 m	)	18.323)	
QR14, 59.4 m	)	18.369)	
QR7A, 245 m	)	18.328)	
QR7B, 245 m	) Bulk	18.317)	All
QR8, 250 m	) Sulphides	18.346)	>1%
QR9, 257.9 m	)	18.328)	galena
QR17, 152 m	)	18.331)	
QR18, 154 m	)	18.328)	
QR19A, 159 m	)	18.359)	
QR19B, 159 m	)	18.355)	
Hellyer ores			
MG3, 204.7 m	)	18.372)	
MG3, 213.0 m	)	18.349)	
MG3, 222.0 m	)	18.354)	
MG5, 296.7 m	)	18.372)	
MG5, 312.15 m	)	18.342)	
MG5, 318.5 m	) Bulk	18.373)	All
MG5, 366.2 m	) Sulphides	18.368)	>1%
MG5, 392.1 m	)	18.363)	galena
MG18, 277.55 m	)	18.364)	
MG18, 284.7 m	)	18.322)	
MG18. 287.4 m	)	18.322)	
MG18, 295.0 m	)	18.351)	
MG18, 304.55 m	)	18.350)	
Rosebery			
67818A, F lens	gl	18.271	-
678188	gl	18.273	-
67818C	gl	18.272	-
68649, D lens	gl	18.266	-
68471A, E lens	gl	18.279	-
68471B	gl	18.273	-
P668, H lens	gl	18.277	-
68466, H lens	gl	18.272	-
Hercules			
70388	gl	18.286	-
70389	gl	18.276	-
70390	gl	18.268	-
Ostic et al. (1967)	gl	18.268	-
Lakeside Prospect			
14055	) Bulk	18.603	0.23%
13832	) Sulphides	18.644	0.71%
13631	)	18.612	30.7%
Murchison Mine			
Murch. 32	-	18.604	1,850
Murch. 30	-	18.584	3,250
Sterling Valley Mine			
-	-	18.455	-
-	-	18.422	>1%

gl = galena; py = pyrite; st = stannite; ccpy = chalcopyrite